Osaka University Knowledge Archive

Title	Studies on Selective Organic Transformations by Semiconductor Photocatalysts Loaded with Platinum and Palladium Nanoparticles
Author(s)	Sugano, Yoshitsune
Citation	大阪大学, 2013, 博士論文
Version Type	VoR
URL	https://hdl.handle.net/11094/27496
rights	
Note	

Osaka University Knowledge Archive : OUKA

https://ir.library.osaka-u.ac.jp/

Osaka University

工博 16309

Studies on Selective Organic Transformations by Semiconductor Photocatalysts Loaded with Platinum and Palladium Nanoparticles

Yoshitsune Sugano

March 2013

Studies on Selective Organic Transformations by Semiconductor Photocatalysts Loaded with Platinum and Palladium Nanoparticles

A dissertation submitted to
The Graduate School of Engineering Science
Osaka University
in partial fulfillment of the requirements for the degree of
Doctor of Philosophy in Engineering

Yoshitsune Sugano

March 2013

Abstract

There has been much interest in the development of environmentally- and economically-friendly chemical processes for organic synthesis from the viewpoint of green and sustainable chemistry. The main objective of this thesis is to develop the photocatalytic processes for selective organic transformations. Semiconductor metal oxides loaded with platinum (Pt) and palladium (Pd) nanoparticles were used for photocatalytic transformations under UV and visible light irradiations. This thesis consists of following six chapters.

In Chapter I, photocatalytic synthesis of benzimidazoles from alcohols and *o*-arylenediamines was studied using titanium dioxide loaded with Pt nanoparticles (Pt/TiO_2) under UV irradiation. The catalytic system efficiently produces benzimidazoles with high selectivity. Experimental results reveal that the reaction is achieved by Pt-assisted photocatalytic oxidation of alcohols to aldehydes on the TiO_2 surface, followed by dehydrogenation of benzimidazoline intermediate on the Pt surface. Amount and size of Pt particles play crucial roles on reaction. The catalyst loaded with 0.2 wt% Pt, which contains 2.0 nm Pt particles, exhibits the highest activity and selectivity.

In Chapter II, TiO_2 loaded with Pd nanoparticles (Pd/TiO_2) were used for photocatalytic hydrodenitrogenation of aromatic cyanides with ethanol as a hydrogen source under UV irradiation. The catalyst promotes selective hydrodenitrogenation of aromatic cyanides, and produces corresponding toluene derivatives and triethylamine with almost quantitative yields. Experimental evidences and model calculation revealed that the catalytic activity strongly depends on the amount of Pd loaded. The catalyst containing 2 wt% Pd, with a relatively low Schottky barrier height at the Pd-TiO_2 heterojunction and a large number of surface Pd atoms, exhibits the highest denitrogenation activity.

In Chapter III, the Pd/TiO_2 catalysts were used for *N*-monoalkylation of primary amine with alcohol under UV irradiation. The catalyst efficiently promotes the corresponding secondary amine with almost quantitative yields. The reaction occurs via tandem photocatalytic and catalytic reactions, consisting of Pd-assisted photocatalytic alcohol oxidation to produce aldehyde, catalytic condensation of aldehydes with amines, and catalytic hydrogenation of formed imines with the hydrogen atom formed on the Pd particles (H-Pd species). Experimental evidences and model calculation reveal that the rate-determining step is the imine hydrogenation, and the reaction depends strongly on the size of Pd particles. The catalyst with 0.3 wt% Pd, containing 2-2.5 nm Pd particles, shows the highest activity for imine hydrogenation, and smaller or larger Pd particles are inefficient.

In Chapter IV, TiO_2 loaded with bimetallic Pd-Pt alloy nanoparticles were used for photocatalytic dehalogenation of aromatic halides with alcohol as a hydrogen source under UV irradiation. The alloy catalytic system efficiently promotes dehalogenation, and the activity is three times higher than that of the catalyst loaded with Pd alone and is also higher than that obtained with molecular hydrogen as a hydrogen source. The high catalytic activity of the alloy catalyst is due to the enhanced consumption of photoformed

electrons on the Pt site and the efficient transfer of the formed hydrogen atom to the adjacent Pd site within the alloy particles, leading to efficient formation of the hydride species, which act as the active species for dehalogenation.

In Chapter V, tungsten trioxide (WO_3) loaded with Pt nanoparticles (Pd/WO_3) were used for partial oxidation of cyclohexane (CHA) with molecular oxygen (O_2) under visible light irradiation (λ >420 nm). The Pt/WO_3 catalysts produce cyclohexanol (CHA-ol) and cyclohexanone (CHA-one) with high selectivity (ca. 93%). The high selectivity for partial oxidation on Pt/WO_3 is because subsequent decomposition of CHA-ol and CHA-one is suppressed. In the Pt/WO_3 system, the photoformed electrons on the conduction band of WO_3 are efficiently consumed by a multi-electron reduction of O_2 (formation of water and hydrogen peroxide), where a single-electron reduction of O_2 is unfavored. This suppresses the formation of a superoxide anion that promotes decomposition of CHA-ol and CHA-one and, hence, results in selective formation of partial oxidation products.

In chapter VI, Pt particles loaded on anatase TiO_2 (Pt/anatase) were used for aerobic oxidation of alcohols under visible light irradiation (λ >450 nm). The reaction is initiated by the absorption of visible region light by Pt nanoparticles. This promotes interband excitation of d electrons on Pt nanoparticles. This then leads to smooth electron transfer to anatase and promotes the reduction of O_2 on anatase. Model calculation with Pt nanoparticles also reveals that this activity depends on the height of Schottky barrier and the number of perimeter Pt atoms created at the Pt/anatase heterojunction. The catalyst loaded with 2 wt% Pt, containing 3–4 nm Pt particles, facilitates smooth Pt→anatase electron transfer, resulting in the highest photocatalytic activity. The catalyst also promotes efficient and selective aerobic oxidation of alcohols by sunlight exposure.

This thesis described the selective organic transformations by semiconductor photocatalysts loaded with Pt and/or Pd nanoparticles. These results presented in this thesis may contribute to the development of selective photocatalytic organic transformations and the design of more environmentally- and economically-friendly synthesis processes by sunlight.

Preface

This dissertation work was carried out under the joint supervision of Professor Dr. Takayuki Hirai and Associate Professor Dr. Yasuhiro Shiraishi at the Research Center for Solar Energy Chemistry, and Division of Chemical Engineering, Graduate School of Engineering Science, Osaka University from 2007 to 2013.

The objective of this thesis is the design and development of selective systems for photocatalytic organic transformations by semiconductor metal oxides loaded with platinum and palladium nanoparticles. The author hopes that the results obtained in this work would give some suggestions for the future construction of photocatalytic systems for organic synthesis.

Yoshitsune Sugano
Division of Chemical Engineering
Graduate School of Engineering Science
Osaka University
Toyonaka 560-8531, Japan

CONTENTS

General Introduction 1

Chapter I

One-Pot Synthesis of benzimidazoles by Simultaneous Photocatalytic and Catalytic Reaction on TiO_2 Loaded with Pt Nanoparticles 16

1. Introduction 16

2. Experimental 17

2-1. Materials and procedure 17

3. Results and discussion 18

3-1. Synthesis and characterization of catalysts 18

3-2. Photocatalytic activity of Pt/TiO_2 catalyst. 20

3-3. Reaction mechanism 21

3-4. Effect of Pt amount and size on the catalyric activity 23

3.5. Synthesis of various benzimidazole 25

4. Conclusion 26

5. References 27

Chapter II

Photocatalytic Hydrodenitrogenation of Aromatic Cyanides on TiO_2 Loaded with Pd Nanoparticles 29

1. Introduction 29

2. Experimental 30

2-1. Materials 30

2-2. Photoreaction procedure 30

2-3. Analysis 31

3. Results and discussion 31

3-1. Synthesis and characterization of catalysts 31

3-2. Photocatalytic activity of Pd/TiO_2 catalysts 34

3-3. Mechanism for photocatalytic hydrodenitrogenation 36

3-4. Hydrodenitrogenation of substituted benzonitrile 38

3-5. Effect of Pd amount on the catalytic activity 39

4. Conclusion 42

5. References 42

Chapter III

***N*-Monoalkylation of Amines with Alcohols by Tandem Photocatalytic and Catalytic Reactions on TiO_2 Loaded with Pd Nanoparticles 44**

1. Introduction 44

2. Experimental 45

2-1. Materials 45

2-2. Photoreaction 46

2-3. Hydrogenation by H_2 46

2-4. Analysis 46

3. Results and discussion 47

3-1. Catalytic activity of metal-loaded TiO_2 47

3-2. Catalytic activity of Pd/TiO_2 48

3-3. Mechanism for *N*-alkylation 52

3-4. Effect of Pd amount on the reaction steps 53

3-5. Active site for imine hydrogenation 56

3-6. Effect of alcohol on the imine hydrogenation 60

4. Conclusion 62

5. References 63

Chapter IV

Highly Efficient Photocatalytic Dehalogenation of Organic Halides on TiO_2 Loaded with Bimetallic Pd-Pt Alloy Nanoparticles 66

1. Introduction 66

2. Experimental 67

2-1. Materials 67

2-2. Photoreaction procedure 67

2-3. Analysis 67

3. Results and discussion 68

3-1. Synthesis and characterization of catalysts 68

3-2. Photocatalytic activity of PdPt/TiO_2 catalysts 73

3-3. Reaction mechanism 75

3-4. Dehalogenation of various aromatic halides 78

4. Conclusion 78

5. References 79

Chapter V

Visible Light-Induced Partial Oxidation of Cyclohexane on WO_3 Loaded with Pt Nanoparticles **80**

1. Introduction **80**

2. Experimental **82**

2-1. Materials 82

2-2. Catalyst preparation 82

2-3. Photoreaction 83

2-4. ESR measurement 83

2-5. Analysis 83

3. Results and discussion **83**

3-1. Catalyst properties 83

3-2. Photocatalytic activity 85

3-3. Multi-electron reduction on WO_3 87

3-4. Suppression of subsequent decomposition of products 89

4. Conclusion **91**

5. References **91**

Chapter VI

Platinum Nanoparticle Supported on Anatase Titanium Dioxide as Highly Active Catalysts for Aerobic Oxidation under Visible Light Irradiation ..**94**

1. Introduction **94**

2. Experimental **96**

2-1. Preparation of catalysts 96

2-2. Reaction procedure 96

2-3. Action spectra analysis 97

2-4. ESR measurement 97

2-5. Analysis 97

3. Results and discussion **98**

3-1. Preparation and properties of catalysts 98

3-2. Catalytic activity 100

3-3. Electron transfer at the Pt/anatase heterojunction 103

3-4. Effect of Pt amount 106

3-5. Effect of Pt particle size 109

4. Conclusion **114**

5. References **114**

General Conclusions **118**

Suggestions for Future Work **121**
List of Publication **125**
Acknowledgment **126**

General Introduction

ENERGY and ENVIRONMENT are two of the humanity's top ten problems for next 50 years.[1] Since the industrial revolution in 18th century, human beings used large amount of resources and energies, and built up enough material civilization, leading to obtaining an easy and comfortable life. The human beings who are one of the species on the earth, however, have caused a crisis of biogeocenosis of the earth. The origin of this disaster is not only the development and expansion of industry based on technologies but our lifestyle which have grown dramatically since the industrial revolution. Increase of energy consumption, world population, and food consumption, gave rise to the global disasters such as warming temperature, acid rains, and ozone depletion. Therefore, businesses, governments, and consumers shall cooperate for taking measures against the protection of earth resources and environment. Chemical industry, which is one of the various industries, produces various chemical precursors of automobiles, constructs, clothes, and drugs to other industries and has an important part in our lifestyle. Chemical industry, therefore, has the potential to contribute to environmental protection of the earth by reviewing lifecycle (from production to disposal) of chemical products.

One of the solutions by approaching from the chemical industry is the introduction of the concept of "Green chemistry". This concept means "the design of chemical products and processes that reduce or eliminate the use and generation of hazardous substances,"[2] which is a comprehensive approach applicable to all aspects of chemistry. From feed stocks to solvents, synthesis, and process, green chemistry actively seeks ways to produce materials which are more benign to human health and the environment. The current attention on green chemistry reflects a shift away from the historic "command and control" approach to environmental problems that restrictive waste treatment and control and clean up through regulation, and toward preventing pollution at its source. Therefore, rather than accepting waste production and disposal as unavoidable, green chemistry seeks new technologies that are cleaner and economically competitive.

The economic benefits of green chemistry are central locomotives in its advancement. Industry is also able to adopt green chemistry methodologies because they improve the corporate bottom line; a wide variety of operating costs is decreased through the use of green chemistry. When less waste is generated, environmental compliance costs go down, leading to the decrease of needs of treatment and disposal. Decreased solvent usage and fewer processing steps lessen the material and energy costs of manufacturing and increase material efficiency. The environment, human health, and the economic

advantages realized through green chemistry are, therefore, serving as a strong incentive to industry to adopt greener technologies.

Developing the green chemistry methodologies is a challenge that may be viewed through the framework of "Twelve Principles of Green Chemistry".[3] These principles identify *CATALYSIS* as one of the most important tools for implementing green chemistry. In addition, even from the chemical industry, an improvement of catalysis process, which is one of the main and fundamental parts of manufacturing process, hold the promise of reduction of produce costs. The design and application of new catalysts and catalytic systems, therefore, offer numerous green chemistry benefits including lower energy requirements, catalytic versus stoichiometric amounts of materials, increased selectivity, and decreased use of processing and separation agents. These also allow the use of less toxic materials, which leads to achieving the dual goals of environmental protection and economic benefit simultaneously. Especially, heterogeneous catalysis has received a tremendous amount of interest, both from a scientific and an industrial perspective. This is demonstrated by the 2007 Nobel Prize in Chemistry awarded to Prof. Ertl, a pioneer in introducing surface science techniques to the field of heterogeneous catalysis leading to a deeper understanding of how chemical reactions take place at surfaces.[4] Since more than 90% of chemical manufacturing processes utilize catalysts,[5] heterogeneous catalysis has an enormous impact on the world economy. The current manufacturing processes, however, have taken large energy to purify the chemical products and precursors due to the low yields of catalytic reaction products. These processes also need severe reaction conditions (high temperature and high pressure) to increase the yields per unit time, although sub-reactions proceed and specific reactors are required. For the improvement of these processes, catalytic productions of an only main product under more economically and environmentally benign conditions are desirable.

Metal nanoparticle catalysis is one of the most attracted fields in heterogeneous catalysis. Several remarkable novel catalytic properties including enhanced reactivity and selectivity have been reported for nanoparticle catalysts as compared to their bulk counterparts. To utilize the power of these nanoparticle catalysts, detailed understanding of the origin of their enhanced performance is necessary. Many experimental studies on nanoparticles have focused on correlating catalytic activity with particles size. While particle size is an important consideration, many other factors such as geometry, composition, oxidation state, and chemical/physical environment can also play an important role in determining nanoparticle reactivity. The exact relationship between these parameters and the catalytic performance may, however, be system dependent. A systematic understanding of the factors that control catalyst reactivity and selectivity is therefore very important task.

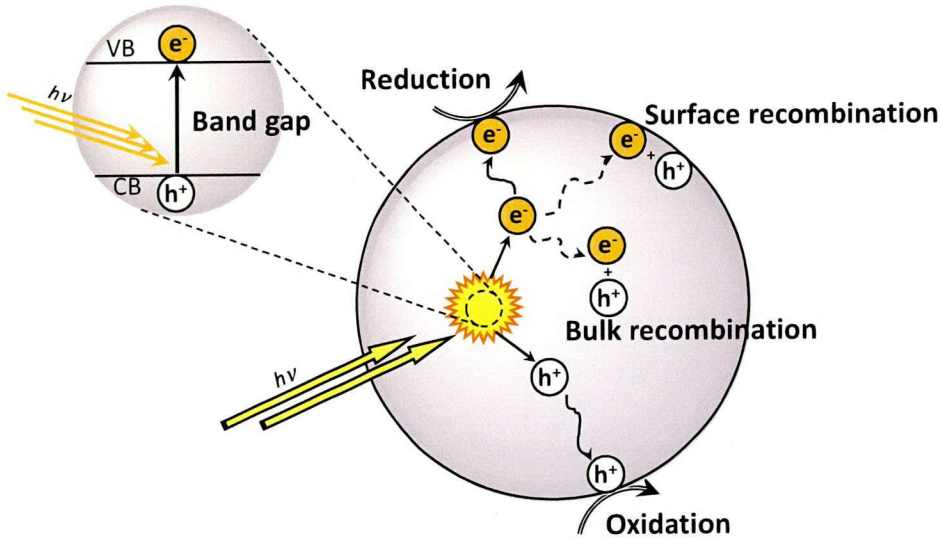

Figure 1. Photocatalytic reaction occurring on semiconductor photocatalyst.

Metal nanoparticles are often used in the field of photocatalysis. Photocatalytic reaction is a recent discipline particularly well adapted to environmental problems since it operates at room temperature by catalytic photoactivation instead of thermal activation. Among them, titanium dioxide (TiO_2) has been widely used as a pigment in sunscreens, paints, ointments, or toothpaste, because it is chemically stable, harmless, and inexpensive. In 1972, Fujishima and Honda discovered the photocatalytic splitting of water on TiO_2 electrodes.[6] As a result of this, the application of TiO_2 photocatalysis was extended to environmental frontiers. Frank and Bard[7] reported the application of TiO_2 in photocatalytic oxidation of CN^- and SO_3^{2-} in aqueous medium under sunlight irradiation. Photocatalytic reduction of CO_2 on TiO_2 reported by Inoue et al.[8] have attracted much attention in this field. Moreover, Izuml et al.[9] have reported that photo-kolbe decarboxylation route to butane, which includes the generation of hydroxyl radical. This opened a new chapter for application of TiO_2 photocatalysis in organic transformations. Kraeutler and Bard.[10] have applied the decomposition of organic compounds by TiO_2 photocatalysis.

The mechanism for heterogeneous photocatalysis has been studied extensively so far, and a number of excellent reviews and books have been published by many researchers.[11] Despite many applications, the basic mechanisms are almost similar. **Figure 1** shows schematic representation of the photocatalytic reaction on TiO_2. When TiO_2 absorb light with energy larger than its bandgap energy ($>E_g$), photoexcited electron (e^-) and holes (h^+) pairs are generated in the conduction band and valence band, respectively. The e^- and h^+ produced inside the particles migrates to the particle surface and promotes oxidation and reduction reactions, while some of these pairs are deactivated by recombination of them at bulk or surface. In the presence of molecular oxygen (O_2), the reduction of O_2 by conduction band e^- proceeds.

In contrast, the h^+ oxidizes substrates or H_2O.

In 2000s, the growing awareness of green chemistry has given a boost to develop the process for organic synthesis with photocatalysts under mild conditions,[12] which avoid stoichiometric consumption of expensive and harmful oxidants.[13] Wide application of TiO_2 photocatalysis for organic transformations has been reported.[14] Some of the transformations were accomplished, which can be categorized as oxidations and oxidative cleavages,[15] reductions,[16] geometric and valence isomerizations,[17] substitutions,[18] condensations,[19] and polymerizations.[20] However, except for above some successful examples, photocatalytic organic transformations on TiO_2 basically do not proceed efficiently.

One of the reasons for unsuccessful organic transformations on bare TiO_2 is the low activity for photocatalytic reactions. As shown in **Figure 1**, photoexcited semiconductor materials produce e^- and h^+. They migrate thorough the material and appear on the surface, promoting oxidation and reduction reactions of substrates. The parts of e^- and h^+ are, however, recombined during migration and are deactivated. To improve the activity for photocatalysis, therefore, it is necessary to suppress the charge recombination between photogenerated e^- and h^+ (**Figure 2a**). One of the most famous methods to solve this problem is the surface modification of photocatalysts with noble metal nanoparticles such as Pt, Ag, Au, and Pd. Among them, modification of TiO_2 surface with Pt nanoparticles (Pt/TiO_2) is a popular method, which was firstly reported by Kraeutler and Bard.[21] The Pt/TiO_2 catalyst exhibits enhanced activity for various photocatalytic reactions.[22] This is basically due to their different Fermi levels (E_F), characterized by the work function of the metals and the band structure of the semiconductors.[23] When metal nanoparticles are loaded on the semiconductor surface, the electrons migrate from semiconductor to metal occurs until the two Fermi levels are aligned similar, and energy barrier is created at the interface of heterojunction, which is called the Schottky barrier (**Figure 2b**). Photoexcitation of semiconductor generates electrons in the conduction band of the semiconductor and raises its Fermi level to more negative values.[24] Then, the generated energetic difference at the semiconductor and metal interface drives the electrons from the conduction band of the semiconductor into the metal nanoparticle. The Schottky barrier produced at the metal-semiconductor interface can serve as an efficient electron trap preventing electron-hole recombination in photocatalysis, which leads to the enhancement of photocatalytic reactivity. The activity of these photocatalyst is usually tested by degradation of organic pollutants in water or photocatalytic H_2 evolution from aqueous alcohols solutions under UV light irradiation. Application of these modified TiO_2 photocatalysts for photochemical organic transformation is scarce.

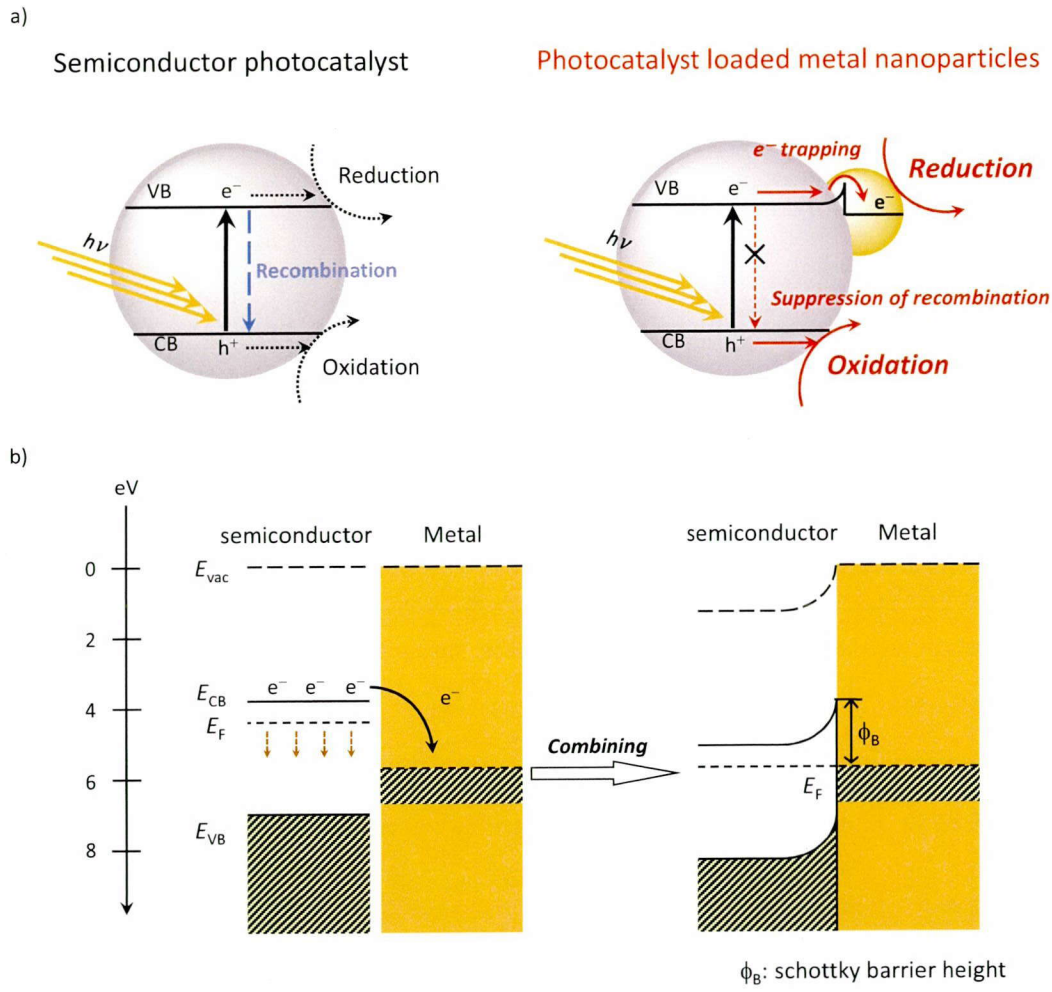

Figure 2. Schematic representation for (a) the photocatalyst with/without metal nanoparticles and (b) the Schottky barrier created at the metal and semiconductor photocatalyst heterojunction.

As mentioned before, in the last century, catalysis developed into one of the most powerful technologies in the petroleum, bulk chemical, fine chemical and pharmaceutical industries.[25] In parallel to developing technologies, the fundamental understanding of catalytic processes has been advancing rapidly by developing model catalytic system using experimental and theoretical techniques at the molecular level.[26] In particular, *noble metal nanoparticle* catalysts possess marvelous and specific activities about various reactions. The pioneering catalytic applications of noble metal nanoparticles were reported in 1940 by Nord and co-workers for nitrobenzene reduction.[27] In the late 1950s, Boreskov stated a chemical approach to the kinetics of heterogeneous catalysis by metals based on the influence of the reaction mixture and reaction conditions on the properties and chemical composition of the catalyst.[28] Since the 1970s, metal nanoparticles have been more frequently used in catalysis,[29] and are even suspected to be involved in organometallic catalysis. Since the turn of the millennium, interest in

metal nanoparticle catalysis has considerably increased because this class of catalysts appears as one of the most promising solutions toward efficient reaction under mild, environmentally benign conditions in the context of Green Chemistry.[30] As present, these preparation, structure determination, and applications are topics of current interest.[31] Especially, attention is focused on that a change in the catalytic properties of metals, caused by the transformation from bulk metal to nanoparticles (1-100 nm), is one of the fundamental problems of heterogeneous catalysis.[32] Supported metal particle size can also essentially affect the specific catalytic activity (reaction rate per one surface atom), the number of reaction cycles, as well as the rate of the catalytic reaction. As suggested,[33] these changes may be associated both with the electronic properties of nanoparticles and with features of their crystal structure (compared with bulk metal or coarse particles, the most part of surface atoms with low coordination numbers and with residing at the angles and edges of fine particles).

Among metal nanoparticles, platinum (Pt) and palladium (Pd), which are well known as platinum group metals, possess dominantly specific and various catalytic activities. Extensive studies for Pt and Pd nanoparticles have been performed for various catalytic applications. Pt nanoparticles show outstanding catalytic and electrical properties and superior resistant characteristics to corrosion, and have been widely applied in chemical, petrochemical, pharmaceutical, electronic, and automotive industries.[34] They possesses distinctive ability in catalyzing partial oxidation, hydrogenation and dehydrogenation of a variety of important molecules that are essential in many industrial processes.[35] In contrast, Pd nanoparticles are well known as noble metal catalysts which possess the high activity for various reactions.[36] The main parts of these reactions by Pd nanoparticles are hydrogenations and C-C couplings (Suzuki, Heck, Stille),[37] and a few reports are related to other processes like dehalogenation, hydrodechlorination, carbonylation or oxidation.

In addition, bimetallic nanoparticles, composed of two different metal elements, are of greater interest than monometallic ones, from both the scientific and technological views, for the improvement of the catalytic properties of metal nanoparticles.[38] In fact, bimetallic catalysts have long been valuable for in-depth investigations of the relationship between catalytic activity and catalyst particle structure.[39] This is because bimetallization can improve catalytic properties of the original monometallic catalysts and create a new property, which may not be achieved by monometallic catalysts. These effects of the added metal component can often be explained in terms of an ensemble and/or a ligand effect in catalyses. Sinfelt et al. have made a series of studies on bimetallic nanoparticle catalysts supported on inorganic supports, for example Ru-Cu[40] and Pt-Ir[41] on silica. They analyzed the detailed structures of their samples by an extended X-ray absorption fine structure (EXAFS) technique, and showed that these

nanoparticles with a diameter of 1-3 nm had an alloy structure, associated with their properties.[42]

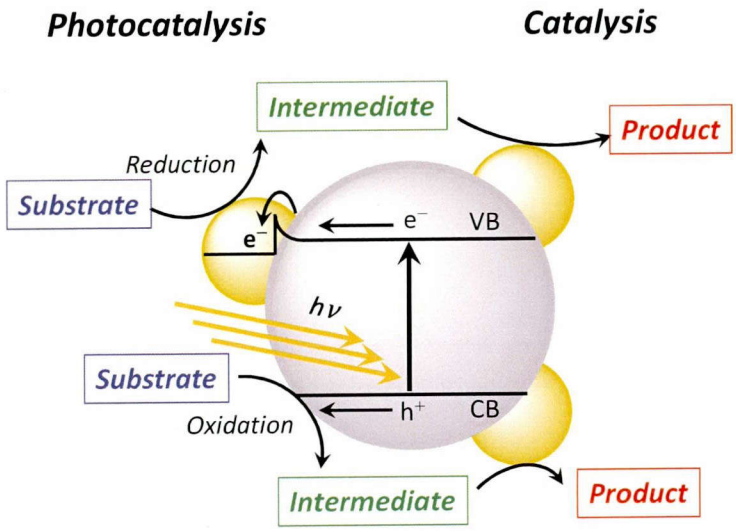

Figure 3. Schematic representation for the concept of selective photocatalytic and catalytic organic transformations by photocatalyst loaded with noble metal nanoparticles.

On the basis of these findings, if photocatalyst and noble metal nanoparticles are combined, some new photocatalytic reactions for selective organic transformation under mild reaction conditions are prospective (**Figure 3**). TiO_2 is an efficient photocatalyst under UV irradiation. It has wide band-gap (3.0–3.2 eV), which almost corresponds to an absorption threshold of ca. 400 nm. This limits the use in the visible wavelength region (400–800 nm). It is well known that <400 nm UV light is contained in solar radiation with only 3–5%. This means that only a small portion of light can be used for chemical reactions. *Development of photocatalysts that work under visible light irradiation* is an important issue for practical application of "sunlight" as the light source. One approach is the use of semiconductor photocatalysts with narrow band gap (<3.0 eV). Warrier et al. reported that CdS and CdSe quantum dots in the presence of sacrificial electron donors promote chemoselective photocatalytic reduction of aromatic azides to aromatic amines.[43] Ohmori et al. reported that α-Fe_2O_3 is capable of oxidizing water and evolving oxygen gas, in the presence of Fe^{3+} as the electron scavengers.[44] Tungsten trioxide (WO_3) is also a visible-light-responsive photocatalyst, which possesses narrow band gap (2.8 eV), deep oxidation potential of valence band, nontoxicity, and stability (**Figure 4**).[45] Abe et al. have proposed that Pt loading is an attractive solution to enhance the photocatalytic properties because loaded Pt enable to trap photogenerated electron from WO_3 to reduce O_2 to H_2O_2 and H_2O.[46] Arai et al. reported that WO_3 loaded with Pd catalyst proceed complete oxidation of acetaldehyde and toluene under visible light irradiation.[47]

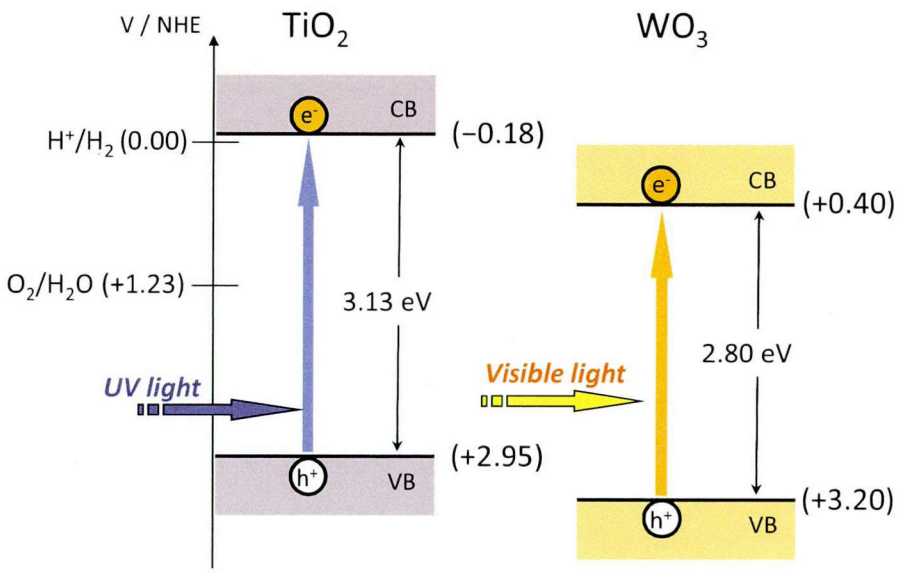

Figure 4. Redox potential of TiO_2 and WO_3 (pH 0).

The other approach is the use of localized surface plasmon resonance (SPR) of a portion of noble metal nanoparticles. In 2004, Tian et al. found that Au or Ag particles loaded on a semiconductor TiO_2 film that is coated on an indium tin oxide electrode generates an anodic photocurrent in the presence of Fe^{2+} under visible light irradiation (λ >420 nm) (**Figure 5**). This photoelectrochemical response is explained by an electron transfer mechanism similar to that for dye-sensitized TiO_2:[48] collective oscillations of electrons on the Au particles irradiated by the incident light transfers the electrons from the Au particles to the TiO_2 conduction band, while the positively charged Au particles receive electrons from the electron donor (Fe^{2+}). On the basis of these findings, they proposed that semiconductor materials loaded with a portion of noble metal nanoparticles behaves as a new class of visible light-driven catalysts.[49] Since then, effects of preparation procedure, metal particle sizes, loading amount, and on photocatalytic activity has been investigated for photodegradation of organic substrates,[50] and H_2 and O_2 evolution from water.[51] Application to organic transformations has scarcely been carried out.

The purpose of this thesis is to develop selective organic transformations by semiconductor photocatalysts loaded with Pt and Pd nanoparticles. The author tried to apply the TiO_2-based photocatalysts loaded with Pd and Pd nanoparticles for benzimidazole synthesis, hydrodenitrogenation of aromatic cyanide, and *N*-alkylation of primary amines under UV irradiation. Moreover, the author used the synergetic effect promoted by bimetallic Pt-Pd alloy nanoparticles for selective hydrodehalogenation of organic halides. To create the photocatalytic system driven by visible light irradiation, the author used WO_3 catalysts loaded with Pt nanoparticles for partial oxidation of CHA. In addition, the author tried to clarify the visible light activity of Pt nanoparticles loaded on TiO_2 surface

and clarified the potential for sunlight-driven organic transformations. The framework of the present study is shown in **Figure 6**.

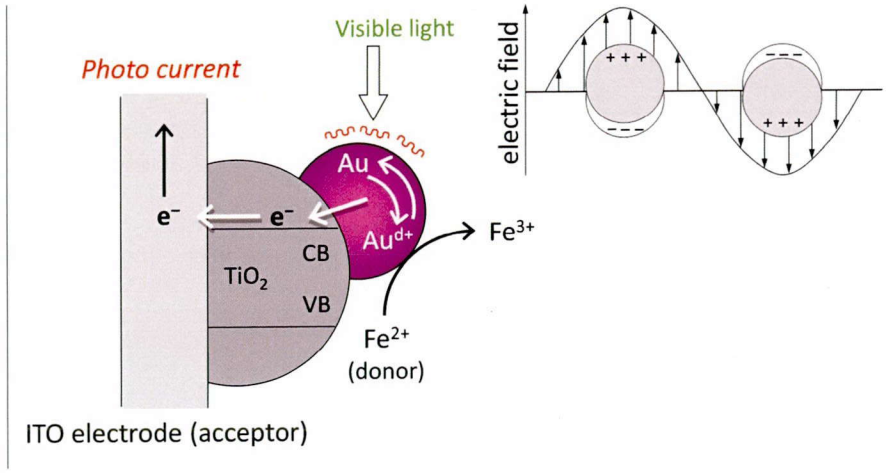

Figure 5. TiO_2-loaded with Au metal nanoparticles showing surface plasmon resonance.

Photocatalytic Activation by UV Light

Chapter I.
Synthesis of Benzimidazoles on TiO_2 Loaded with Pt Nanoparticles

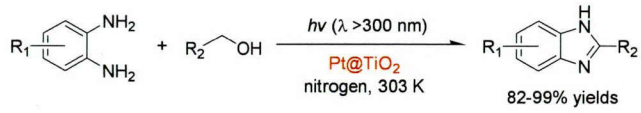

Chapter II.
Hydrodenitrogenation of Aromatic Cyanides on TiO_2 Loaded with Pd Nanoparticles

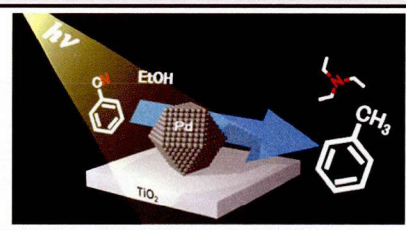

Chapter III.
N-Monoalkylation of Amines with Alcohols on TiO_2 Loaded with Pd Nanoparticles

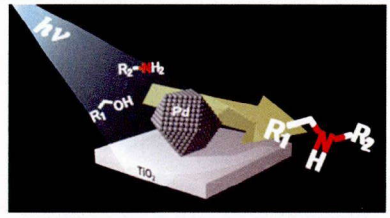

Chapter IV.
Dehalogenation of Organic Halides on TiO_2 Loaded with Bimetallic Pd-Pt Alloy Nanoparticles

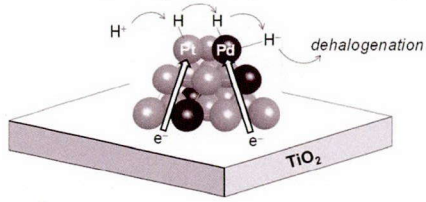

Photocatalytic Activation by Visible Light

Chapter V.
Partial Oxidation of Cyclohexane on WO_3 Loaded with Pt Nanoparticles under Visible Light Irradiation

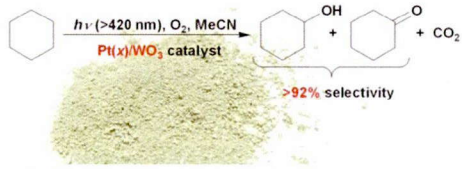

Chapter VI.
Aerobic Oxidation by Platinum Nanoparticle Supported on Anatase Titanium Dioxide under Visile Light Irradiation

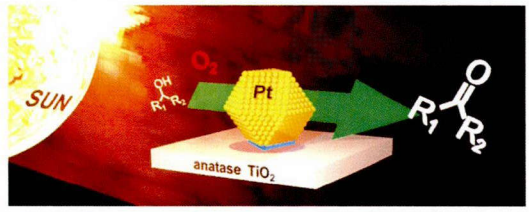

Figure 6. Framework of the present study.

This thesis consists of six chapters. The first four chapters (Chapters I–IV) describe photocatalytic organic transformations under UV irradiation, where TiO_2 loaded with Pt or Pd nanoparticles and TiO_2 loaded with Pd–Pt bimetallic alloy nanoparticles were employed. The chapters V and VI describe visible light-driven photocatalysts, where WO_3 loaded Pt nanoparticles and TiO_2 loaded with Pt nanoparticles are used for selective organic transformations.

In Chapter I, TiO_2 particles loaded with Pt nanoparticle (Pt/TiO_2), prepared by photodeposition method, was used for one-pot catalytic synthesis of benzimidazole from *o*-phenylenediamines and alcohols. We found that the process successfully produces corresponding benzimidazoles rapidly and selectively. This process is promotes by Pt-assisted photocatalytic oxidation of alcohols to aldehydes and catalytic dehydrogenation of formed intermediate. In this reaction, the amount and size of Pt nanoparticles on catalysts are important factors. The catalyst containing 0.2 wt% Pd, with a relatively large amount of Pt atoms and a small Pt particle size (<4 nm), exhibits the highest activity and selectivity of benzimidazole synthesis.

In Chapter II, TiO_2 loaded with Pd nanoparticles (Pd/TiO_2) was used for photocatalytic reaction of aromatic cyanide with ethanol under UV irradiation (λ >300 nm). This catalytic system successfully promoted hydrodenitrogenation of aromatic cyanides and produced toluene derivatives with high selectivity at room temperature. This reaction proceeds by photocatalytic oxidation of ethanol to produce acetaldehyde and hydrogen atom on the Pd surface (H-Pd species). The H-Pd species promotes hydrodenitrogenation of aromatic cyanides and subsequent condensation with aldehydes, leading to successful hydrodenitrogenation. The catalytic activity strongly depends on the amount of Pd loaded. The catalyst containing 2 wt% Pd, with a relatively low Schottky barrier height at the Pd/TiO_2 heterojunction and a large number of surface Pd atoms, exhibits the highest denitrogenation activity.

In Chapter III, the author studied *N*-alkylation of primary amines with alcohols in the presence of metal-loaded TiO_2 under photoirradiation (λ >300 nm). The author found that TiO_2 loaded with Pd nanoparticles successfully promotes *N*-monoalkylation of primary amines at room temperature, This reaction proceeds via three consecutive steps involving (i) Pd-assisted photocatalytic oxidation of alcohols; (ii) catalytic condensation of the formed aldehyde and amine on the TiO_2 surface; and, (iii) catalytic hydrogenation of the formed imine on Pd nanoparticles. The catalyst with 0.3 wt% Pd, containing 2-2.5 nm Pd particles, shows the highest activity for imine hydrogenation, and smaller or larger Pd particles are inefficient.

In Chapter IV, the author found that TiO_2 loaded with bimetallic Pd-Pt alloy nanoparticles ($PdPt/TiO_2$) promotes highly efficient photocatalytic dehalogenation of organic halides with alcohol as a

hydrogen source. The activity is more than three times that of TiO_2 loaded with Pd particles and higher than the conventional method with molecular hydrogen. The high activity is due to the enhancement consumption of photoformed e^- on the Pt site by H^+ reduction and efficient transfer of the formed hydrogen atom to the adjacent Pd site within the alloy particles.

In Chapter V, WO_3 loaded with Pt nanoparticles (Pt/WO_3) were employed for photocatalytic oxidation of cyclohexane with molecular oxygen under visible light irradiation (λ >420 nm) to produce cyclohexanol and cyclohexanone. The catalysts successfully promote partial oxidation with ca. 93% selectivity, without the formation of subsequent decomposition of these products. The ESR measurement with a spin trapping reagent and the photocatalytic reaction with a superoxide radical scavenger indicate that selective oxidation of cyclohexane on the catalysts is indeed achieved due to the decreased formation of superoxide radicals that promotes decomposition of the products.

In chapter VI, the author found that Pt nanoparticles loaded on anatase TiO_2, when used for aerobic oxidation under visible light (λ >450 nm), facilitate direct e^- transfer to anatase and promote the reaction highly efficiently. This occurs via the electronic excitation of Pt particles by visible light followed by the transfer of their e^- to anatase conduction band. The positively charged Pt particles oxidize substrates. Whereas the conduction band e^- are consumed by the reduction of molecular oxygen. The catalyst loaded with 2 wt% Pt, containing 3-4 nm Pt particles, creates a relatively low Schottky barrier and a relatively large number of perimeter Pt atoms and, hence, facilitates smooth Pt→anatase e^- transfer, resulting in very high photocatalytic activity.

The results obtained in this work are summarized in general conclusions. Suggestions for future work are described as an extension of the present work.

Reference

[1] Smalley, R. E. *Energy & NanoTechnology Conference*, Rice University, May 3, **2003**.

[2] Anastas, P. T.; Heine, L. G.; Williamson, T. C. *Green Chemical Syntheses and Processes: Introduction. In Green Chemical Syntheses and Processes*; Anastas, P. T.; Heine, L. G.; Williamson, T. C.; Eds.; American Chemical Society: Washington, DC, **2000**; Chapter 1.

[3] Anastas, P. T.; Warner, J. C. *Green Chemistry: Theory and Practice*; Oxford University Press: New York, **1998**; p 30. (b) Anastas, P. T.; Kirchhoff, M.; Willamson, T. C. *Appl. Catal. A* **2001**, *221*, 3.

[4] (a) Kim, M.; Bertram, M.; Pollmann, M.; von Oertzen, A.; Mikhailov, A. S.; Rotermund, H. H.; Ertl, G. *Science* **2001**, *292*, 1357. (b) Ertl, G. *Angew. Chem. Int. Ed.* **2008**, *47*, 3524. (c) Beta, C.; Moula, M. G.; Mikhailov, A. S.; Rotermund, H. H.; Ertl, G. *Phys. Rev. Lett.* **2004**, *93*, 188302.

[5] Thomas, J. M.; Thomas, W. J. (Eds.), *Principles and Practice of Heterogeneous Catalysis*, VCH, Weinheim, **1997**.

[6] Fujishima, A.; Honda, K. *Nature* **1972**, *238*, 37.

[7] Frank, S.N.; Bard, A.J. *J. Phys. Chem.* **1977**, *81*, 1484.

[8] Inoue, T.; Fujishima, A.; Konishi, S.; Honda, K. *Nature* **1979**, *277*, 637.

[9] Izuml, I.; Fan, F.-R. F.; Bard, A. J. *J. Phys. Chem.* **1981**, *85*, 218.

[10] Kraeutler, B.; Bard, A. J. *J. Am. Chem. Soc.* **1978**, *100*, 5958.

[11] (a) Augugliaro, V.; Litter, M.; Palmisano, L.; Soria, J. *J. Photochem. Photobiol. C* **2006**, *7*, 127. (b) Carp, O.; Huisman, C. L.; Reller, A. *Prog. Solid State Chem.* **2004**, *32*, 33.

[12] (a) Anpo, M. *Pure Appl. Chem.* **2000**, *72*, 1265. (b) Shiraishi, Y.; Hirai, T. *J. Photochem. Photobiol. C: Photochem. Rev.* **2008**, 9, 157.

[13] Fox, M. A. *Top. Curt. Chem.* **1991**, *142*, 172.

[14] Serpone, N.; Pelizzetti, E.; Eda. *Photocatalysis-Funddamental and Applications*, Wiley Interscience, New York, **1989**, p421.

[15] (a) Kraeutler, B.; Bard, A. *J. Am. Chem. Soc.* **1978**, *100*, 2339. (b) Fox, M. A.; Chen, C. C. *J. Am. Chem. Soc.* **1981**, *103*, 6757. (c) Fox, M. A.; Chen, M. J. *J. Am. Chem. Soc.* **1983**, *105*, 4497. (d) Sakata, T.; Kawai, T.; Hashimoto, K. *J. Phys. Chem.* **1984**, *88*, 2344.

[16] Lin, L.; Kuntz, R. R. *Langmuir* **1992**, *8*, 870.

[17] Ikezawa, H.; Kutal, C. *J. Org, Chem.* **1987**, *52*, 3299.

[18] Wsng, C. M.; Mallouk, T. E. *J. Am. Chem. Soc.* **1990**, *112*, 2016.

[19] (a) Denn, W. W.; Aikawa, Y.; Bard, A. J. *J. Am. Chem. Soc.* **1981**, *103*, 6893. (b) Harada, H.; Ueda, T.; Sakata, T. *J. Phys. Chem.* **1989**, *93*, 1542.

[20] (a) Becker, W. G.; Truong, M. M.; Ai, C. C.; Hamel. N. N. *J. Phys. Chem.* **1989**, *93*, 82. (b) Tada, H.; Hyodo, M.; Kawahara, H. *J. Phys. Chem.* **1991**, *95*, 10185. (c) Fox, M. A.; Worthen, K. L. *Chem. Mater.* **1991**, *3*, 253.

[21] Kraeutler, B.; Bard, A. J. *J. Am. Chem. Soc.* **1978**, *100*, 4317.

[22] (a) Baba, R.; Nakabayashi, S.; Fujishima, A.; Honda, K. *J. Phys. Chem.* **1985**, *89*, 1902. (b) Ranjit, K. T.; Viswanathan, B. *J. Photochem. Photobiol. A* **1997**, *108*, 73. (c) Hwang, S.; Lee, M. C.; Choi, W. *Appl. Catal. B* **2003**, *46*, 49. (d) Choi, W.; Lee, J.; Kim, S.; Hwang, S.; Lee, M. C.; Lee, T. K. *J. Ind. Eng. Chem.* **2003**, *9*, 96.

[23] (a) Pichat, P. *New. J. Chem.* **1987**, *11*, 135. (b) Ohtani, B.; Kakimoto, M.; Nishimoto, S.; Kagiya, T. *J. Photochem. Photobiol. A* **1993**, *70*, 265.

[24] Subramanian, V.; Wolf, E. E.; Kamat, P. V. *J. Am. Chem. Soc.* **2004**, *126*, 4943.

[25] Derouane, E. G. *CATTECH* **2001**, *5*, 214.

[26] (a) Somorjai, G. A. *Introduction to surface chemistry and catalysis*, Wiley, New York, **1994**. (b) Christensen, C. H.; Norskov, J. K. *J. Chem. Phys.* **2008**, *128*, 182503.

[27] (a) Rapino, L. D.; Nord, F. F. *J. Am. Chem. Soc.* **1941**, *63*, 2745. (b) Kavanagh, K. E.; Nord, F. F. *J. Am. Chem. Soc.* **1943**, *65*, 2121.

[28] Boreskov, G. K. *J. Chim. Phys.* **1954**, *51*, 759.

[29] (a) Michel, J. B.; Scharz, J. T. *Catalyst Preparation Science*, Elsevier, Amsterdam, **1987**, p669. (b) Schmid, G. *Chem. Rev.* **1992**, *92*, 1709. (c) Lewis, L. N. *Chem. Rev.* **1993**, *93*, 2693.

[30] (a) El-Sayed, M. A. *Acc. Chem. Res.* **2001**, *34*, 257. (b) Bell, A. T. *Science* **2003**, *299*, 1688.

[31] (a) Mori, K.; Kumami, A.; Tomonari M.; Yamashita, H. *J. Phys. Chem. C*, 2009, **113**, 16850. (b) Abad, A.; Corma, A.; García, H. *Chem. Eur. J.*, 2008, **14**, 212-222.

[32] (a) Che, M.; Benett, C. O. *Adv. Catal.* **1989**, *36*, 55. (b) Bond, G. C. *Chem. Soc. Rev.* **1991**, *20*, 441.

[33] (a) Ponec, V. *Adv. Catal.* **1983**, *32*, 149. (b) Sachtler, W. M. H. *Catal. Rev. Sci. Eng.* **1976**, *14*, 193. (c) Guszi, L.; Sarkany, A. *Catalysis*, Spivey, J. J.; Agarwal, S. K., Ed., Royal Society of Chemistry, Cambridge, **1994**, *11*, p318.

[34] (a) Barefoot, R. R.; VanLoon, J. C. *Anal. Chim. Acta* **1996**, *334*, 5. (b) Gasteiger, H. A.; Kocha, S. S.; Sompalli, B.; Wanger, F. T. *Appl. Catal. B* **2005**, *56*, 9. (c) Lu, W.; Mi, B.-X.; Chan, M. C. W.; Hui, Z.; Che, C.-M.; Zhu, N.; Lee, S.-T. *J. Am. Chem. Soc.* **2004**, *126*, 4958.

[35] Lipkowski, J.; Ross, P. N. *Electrocatalysis*, Wiley-VCH, New York, **1998**.

[36] (a) Moiseev, I. I. *Kinet. Katal.* **2001**, *42*, 5. (b) Rozenberg, J. I. Berlin, A. V. *Ross. Khim. Zh.* **2005**, *50*, 4. (c) Karpinski, Z. *Adv. Catal.* **1990**, *37*, 45. (d) Miseev, I. I.; Vargaftik, M. N. *Ross. Khim. Zh.* **2005**, *50*, 72.

[37] Astruc D,; Lu, F, Ruiz, A. J. *Angew. Chem. Int. Ed.* **2005**, *44*, 7852.

[38] Toshima, N. *J. Macromol. Sci. Chem.* **1990**, *A27*, 1225.

[39] Sinfelt, J. H. *Acc. Chem. Res.* **1987**, *20*, 134.

[40] Sinfelt, J. H.; Via, G. H.; Lytle, F. W. *J. Chem. Phys.* **1980**, *72*, 4832.

[41] Sinfelt, J. H.; Via, G. H.; Lytle, F. W. *J. Chem. Phys.* **1982**, *76*, 2779.

[42] (a) Sinfelt, J. H.; Via. G. H.; Lytle, F. W. *J. Chem. Phys.* **1981**, *75*, 5527. (b) Meitzner, G.; Via, G. H.; Lytle, F. W.; Sinfelt, J. H. *J. Chem. Phys.* **1983**, *78*, 882. (c) Meitzner, G.; Via, G. H.; Lytle, F. W.; Sinfelt, J. H. *J. Chem. Phys.* **1983**, *78*, 2533.

[43] Warrier, M.; Lo, M. K. F.; Monbouquette, H.; Garcia-Garibay, M. A. *Photochem. Photoboil. Sci.*

2004, *3*, 859.

[44] Ohmori, T.; Takahashi, H.; Mametsuka, H.; Suzuki, E. *Phys. Chem. Chem. Phys.* **2000**, *2*, 3519.

[45] Kim, J.; Lee, C.; W.; Choi, W. *Environ. Sci. Technol.* **2010**, *44*, 6849.

[46] Abe, R.; Takami, H.; Murakami, N.; Ohtani, B. *J. Am. Chem. Soc.* **2008**, *130*, 7780.

[47] Arai, T.; Horiguchi, M.; Yanagida, M.; Gunji, T.; Sugihara, H.; Sayama, K. *Chem. Commun.* **2008**, 5565.

[48] Grätzel, M. *Nature* **2001**, *414*, 338.

[49] (a) Tian, Y.; Tatsuma, T. *Chem. Commun.* **2004**, 1810. (b) Tian, Y.; Tatsuma, T. *J. Am. Chem. Soc.* **2005**, *127*, 7632.

[50] (a) Kowalska, E.; Abe, R.; Ohtani, B. *Chem. Commun.* **2009**, 241. (b) Rodriguez-Gonzalez, V.; Zanella, R.; del Angel, G.; Gomez, R. *J. Mol. Catal. A* **2008**, *281*, 93.

[51] Silva, C. G.; Juárez, R.; Marino, T.; Molinari, R.; García, H. *J. Am. Chem. Soc.* **2011**, *133*, 595.

Chapter I

Synthesis of benzimidazoles on TiO_2 Loaded with Pt Nanoparticles

1. Introduction

Benzimidazole and its derivatives occupy pivotal positions in the synthesis of natural products and pharmaceutical materials. These compounds have been studied extensively because of their biological activities as bactericides,[1] anticarcinogens,[2] and peptic ulcer agents.[3] There is particular interest in their activity against several viruses such as HIV,[4] herpes (HSV-1),[5] and influenza.[6] Classical method for benzimidazole synthesis is the coupling of o-arylenediamines with carboxylic acids or their derivatives,[7] which requires strong acidic conditions and high temperature (ca. >200 °C). The other method is the oxidation of benzimidazoline intermediates generated from the condensation of *o*-arylenediamines and aldehydes.[8] This method produces benzimidazoles at relatively low temperature (~100 °C), but requires unstable aldehydes as reactants and stoichiometric or excess amounts of strong oxidants such as DDQ. Recent advances in this method allow the use of molecular oxygen as an oxidant,[9] but these processes require homogeneous catalysts such as metal triflates and a free radical. Alternative methods that proceed under mild reaction conditions with stable reactants such as alcohols and carboxylic acids and easy-handling heterogeneous catalysts are therefore necessary for economically and environmentally benign benzimidazole production.

Here we present a new strategy for benzimidazole synthesis without acids and oxidants at room temperature (**Scheme 1-1**). This promotes efficient and selective benzimidazole production with *o*-arylenediamines and alcohols as reactants under photoirradiation (λ >300 nm). The process employs a semiconductor TiO_2 loaded with Pt nanoparticles (Pt/TiO_2) as a heterogeneous catalyst. The catalyst promotes two different transformations in one pot by simultaneous photocatalytic and catalytic actions; one is the conversion of alcohols to aldehydes via a Pt-assisted photocatalytic oxidation on the TiO_2 surface,[10] and the other is the catalytic dehydrogenation of benzimidazoline intermediates, generated from the condensation of *o*-arylenediamines and aldehydes, on the surface of Pt particles. Various catalytic systems enabling one-pot organic transformations have been proposed.[11] There are, however, only two reports of one-pot system that combines photocatalysis and catalysis,[12] where both systems use a set of homogeneous photocatalyst (photoredox catalyst) and catalyst for one-pot transformations.

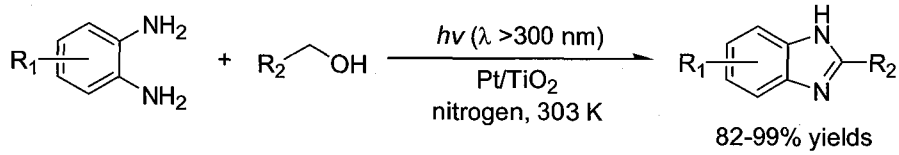

Scheme 1-1. One-pot benzimidazole synthesis with Pt/TiO_2 catalyst under photoirradiation.

2. Experimental

2-1. Materials and procedure

All of the reagents used were supplied from Wako, Tokyo Kasei, and Sigma-Aldrich and used without further purification. Water was purified by the Milli-Q system. JRC-TIO-4 TiO_2 (equivalent to Deggusa P25; particle diameter, 24 nm; BET surface area, 54 $m^2\ g^{-1}$; anatase/rutile = ca. 83/17) were kindly supplied from the Catalyst Society of Japan.

The Pt_x/TiO_2 catalyst [x (wt%) = $Pt/(Pt + TiO_2) \times 100$; x = 0.05, 0.1, 0.2, 0.5, 1.0] were synthesized as hollows: TiO_2 (0.1 g) and H_2PtCl_6 (0.11, 0.21, 0.42, 1.06, and 2.12 mg) were added to a water/MeOH (24/1 v/v) mixture (10 mL) within a Pyrex glass tube (20 cm^3) and purged with nitrogen gas. The tube was photoirradiated with magnetic stirring by a high-pressure Hg lamp (300 W; Eikohsha Co. Ltd.; light intensity at 300–400 nm, 19.1 W m^{-2}) at 303 K for 30 min. The resultant was recovered by filtration, washed thoroughly with water, and dried in vacuo at 353 K for 12 h. The Pt amount on the catalysts was determined by X-ray fluorescence spectrometer.

Photoreaction were carried out as follows; *o*-arylenediamine, alcohol, and catalyst were added to a Pyrex glass tube (20 cm^3). The tube was purged with nitrogen gas and photoirradiated with magnetic stirring by a Xe lamp (2 kW; Ushio Inc.; light intensity, 18.2 W m^{-2} at 300-400 nm) at 303 K. The reactant and product concentrations were determined by GC systems equipped with FID or TCD.

Intermediate **3** (1-(1-ethoxyethyl)-2-methyl-1*H*-benzimidazole) were synthesized as hollows: An EtOH solution containing **1** was photoirradiated in the presence of pure TiO_2 for 12 h at 303 K. The resulting solution was concentrated by evaporation and subjected to flash chromatography using silica gel with ethyl acetate as an eluent. The obtained solution was concentrated by evaporation and dried in vacuo, affording a yellow crystal of **3**. ^1H NMR (400 MHz, $CDCl_3$, TMS): δ (ppm) = 7.69–7.66 (q, 1H), 7.60–7.58 (q, 1H), 7.23–7.17 (m, 2H), 5.67–5.62 (q, 1H), 3.43–3.25 (m, 2H), 2.63 (s, 3H), 1.73–1.72 (d, 3H), 1.17–1.14 (t, 3H). ^{13}C NMR (400 MHz, CDCl3, TMS): δ (ppm) = 150.38, 142.68, 133.29, 122.08, 121.85, 118.94, 111.18, 82.82, 63.82, 21.32, 14.82, 14.74. EI-MS: Calcd for $C_{12}H_{16}N_2O$ 204.3, found m/z 204.2 (M^+).

3. Results and discussion

3-1. Synthesis and characterization of catalysts

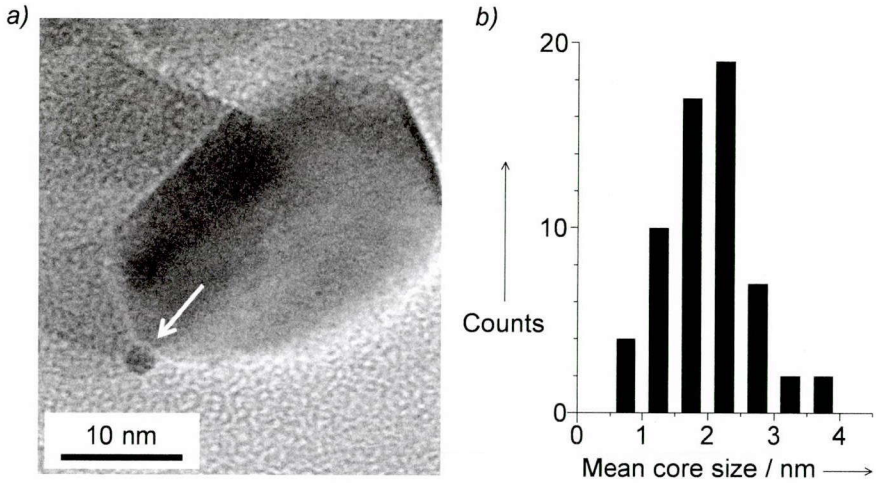

Figure 1-4. a) TEM micrograph and b) size distribution of Pt particles on $Pt_{0.2}/TiO_2$.

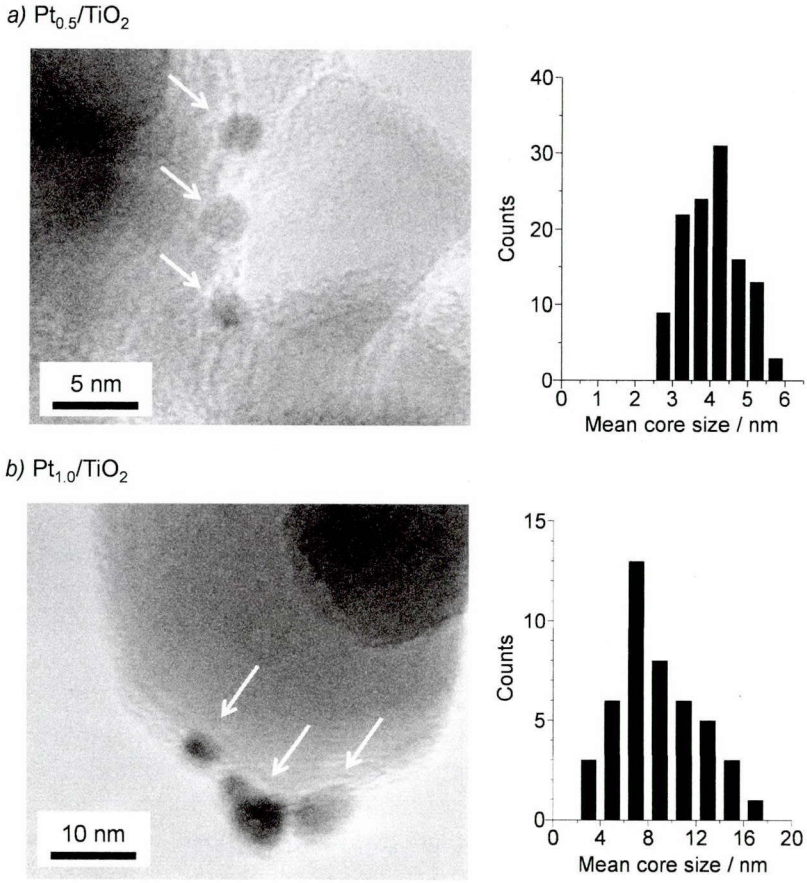

Figure 1-5. TEM micrograph and size distribution of Pt nanoparticles on a) $Pt_{0.5}/TiO_2$ and b) $Pt_{1.0}/TiO_2$ catalysts.

a)

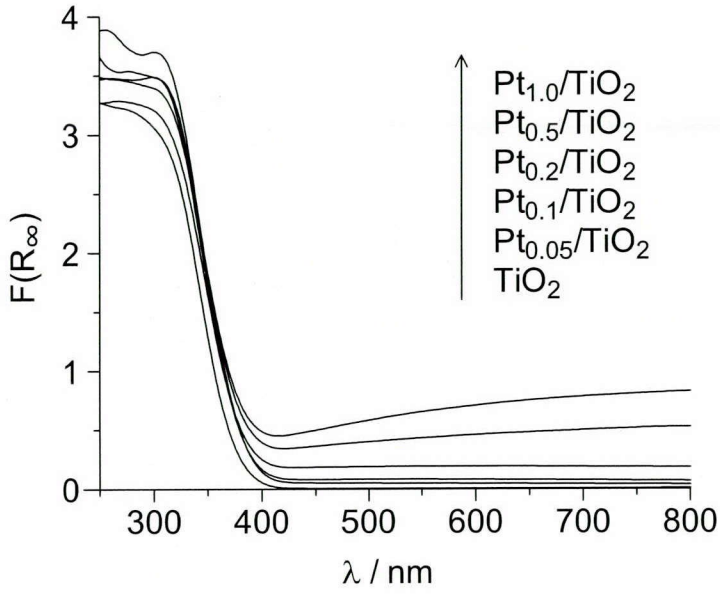

b)

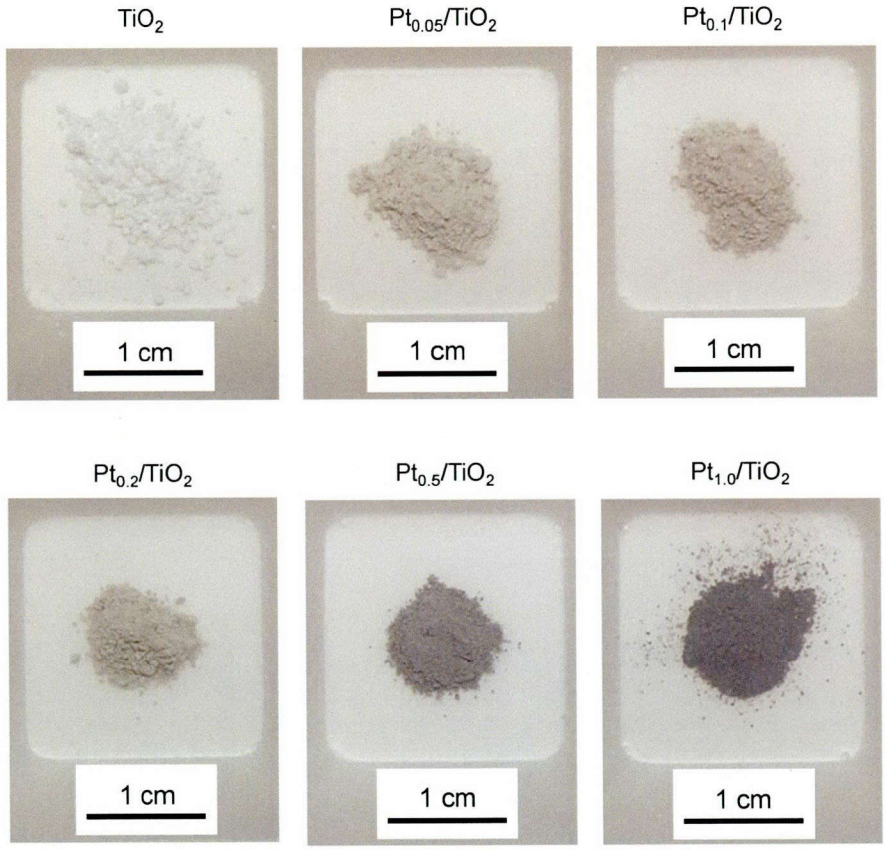

Figure 1-6. a) Diffuse reflectance UV-vis spectra and b) photographs for the respective catalysts.

Pt_x/TiO_2 with different Pt amount [x (wt%) = $Pt/(TiO_2 + Pt) \times 100$; x = 0.05, 0.1, 0.2, 0.5, 1.0] were prepared by a conventional photodeposition method,[13] where photoirradiation of an aqueous solution containing JRC-TIO-4 TiO_2 particles (equivalent to Degussa P25) and H_2PtCl_6 affords gray powders of catalysts. **Figure 1-4** shows the transmission electron microscopy (TEM) image of $Pt_{0.2}/TiO_2$. A spherical Pt particle is observed with an average diameter 2.0 nm. The Pt particle size increases with an increase in the Pt amount on TiO_2, where x = 0.5 and 1.0 catalysts contain 4.0 nm and 9.3 nm particles, respectively (**Figure 1-5**). In addition, the catalysts with larger Pt amount show increased absorbance at λ >300 nm due to light scattering by the Pt particles[14] (**Figure 1-6**), although the band gap energies of the catalysts are similar (3.2–3.3 eV).

3-2. Photocatalytic activity of Pt/TiO_2 catalyst.

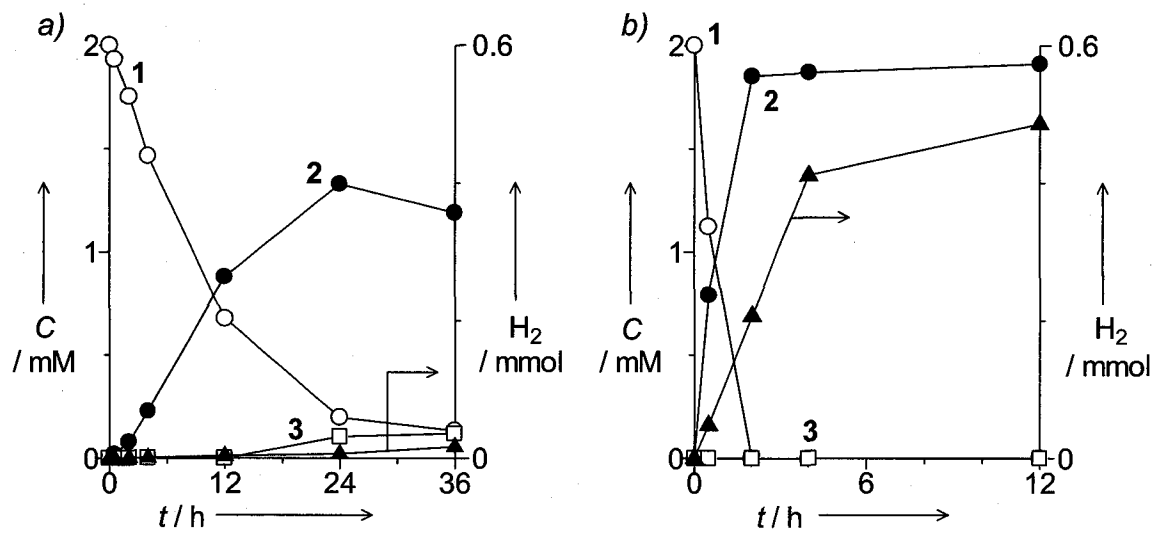

Figure 1-7. Time-dependent change in the concentrations of substrate and products during photoirradiation of **1** in EtOH with a) TiO_2 and b) $Pt_{0.2}/TiO_2$ catalysts. Reaction conditions: catalyst (10 mg), **1** (20 μmol), EtOH (10 mL), nitrogen (1 atm), λ >300 nm, 303 K, where 10 mg $Pt_{0.2}/TiO_2$ contains 0.10 μmol Pt.

The efficacy of Pt/TiO_2 catalyst on benzimidazole production is evident from the reaction of *o*-phenylenediamine (**1**) with EtOH. **Figure 1-7** shows the time-dependent change in the concentrations of **1** and the product, 2-methylbenzimidazole (**2**), during photoirradiation (λ >300 nm) of an EtOH solution containing **1** under nitrogen atmosphere. With pure TiO_2 (**Figure 1-7a**), 24 h photoirradiation is required to achieve >90% conversion of **1**, where the **2** yield is only ca. 60%. The major byproduct is

determined by ^{1}H, ^{13}C NMR and EI-MS analysis to be 1-(1-ethoxyethyl)-2-methyl-1H-benzimidazole (**3**) (**Figures 1-1–3**), where the **3** yield after 36 h irradiation is 5.2%. In contrast, as shown in **Figure 1-7b**, $Pt_{0.2}/TiO_2$ promotes rapid and selective production of **2**; only 2 h irradiation achieves >99% **1** conversion and produces **2** with >93% yield. This indicates that the present process with Pt/TiO_2 indeed promotes rapid and selective benzimidazole production.

3-3. Reaction mechanism

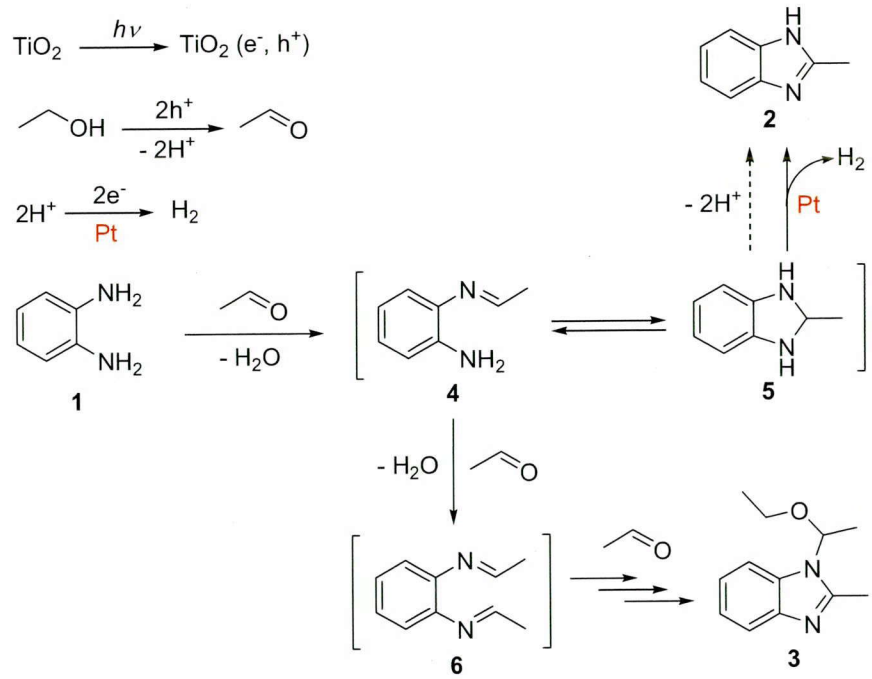

Scheme 1-2. Proposed mechanism for one-pot benzimidazole production promoted by Pt/TiO_2 catalyst under photoirradiation.

The rapid and selective **2** formation is achieved by simultaneous photocatalytic and catalytic reactions on Pt/TiO_2, as depicted in **Scheme 1-2**. The reaction is initiated by photoexcitation of TiO_2 particles. The excited TiO_2 produces electron (e^-) and positive hole (h^+) pairs. The h^+ oxidizes EtOH to acetaldehyde on the TiO_2 surface.[15] Spontaneous condensation of the formed aldehyde and **1** produces a monoimine intermediate (**4**).[16] The rapid consumption of **1** during the reaction with Pt/TiO_2 (**Figure 1-7b**) is because the Pt particles efficiently trap e^- on the excited TiO_2 and enhance the charge separation between e^- and h^+.[17] This accelerates the alcohol oxidation (production of large amount of aldehyde) and thus allows rapid condensation of **1** and the aldehyde. As shown in **Figure 1-7**, the amount of H_2 produced during 12 h irradiation with Pt/TiO_2 is 486 μmol, whereas pure TiO_2 produces only 3 μmol H_2.

This indicates that the e^- formed on TiO_2 is indeed trapped by the Pt particles and consumed efficiently by the reduction of H^+ formed during alcohol oxidation.[15] These suggest that the enhanced photocatalytic transformation of alcohol to aldehyde on Pt/TiO_2 allows efficient production of the intermediate **4**.

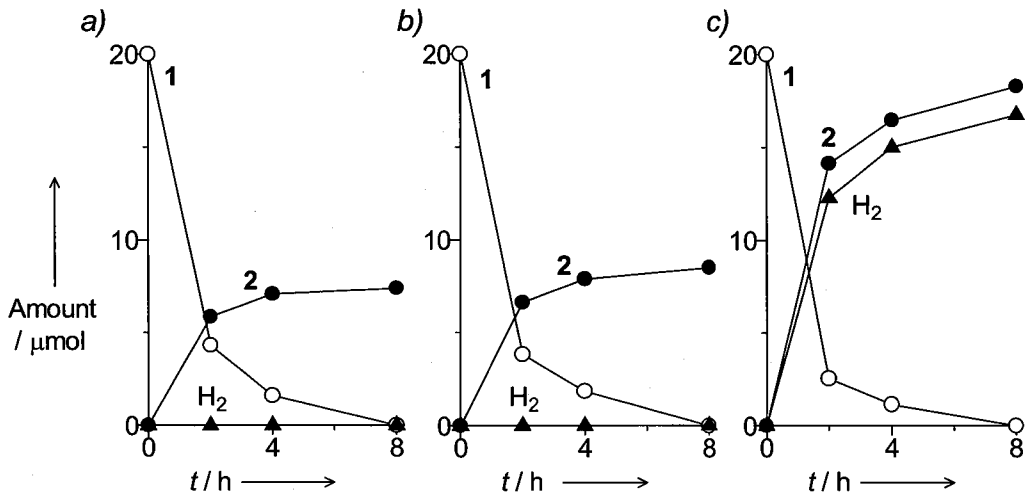

Figure 1-8. Time-dependent change in the amount of **1**, **2**, and H_2 during the reaction of **1** with 1 equiv of acetaldehyde in the dark condition, a) without catalyst, b) with TiO_2, and c) with $Pt_{0.2}/TiO_2$. Reaction conditions: catalyst (10 mg), **1** (20 μmol), acetaldehyde (20 μmol), EtOH (10 mL), nitrogen (1 atm), 303 K, where 10 mg $Pt_{0.2}/TiO_2$ contains 0.10 μmol Pt.

The product **2** is formed by cyclization of **4** followed by autooxidation of a benzimidazoline intermediate (**5**) with a release of H^+,[18] where **4** and **5** are in equilibrium.[19] The **4** reacts easily with the other aldehyde and produces a diimine intermediate (**6**), leading to a byproduct (**3**) formation.[20] Therefore, in the classical method with *o*-arylenediamines and aldehydes,[8,9] oxidants that promote rapid transformation of **5** to **2** are necessary for selective formation of **2** while suppressing byproduct formation. In the present process with Pt/TiO_2, Pt particles promote rapid and selective transformation of **5** to **2** via a catalytic dehydrogenation (**Scheme 1-2**). This is confirmed by the reaction of **1** with equimolar acetaldehyde in the dark condition. **Figure 1-8** shows the time-dependent change in the amounts of **1** and the products at 303 K. The rate of decrease of **1** with Pt/TiO_2 (**Figure 1-8c**) is similar to that obtained without catalyst and with pure TiO_2 (**Figure 1-8a** and **b**), indicating that the rate of condensation of **1** and aldehyde is similar. The **2** yields obtained without catalyst and with TiO_2 are low (<40%), but Pt/TiO_2 produces **2** quantitatively, indicating that Pt particles successfully promote transformation of **5** to **2**. In this case, H_2 gas with an equivalent quantity of **2** was produced, whereas

other systems do not produce H_2. This suggests that the Pt particles indeed catalyze dehydrogenation of **5**. The rapid transformation of **5** to **2** in the Pt/TiO_2 system, therefore, leads to a shift of the equilibrium between **4** and **5** to the **5** formation (**Scheme 1-2**). This thus allows selective **2** formation while suppressing byproduct formation. The high dehydrogenation activity of Pt particles at room temperature is probably due to the strong affinity of the amine nitrogens of **5** to the Pt surface, as observed for ethylenediamine dehydrogenation on the Pt surface.[21]

3-4. Effect of Pt amount and size on the catalytic activity

The amount and size of Pt particles are important factors for rapid and selective benzimidazole production. **Figure 1-9** shows the conversion of **1** and the selectivity of **2** during 4 h photoirradiation of an EtOH solution containing **1** with respective catalysts. Conversion of **1** increases with an increase in the Pt amount on TiO_2 because larger amount of Pt allows efficient charge separation on the photoexcited TiO_2. The highest conversion is obtained with $Pt_{0.2}/TiO_2$, and the catalysts with larger Pt amount show lower conversion. This is because excess amount of Pt suppresses the incident light absorption by TiO_2.[22]

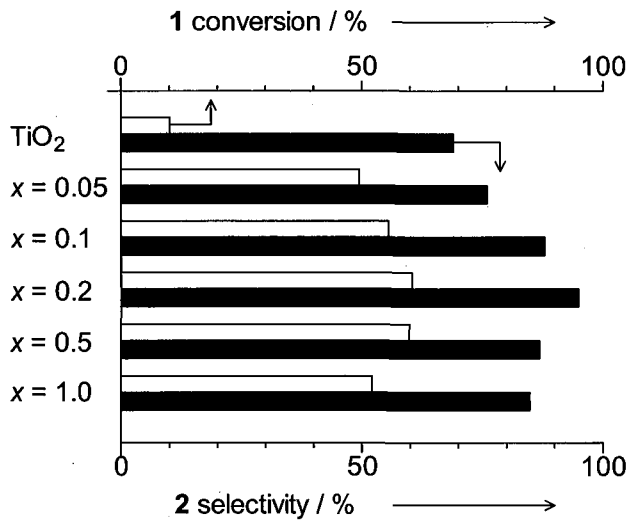

Figure 1-9. Conversion of **1** and selectivity of **2** obtained by photoirradiation of an EtOH solution containing **1** with TiO_2 and Pt_x/TiO_2 catalysts for 4 h. Reaction conditions: EtOH (10 mL), **1** (0.1 mmol), catalyst (10 mg), nitrogen (1 atm), λ >300 nm, 303 K.

The **2** selectivity is also affected by the Pt amount. As shown in **Figure 1-9**, the selectivity increases with an increase in the Pt amount, but the catalysts with >0.2 wt% Pt show lower selectivity. This is because larger size Pt particles have lower dehydrogenation activity. As reported,[23] dehydrogenation

activity of Pt particles increases with a decrease in their size; in particular, <4 nm particles show very high activity. The size of Pt particles on $Pt_{0.2}/TiO_2$ is 2.0 nm, whereas that on $x = 0.5$ and 1.0 catalysts are 4.0 and 9.3 nm, respectively. As shown in **Table 1-1**, the reaction of **1** and equimolar acetaldehyde in the dark with $Pt_{0.2}/TiO_2$ (4 h, 303 K) produces **2** with 91% yield, along with 82% H_2 formation. In contrast, $x = 0.5$ and 1.0 catalysts show lower yields of **2** (<80%) and H_2 (<48%). This indicates that smaller Pt particles with a <4 nm diameter indeed have higher dehydrogenation activity and are responsible for efficient benzimidazole formation. TEM analysis of $Pt_{0.2}/TiO_2$ recovered after 12 h photoreaction for **2** synthesis (**Figure 1-7b**) reveals that the Pt particle size scarcely changes during the reaction (**Figure 1-10**). In addition, the catalyst is reusable at least three times without loss of activity (**Table 1-2**).

Table 1-1. Conversion and product yields obtained by the reaction of **1** with acetaldehyde in the presence of various catalysts in the dark condition.[a]

Entry	Catalyst	Pt particle size / nm	Conversion / %	Yield / %	
			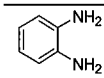 **1**	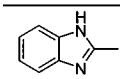 **2**	H_2
1	TiO_2		96	69	–[b]
2	$Pt_{0.05}/TiO_2$		>99	86	59
3[c]	$Pt_{0.05}/TiO_2$		>99	89	81
4	$Pt_{0.1}/TiO_2$		98	91	65
5[d]	$Pt_{0.1}/TiO_2$		>99	92	84
6	$Pt_{0.2}/TiO_2$	2.0[e]	>99	91	82
7	$Pt_{0.5}/TiO_2$	4.0[e]	>99	80	48
8	$Pt_{1.0}/TiO_2$	9.3[e]	97	79	40
9	TiO_2 + Pt black	3400[f]	93	77	39

[a] Reaction condition: Catalyst (10 mg), **1** (0.1 mmol), acetaldehyde (0.1 mmol), EtOH (10 mL), nitrogen (1 atm), reaction time (4 h), 303 K. [b] The amount of H_2 formed is less than detection limit (<0.12 μmol). [c] catalyst (40 mg). [d] catalyst (20 mg). [e] determined by TEM analysis. [f] determined by dynamic light scattering measurement.

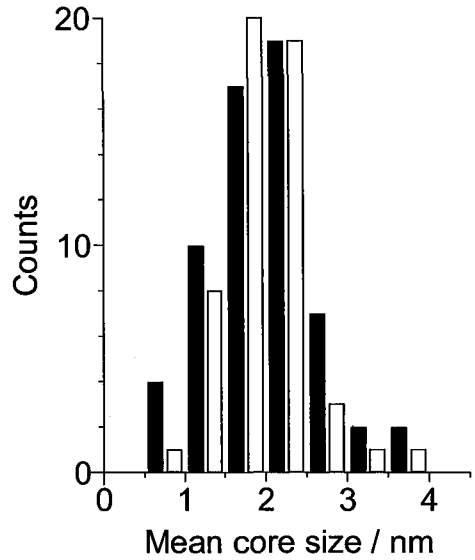

Figure 1-10. Size distribution of Pt nanoparticles on (black bar) fresh $Pt_{0.2}/TiO_2$ and (white bar) $Pt_{0.2}/TiO_2$ recovered after 12 h photoreaction with **1** (**Figure 2b**).

Table 1-2. Reuse of $Pt_{0.2}/TiO_2$ catalyst for **2** synthesis.[a]

Entry	Catalyst	Conversion / %	Yield / %
		1	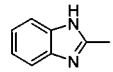 **2**
1	Fresh	>99	95
2	1st reuse	>99	95
3	2nd reuse	>99	95
4	3rd reuse	>99	94

[a] Reaction conditions: catalyst (10 mg), **1** (20 μmol), EtOH (10 mL), nitrogen (1 atm), λ >300 nm, 303 K, photoirradiation time (12 h).

3.5. Synthesis of various benzimidazole

The present process is tolerant for synthesis of various kinds of benzimidazoles. As shown in **Table 1-3**, photoirradiation of alcohol solutions containing various *o*-arylenediamines with $Pt_{0.2}/TiO_2$ successfully produces the corresponding benzimidazoles. In that, 2-alkyl- and 2-aryl-substituted benzimidazoles are produced with very high yields. In addition, 5- and/or 6-substituted derivatives are also produced successfully.

Table 1-3. Synthesis of benzimidazoles from *o*-arylenediamines and alcohols.[a]

Entry	Diamines	Amount / μmol	Alcohol	*t* / h	Catalyst	Diamine conv. / %	Product	GC yield / %
1		20		4	TiO_2	27		11
2		20		4	$Pt_{0.2}/TiO_2$	>99		93
3		20		4	TiO_2	56		34
4		20		4	$Pt_{0.2}/TiO_2$	>99		>99
5		20		4	TiO_2	54		37
6		20		4	$Pt_{0.2}/TiO_2$	>99		>99
7		20		4	TiO_2	62		43
8		20		4	$Pt_{0.2}/TiO_2$	>99		95
9[b]		10		24	TiO_2	93		1.8
10[b]		10		24	$Pt_{0.2}/TiO_2$	>99		89
11[c]		10		12	TiO_2	>99		57
12[c]		10		12	$Pt_{0.2}/TiO_2$	>99		82
13		20		4	TiO_2	43		23
14		20		4	$Pt_{0.2}/TiO_2$	>99		94
15		20		4	TiO_2	63		11
16		20		4	$Pt_{0.2}/TiO_2$	>99		>99
17		20		4	TiO_2	64		20
18		20		4	$Pt_{0.2}/TiO_2$	>99		83

[a] Reaction conditions: catalyst (10 mg), alcohol (10 mL), nitrogen (1 atm), λ >300 nm. [b] catalyst (80 mg), alcohol (5 mL). [c] catalyst (5 mg), alcohol (750 μmol), MeCN (5 mL).

4. Conclusion

In conclusion, we found that the Pt/TiO_2 system enables efficient benzimidazole production under photoirradiation. This is promoted by one-pot multiple catalytic transformations on Pt/TiO_2, which involve Pt-assisted photocatalytic oxidation on TiO_2 and catalytic dehydrogenation on the surface of Pt particles. The process has significant advantages as compared to the other methods:[24] (i) cheap and stable reactant (alcohol); (ii) no requirement of acids and oxidants; (iii) no harmful byproduct formation (only water and H_2 form during reaction); (iv) mild reaction condition (room temperature). The process therefore has a potential to enable green benzimidazole synthesis. Recently, organic transformation with semiconductor photocatalysts has attracted much attention,[25] but successful examples are still scarce. The basic idea presented here based on the combination of photocatalytic and catalytic reactions may help open a new strategy towards the development of photocatalysis-based organic synthesis.

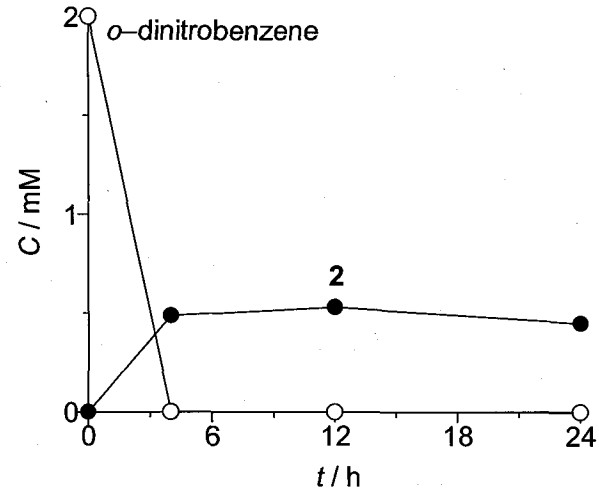

Figure 1-11. Time-dependent change in the concentrations of *o*-dinitrobenzene and the product **2** during photoirradiation of an EtOH solution containing *o*-dinitrobenzene. Reaction conditions: Degussa P25 TiO_2 (10 mg), *o*-dinitrobenzene (20 μmol), EtOH (10 mL), nitrogen (1 atm), λ >300 nm (Xe lamp; 2 kW; Ushio Inc.; light intensity, 18.2 W m^{-2} at 300–400 nm), 303 K.

5. References

[1] Charifson, P. S.; Grillot, A.-L.; Grossman, T. H.; Parsons, J. D.; Badia, M.; Bellon, S.; Deininger, D. D.; Drumm, J. E.; Gross, C. H.; LeTiran, A.; Liao, Y.; Mani, N.; Nicolau, D. P.; Perola, E.; Ronkin, S.; Shannon, D.; Swenson, L. L.; Tang, Q.; Tessier, P. R.; Tain, S.-K.; Trudeau, M.; Wang, T.; Wei, Y.; Zhang, H.; Stamos, D. *J. Med. Chem.* **2008**, *51*, 5243.

[2] White, A. W.; Almassy, R.; Calvert, A. H.; Curtin, N. J.; Griffin, R. J.; Hostomsky, Z.; Maegley, K.; Newell, D. R.; Srinivasan, S.; Golding, B. T. *J. Med. Chem.* **2000**, *43*, 4084.

[3] Sewing, K.-Fr. *Trends Pharmacol. Sci.* **1984**, *5*, 262.

[4] Morningstar, M. L.; Roth, T.; Farnsworth, D. W.; Smith, M. K.; Watson, K.; Buckheit, Jr., R. W.; Das, K.; Zhang, W.; Arnold, E.; Julias, J. G.; Hughes, S. H.; Michejda, C. J. *J. Med. Chem.* **2007**, *50*, 4003.

[5] Zhu, Z.; Lippa, B.; Drach, J. C.; Townsend, L. B. *J. Med. Chem.* **2000**, *43*, 2430.

[6] Tamm, I. *Science* **1954**, *120*, 847.

[7] (a) Wright, J. B. *Chem. Rev.* **1951**, *48*, 397. (b) Preston, P. N. *Chem. Rev.* **1974**, *74*, 279. (c) Preston, P. N. *in Chemistry of Heterocyclic Compounds, vol. 40, Benzimidazoles and Congeneric Tricyclic Compounds* (Eds: Weissberger, A.; Taylor, E. C.), Wiley, New York, **1981**, part 1, p. 6–60.

[8] (a) Lee, K. J.; Janda, K. D.; *Can. J. Chem.* **2001**, *79*, 1556. (b) Beaulieu, P. L.; Haché, B.; Von Moos, E.; *Synthesis* **2003**, 1683. (c) Bahrami, K.; Khodaei, M. M.; Kavianinia, I. *Synthesis* **2007**, 547.

[9] (a) Chen, Y.-X.; Qian, L.-F.; Zhang, W.; Han, B. *Angew. Chem. Int. Ed.* **2008**, *47*, 9330. (b) Trivedi,

R.; De, S. K.; Gibbs, R. A.; *J. Mol. Catal. A* **2006**, *245*, 8. (c) Curini, M.; Epifano, F.; Montanari, F.; Rosati, O.; Taccone, S. *Synlett* **2004**, 1832.

[10] Ohtani, B.; Kakimoto, M.; Nishimoto, S.; Kagiya, T.; *J. Photochem. Photobiol. A* **1993**, *70*, 265.

[11] (a) Lee, J. M.; Na, Y.; Han, H.; Chang, S. *Chem. Soc. Rev.* **2004**, *33*, 302. (b) Kolb, H. C.; VanNieuwenhze, M. S.; Sharpless, K. B.; *Chem. Rev.* **1994**, *94*, 2483.

[12] (a) Nicewicz, D. A.; MacMillan, D. W. C. *Science* **2008**, *322*, 77. (b) Nagib, D. A.; Scott, M. E.; MacMillan, D. W. C.; *J. Am. Chem. Soc.* **2009**, *131*, 10875.

[13] Lee, J.; Choi, W. *Environ. Sci. Technol.* **2004**, *38*, 4026.

[14] Kowalska, E.; Remita, H.; Colbeau-Justin, C.; Hupka, J.; Belloni, J. *J. Phys. Chem. C* **2008**, *112*, 1124.

[15] (a) Yang, Y. Z.; Chang, C.-H.; Idriss, H. *Appl. Catal. B* **2006**, *67*, 217. (b) Nishimoto, S.-I.; Ohtani, B.; Kagiya, T. *J. Chem. Soc. Faraday Trans. 1* **1985**, *81*, 2467.

[16] Sharghi, H.; Beyzavi, M. H.; Doroodmand, M. M. *Eur. J. Org. Chem.* **2008**, 4126.

[17] Ohtani, B.; Iwai, K.; Nishimoto, S.; Sato, S. *J. Phys. Chem. B* **1997**, *101*, 3349.

[18] Chikashita, H.; Nishida, S.; Miyazaki, M.; Morita, Y.; Itoh, K. *Bull. Chem. Soc. Jpn.* **1987**, *60*, 737.

[19] Speier, G.; Párkányi, L. *J. Org. Chem.* **1986**, *51*, 218.

[20] Yang, D.; Fokas, D.; Li, J.; Yu, L.; Baldino, C. M. *Synthesis* **2005**, 47.

[21] Kang, D. H.; Trenary, M. *Surf. Sci.* **2000**, *470*, L13.

[22] Zhao, Z.-G.; Miyauchi, M. *Angew. Chem. Int. Ed.* **2008**, *47*, 7051.

[23] (a) Aramendía, M. A.; Benítez, J. A.; Boráu, V.; Jiménez, C.; Marinas, J. M.; Moreno, A. *React. Kinet. Catal. Lett.* **1997**, *62*, 23. (b) Rioux, R. M.; Hsu, B. B.; Grass, M. E.; Song, H.; Somorjai, G. A. *Catal. Lett.* **2008**, *126*, 10.

[24] There is one report of photocatalytic benzimidazole production process, consisting of photoirradiation of an alcohol solution containing *o*-dinitrobenzenes with pure Degussa P25 TiO_2: Wang, H.; Partch, R. E.; Li, Y. *J. Org. Chem.* **1997**, *62*, 5222. However, the benzimidazole selectivity is only ca. 25% (**Figure 1-11**).

[25] (a) Maldotti, A.; Molinari, A.; Amadelli, R. *Chem. Rev.* **2002**, *102*, 3811. (b) Palmisano, G.; Augugliaro, V.; Pagliaro, M.; Palmisano, L. *Chem. Commun.* **2007**, 3425. (c) Shiraishi, Y.; Hirai, T. *J. Photochem. Photobiol. C* **2008**, *9*, 157. (d) Yurdakal, S.; Palmisano, G.; Loddo, V.; Augugliaro, V.; Palmisano, L. *J. Am. Chem. Soc.* **2008**, *130*, 1568.

Chapter II

Hydrodenitrogenation of Aromatic Cyanides on TiO_2 Loaded with Pd Nanoparticles

1. Introduction

Aromatic cyanides are one of the most important chemicals used as solvents, extractants, and intermediates for the synthesis of pharmaceuticals, plastics, rubbers, herbicides, and pesticides.[1] These compounds are therefore often contained in industrial effluents. Since they are highly toxic to living organisms,[2] their decomposition and detoxification are very important tasks. Bioremediation processes have been studied for the treatment of aromatic cyanides.[3] These processes decompose the compounds into harmless ones such as CO_2 and H_2O; however, they require restricted operation conditions in pH and temperature. Photocatalytic decomposition of aromatic cyanides has also been studied with titanium dioxide (TiO_2).[4] Photoirradiation of TiO_2 in water under O_2 produces active oxygen species such as hydroxyl radical (OH•) or superoxide anion ($O_2•^-$), and decomposes aromatic cyanides into CO_2, NO_3^-, and H_2O.[5] These oxidative processes, however, completely decompose the aromatic nuclei of the compounds. Selective decomposition of the –CN moiety and the reuse of resulting aromatic nuclei for upstream processes are desirable for development of green and sustainable processes.

Supported Pd nanoparticles are often employed for catalytic hydrogenation of various compounds such as olefins[6–9] and nitro compounds,[10–12] with molecular hydrogen (H_2) as a hydrogen source. Hydrogenation of aromatic cyanides on Pd catalysts has also been studied at elevated temperatures.[13] These compounds are successfully converted to toluene derivatives and NH_3 via hydrogenation and subsequent cleavage of C–N moiety. This hydrodenitrogenation is promoted by the reaction of aromatic cyanides with activated hydrogen species (H–Pd), formed via a dissociative adsorption of H_2 on the surface of Pd particles. The reaction proceeds selectively without decomposition of aromatic nuclei and enables the reuse of products for upstream processes.

Photoexcitation of semiconductor materials loaded with noble metal particles creates a positive hole (h^+) and conduction band electrons (e^-), and allows subsequent e^- transfer to the metal particles.[14] Photoexcitation of semiconductor loaded with Pd particles, when performed in protic solvents such as alcohols, produces aldehyde via oxidation of alcohol by h^+ and H–Pd species via reduction of protons (H^+) by e^- on the Pd particles.[15] This photocatalytic reaction, if performed out with aromatic cyanides, may successfully promote hydrodenitrogenation by the photoformed H–Pd species at room temperature.

In the present work, TiO_2 loaded with Pd particles (Pd/TiO_2) was used for photocatalytic reaction of

aromatic cyanide with ethanol under UV irradiation (λ >300 nm). This catalytic system successfully promotes hydrodenitrogenation of aromatic cyanides and produces toluene derivatives with high selectivity at room temperature. The denitrogenation mechanism was clarified, and the effect of Pd amount on the catalytic activity was studied.

2. Experimental

2-1. Materials

All of the reagents used were purchased from Wako, Tokyo Kasei, and Sigma-Aldrich, and used without further purification. Water was purified by the Milli Q system. JRC-TIO-4 TiO_2 (equivalent to Deggusa P25; particle diameter, 24 nm; BET surface area, 54 m^2 g^{-1}; anatase/rutile = ca. 83/17) were kindly supplied from the Catalyst Society of Japan.

The Pd_x/TiO_2 catalysts [x (wt%) = Pd/(Pd + TiO_2) × 100; x = 0.5, 1, 2, 4] were prepared according to literature procedure,[16] as follows: TiO_2 (1.0 g) and $Pd(NO_3)_2$ (10.9, 21.9, 44.2, or 90.2 mg) were added to water (40 mL) and solvent were evaporated with vigorous stirring at 353 K for 12 h. The obtained powders were calcined at 673 K under air flow (0.5 L min^{-1}) and then reduced at 673 K under H_2 flow (0.2 L min^{-1}). The heating rate and holding time at 673 K for these treatments were 2 K min^{-1} and 2 h, respectively. Ag_2/TiO_2 and Pt_2/TiO_2 were prepared in a similar manner to those for Pd_x/TiO_2, using $AgNO_3$ (16 mg) or H_2PtCl_6•$6H_2O$ (54 mg) as precursors.

Au_2/TiO_2 was prepared by a deposition-precipitation method, as follows:[17] $HAuCl_4$•$4H_2O$ (45.8 mg) was added to water (50 mL). The pH of the solution was adjusted to 7 by an addition of 1 M NaOH. TiO_2 (1.0 g) was added to the solution and stirred vigorously at 353 K for 3 h. The particles were recovered by centrifugation and washed with water. They were calcined at 673 K under air flow (0.5 L min^{-1}).

2-2. Photoreaction procedure

Each of the respective catalysts (10 mg) was added to ethanol (5 mL) containing aromatic cyanides within a Pyrex glass tube (20 cm^3; φ16.5 mm). The tube was sealed using a rubber septum cap and purged with argon gas. Each tube was photoirradiated with magnetic stirring by a Xe lamp (2 kW; Ushio Inc.). The temperature of solution during photoirradiation was 298 K, and the light intensity was 18.2 W m^{-2} (at 300–400 nm; through a water filter). After photoirradiation, the gas phase product was analyzed by GC-TCD (Shimadzu; GC-8A). The resulting solution was recovered by centrifugation and analyzed by GC-FID (Shimadzu; GC-2010), where the products were identified by GC-MS (EI) (Shimadzu; 40

GCMS-QP5050A).

2-3. Analysis

Total amounts of metals on the catalysts were determined by an inductively-coupled argon plasma atomic emission spectrometer (ICAP-AES; SII Nanotechnology, SPS 7800), after dissolution of catalysts in an aqua regia.[16] Diffuse reflectance UV-vis spectra were measured on an UV-vis spectrophotometer (Jasco Corp.; V-550 with Integrated Sphere Apparatus ISV-469) using $BaSO_4$ as a reference. Transmission electron microscopy (TEM) observations were carried out using an FEI Tecnai G2 20ST analytical electron microscope operated at 200 kV.

3. Results and discussion

3-1. Synthesis and characterization of catalysts

The Pd_x/TiO_2 catalysts with different Pd loadings [x (wt%) = Pd/(Pd + TiO_2) × 100; x = 0.5, 1, 2, 4] were prepared by impregnation of $Pd(NO_3)_2$ onto TiO_2 followed by reduction with H_2. **Figure 2-1** shows the typical TEM images of respective Pd_x/TiO_2 catalysts. All catalysts contain spherical Pd particles. The size of Pd particles increases with the Pd loadings: the average diameters for x = 0.5, 1, 2, and 4 catalysts were 2.6, 4.1, 5.0, and 6.5 nm, respectively. As shown in **Figure 2-2**, the high-resolution TEM images of catalysts revealed that Pd particles can be indexed as *fcc* structures, as same as bulk metallic Pd (JCPDS 46-1043). **Figure 2-3** shows the diffuse reflectance UV-vis spectra of catalysts. The higher Pd loading catalysts exhibit increased absorbance at λ >300 nm, due to the light scattering by the Pd particles.[15] As shown in inset, TiO_2 loaded with 2 wt% Pt (Pt_2/TiO_2) exhibits spectra similar to that of Pd_x/TiO_2,[18] and TiO_2 loaded with 2 wt% Au (Au_2/TiO_2) and Ag (Ag_2/TiO_2) exhibit distinctive absorption bands at 400-500 nm assigned to localized surface plasmon resonance.[17,19]

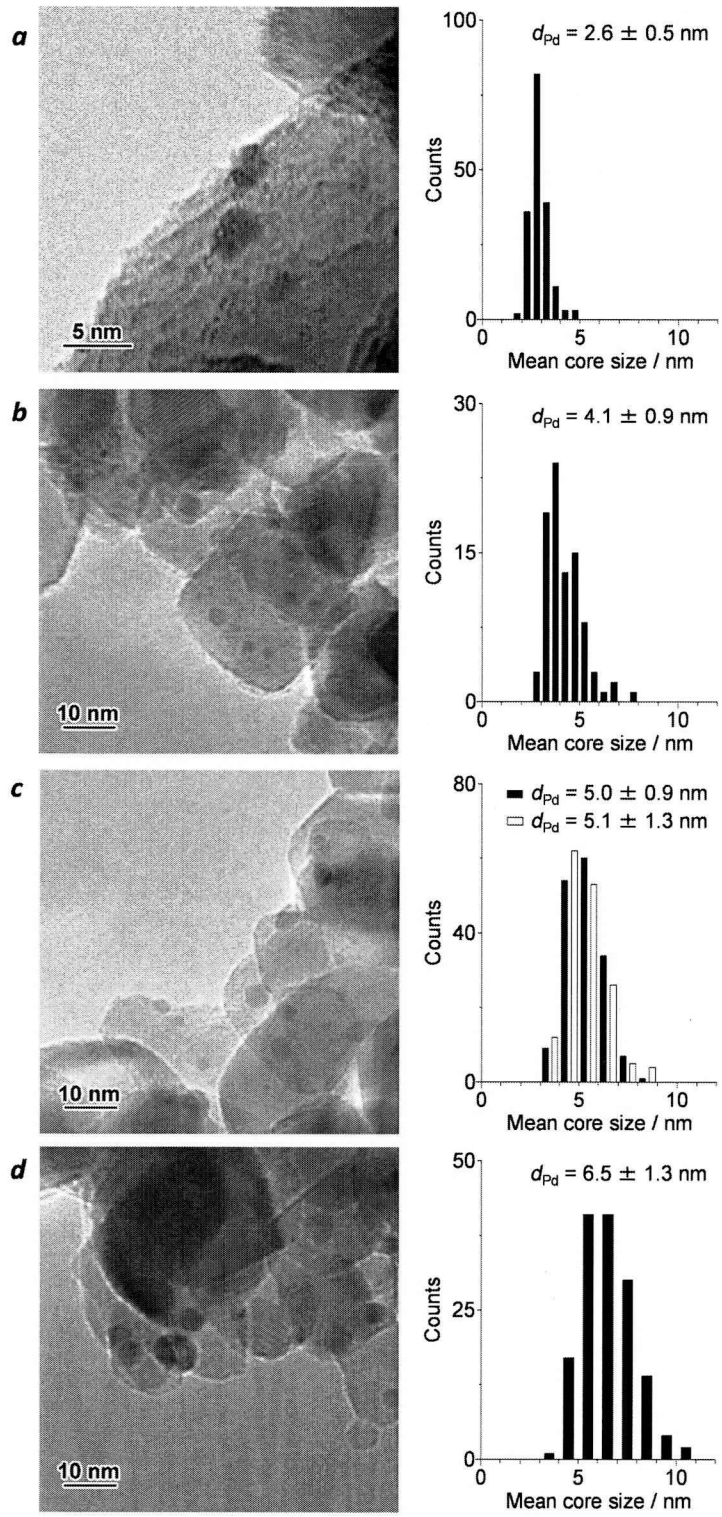

Figure 2-1. TEM images and size distribution of Pd particles for (a) $Pd_{0.5}/TiO_2$, (b) Pd_1/TiO_2, (c) Pd_2/TiO_2, and (d) Pd_4/TiO_2 catalysts. The black bars show the data for fresh catalysts, and the white bars show the data for catalysts recovered after the 3rd reuse for reactions (Table 2, run 4).

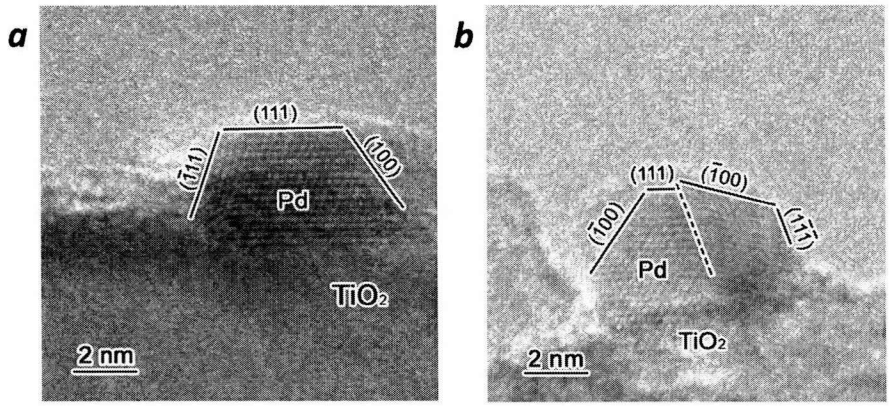

Figure 2-2. High-resolution TEM images of Pd_2/TiO_2 catalyst. (a) The incident beam direction is [0, –1, 1]. (b) This particle is twinned particle. The incident beam directions are [0, –1, 1] and [0, 1, –1].

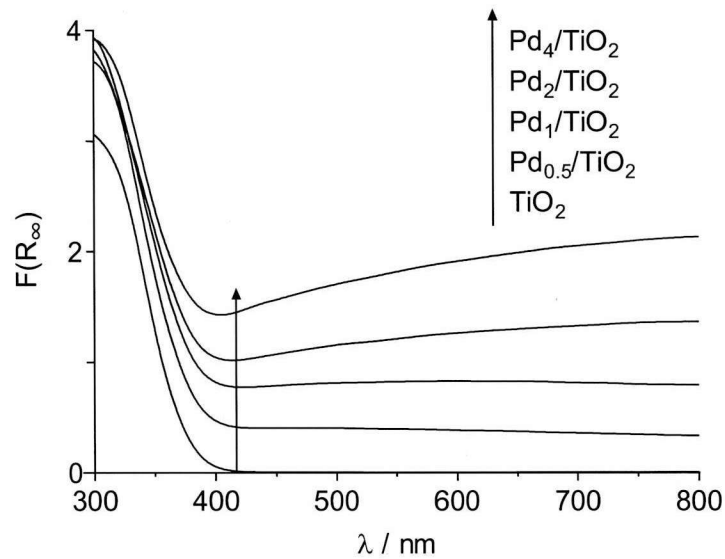

Figure 2-3. Diffuse-reflectance UV-vis spectra of Pd_x/TiO_2, Pt_2/TiO_2, Au_2/TiO_2, and Ag_2/TiO_2 catalysts.

Catalytic activity of Pd/TiO_2 for hydrodenitrogenation was studied with benzonitrile (**1**) as a model compound.[13] **Table 2-1** (runs 1–3) summarizes the results for hydrodenitrogenation of benzonitrile with H_2 (1 atm) as a hydrogen source in the dark. Benzonitrile (2 mM) and Pd_2/TiO_2 (10 mg) were added to an *n*-hexane solution (5 mL) containing 5% ethanol, and the solution was stirred under H_2 (1 atm) for 6 h at different temperature. As shown in run 1, the benzonitrile conversion at 298 K is 84% but the yield of toluene (**2**) is only 15 %, where large amounts of benzylamine (**3**, 30%) and *N*-ethylbenzylamine (**4**, 38%) remain. This suggests that the C–N cleavage is difficult to achieve at this temperature. As shown in runs 2 and 3, the rise in temperature increases the toluene yields, and the reaction at 333 K facilitates almost quantitative conversion to toluene (run 3). Photocatalytic reaction of benzonitrile with alcohol as a hydrogen donor was carried out. The reaction was performed by photoirradiation (λ >300 nm) of the

solution under argon (1 atm) for 6 h. As shown in run 4, the reaction facilitates complete conversion of benzonitrile to toluene at 298 K. This suggests that photocatalytic reaction with alcohol as a hydrogen source successfully promotes hydrodenitrogenation even at room temperature.

Table 2-1. Hydrodenitrogenation of benzonitrile with Pd_2/TiO_2 catalyst.

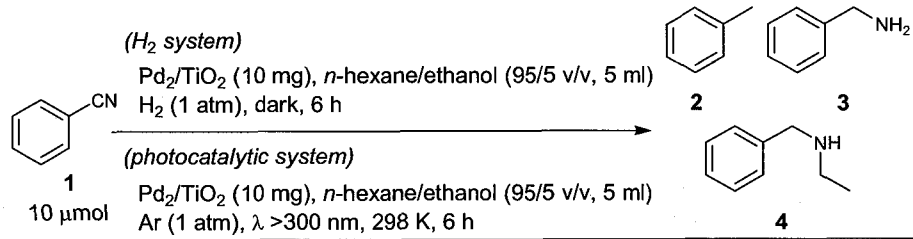

Run	System	Temperature / K	Conversion of **1** / %	Yield / %		
				2	**3**	**4**
1[a]	H_2	298	84	15	30	38
2	H_2	313	98	61	14	23
3	H_2	333	>99	99	0	0
4[b]	Photo	298	99	99	0	0

[a] Dibenzylamine (1%) was also detected as a product. This is produced by nucleophilic attack of a lone pair of nitrogen atom of benzylamine to an electrophilic carbon of semi-hydrogenated intermediate (ref 13). After photoreaction, acetaldehyde (197 μmol) and trace amount of *N,N*-diethylbenzylamine (**5**) were formed.

3-2. Photocatalytic activity of Pd/TiO_2 catalysts

Photocatalytic activity of Pd_x/TiO_2 with different Pd loadings (x) was studied in ethanol. **Table 2-2** summarizes the results for photocatalytic reaction of benzonitrile by 6 h reaction. As shown in run 1, pure TiO_2 promotes almost no reaction of benzonitrile. In contrast, increased Pd loadings (runs 2–5) enhances reaction and produces toluene with high selectivity (>95%). Among the catalysts, Pd_2/TiO_2 exhibits the highest denitrogenation activity, and further Pd loading (Pd_4/TiO_2) decreases the activity. Loading of other metal particles is inefficient for denitrogenation. As shown in runs 6 and 7, Au_2/TiO_2 o Ag_2/TiO_2 promotes almost no reaction of benzonitrile. Pt_2/TiO_2 (run 8) shows relatively high conversion of benzonitrile (45%); however, the toluene yield is only 8%, where *N,N*-diethylbenzylamine (**5**) is produced mainly (36%). These data indicate that Pd/TiO_2 catalyst, especially loaded with 2 wt% Pd, promotes efficient denitrogenation. It must be noted that the catalyst is reusable for further reaction. As shown in run 4, the Pd_2/TiO_2 catalyst, when reused for further reaction, shows activity and selectivity

similar to those of virgin catalyst. In addition, as shown in **Figure 2-1c** (white bars), TEM analysis of the catalyst recovered after the reaction revealed that the size of Pd particles scarcely changes during the reactions. This indicates that the catalyst is reusable without loss of activity and selectivity.

As shown in runs 2–5 (**Table 2-2**), photoreactions with Pd/TiO_2 catalysts produced triethylamine (**6**) with the amount similar to that of toluene formed. **Figure 2-4** shows the time-dependent change in the amounts of benzonitrile and products during photoreaction with Pd_2/TiO_2 catalyst. Photoirradiation leads to a decrease in the amount of benzonitrile, along with a formation of toluene and triethylamine. The profile for the toluene formation is very similar to that for the triethylamine formation. These data clearly suggest that the nitrogen atom of benzonitrile is removed as triethylamine.

Table 2-2. Photocatalytic hydrodenitrogenation of benzonitrile (**1**) in ethanol with various catalysts.[a]

Run	Catalyst	d / nm[b]	Conversion of **1** / %	Yield / %			Acetaldehyde formed / μmol	H_2 formed / μmol
				2	**5**	**6**		
1	TiO_2		0	0	0	0	6	<0.1
2	$Pd_{0.5}/TiO_2$	2.6	42	40	trace	38	293	289
3	Pd_1/TiO_2	4.1	58	57	trace	54	256	242
4	Pd_2/TiO_2	5.0	>99	98	trace	96	206	176
	1st reuse[c]		>99	99	trace	96		
	2nd reuse[c]		>99	97	trace	95		
	3rd reuse[c]	5.1	>99	98	trace	97		
5	Pd_4/TiO_2	6.5	86	85	trace	83	143	119
6	Au_2/TiO_2	3.7	0	0	0	0	207	202
7	Ag_2/TiO_2	4.6	0	0	0	0	55	51
8	Pt_2/TiO_2	3.1	45	8	36	5	153	144
9	Pd_2/TiO_2[d]	5.0					263	248

[a] Reaction conditions: catalyst (10 mg), benzonitrile (10 μmol), ethanol (5 mL), Xe lamp (λ >300 nm), Ar (1 atm), temperature (298 K), photoirradiation time (6 h). [b] Average diameter for metal nanoparticles determined by TEM observations. [c] Catalysts were reused after simple washing with ethanol. [d] Photoreaction was performed without benzonitrile.

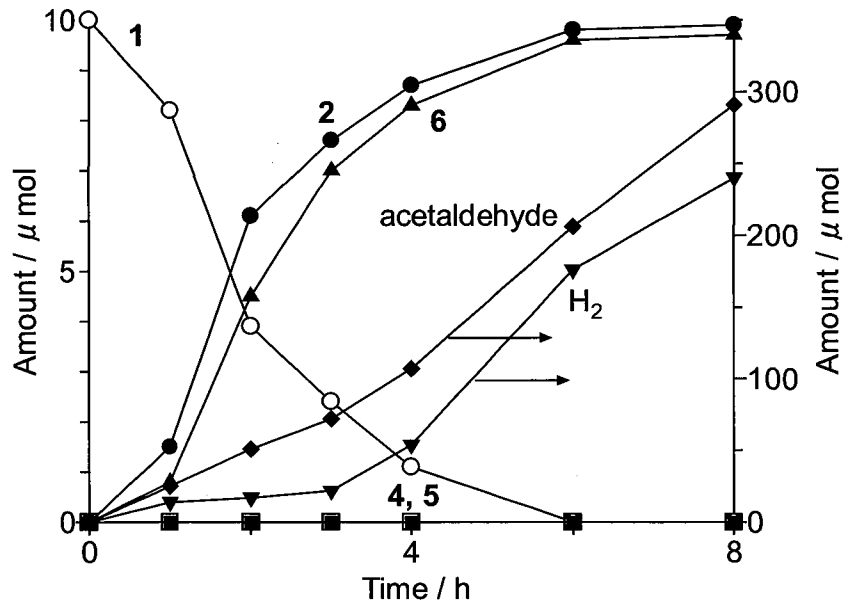

Figure 2-4. Time-dependent change in the amounts of benzonitrile (**1**) and the products obtained during photoreaction of benzonitrile with Pd_2/TiO_2 catalyst. Reaction conditions are identical to those in **Table 2-2**.

3-3. Mechanism for photocatalytic hydrodenitrogenation

Photocatalytic hydrodenitrogenation of benzonitrile is initiated by photoexcitation of TiO_2. This produces the positive hole (h^+) and electron (e^-) pairs, as follows.

$$TiO_2 + h\nu \rightarrow h^+ + e^- \quad (1)$$

The h^+ oxidizes ethanol and produces acetaldehyde and protons (H^+) on the TiO_2 surface.[18,20]

$$CH_3CH_2OH + 2h^+ \rightarrow CH_3CHO + 2H^+ \quad (2)$$

The photoformed conduction band e^- is transferred to the Pd particles. This reduces H^+ and produces a hydrogen atom on the particles (H–Pd species).

$$H^+ + e^- + Pd \rightarrow H\text{–}Pd \quad (3)$$

The parts of the hydrogen atoms on the Pd particles are removed by the coalescence as a H_2 gas.

$$H\text{–}Pd + H\text{–}Pd \rightarrow H_2\uparrow + 2Pd \quad (4)$$

The stoichiometrical conversion of benzonitrile to toluene and triethylamine (**Figure 2-4**) indicates that three aldehyde molecules formed by photocatalytic oxidation of ethanol (eq. 2) are involved in the hydrodenitrogenation of one benzonitrile molecule. The reaction mechanism can therefore be summarized in **Scheme 2-1**, which involves twelve H–Pd species. The substrate benzonitrile (**1**) undergoes hydrogenation by the H–Pd species and produces benzylamine (**3**) intermediately. This is transformed to an imine intermediate (**7**) by condensation with acetaldehyde, and then converted to

N-ethylbenzylamine (**4**) via hydrogenation by H–Pd species. Condensation of **4** with acetaldehyde and subsequent hydrogenation by H–Pd species afford *N,N*-diethylbenzylamine (**5**).[21] Hydrogenolysis of 5 by the H-Pd species produces toluene (**2**) and diethylamine (**8**). Condensation of **8** with acetaldehyde and subsequent hydrogenation produces triethylamine (**6**). During the photoreaction (**Figure 2-4**), trace amounts of **4** and **5** (<0.1 μmol) were detected by GC analysis. In addition, as summarized in **Table 2-3**, photocatalytic reactions of compounds **3**, **4**, or **5** as the starting materials with Pd_2/TiO_2 catalyst also produces toluene and triethylamine with almost quantitative yields. These findings clearly support the proposed denitrogenation mechanism involving the condensation with aldehyde and the hydrogenation by the H–Pd species (**Scheme 2-1**). As shown in **Figure 2-4**, the mass balance of benzonitrile (**1**) and toluene (**2**) is almost 100% during the reaction. This suggests that the hydrogenation of **1** to **3** is the rate-determining step for this reaction sequence. **Table 2-2** (run 9) shows the result of photocatalytic reaction performed in the absence of benzonitrile. The photoreaction produces 248 μmol H_2, which is larger than that obtained with benzonitrile (176 μmol, run 4). This indicates that hydrodenitrogenation and H_2 evolution (eq. 4) take place competitively.

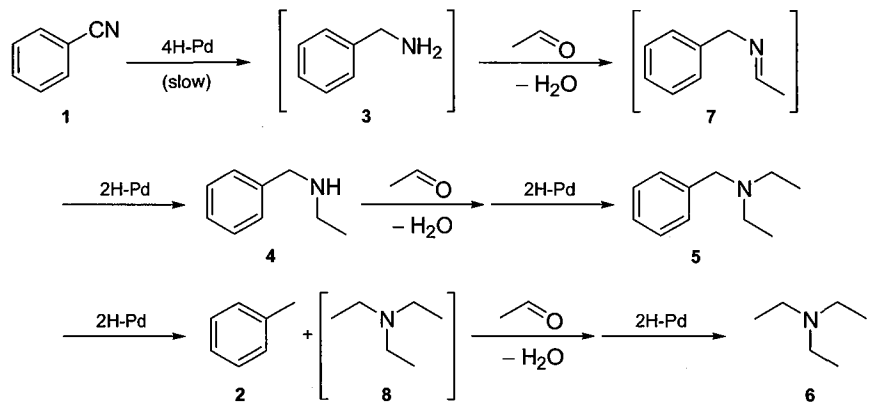

Scheme 2-1. Proposed mechanism for photocatalytic hydrodenitrogenation of benzonitrile with Pd/TiO_2 catalyst in the presence of acetaldehyde.

Table 2-3. Results of photocatalytic reaction of various substrates with Pd_2/TiO_2 catalyst.[a]

Substrate	Conversion / %	Yield / %	
		Toluene (**2**)	Triethylamine (**6**)
3	>99	99	97
4	>99	99	98
5	>99	>99	97

[a] Reaction conditions: Pd_2/TiO_2 (10 mg), substrate (10 μmol), ethanol (5 mL), Xe lamp (λ >300 nm), Ar (1 atm), temperature (298 K), photoirradiation time (6 h).

3-4. Hydrodenitrogenation of substituted benzonitrile

The Pd/TiO_2 catalyst was employed for hydrodenitrogenation of aromatic cyanides with several substituents. The results are summarized in **Table 2-4**. As shown in run 2, terephthalonitrile is successfully transformed to *p*-xylene with 98% yield via the hydrodenitrogenation of two –CN groups. Reaction of 1-naphthonitrile (run 3) produces 1-methylnaphthalene with 93% yield. Reactions of benzonitrile with methyl, methoxy, or hydroxyl substituents (runs 4–6) produce the corresponding toluene derivatives while maintaining these substituents. In contrast, halogen or carbonyl substituent also undergoes reaction. As shown in run 7, the reaction of *p*-chlorobenzonitrile produces toluene because the halogen groups are removed via the reaction with H–Pd species.[15] In addition, carbonyl substituent is converted to the hydroxyl group (run 8) due to the reduction by the H–Pd species. These results suggest that the Pd/TiO_2 catalyst promotes hydrodenitrogenation of –CN group even in the presence of substituents, although some substituents are also transformed during the reaction.

Table 2-4. Results of photocatalytic hydrodenitrogenation of various aromatic cyanides with Pd_2/TiO_2 catalyst.[a]

Run	Substrate	Time / h	Substrate conversion / %	Product	Yield / %
1		12	>99		98
2	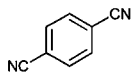	48	>99	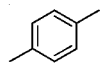	98
3	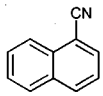	24	>99	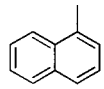	93
4	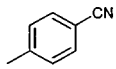	12	>99	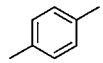	93
5	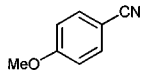	12	>99	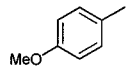	>99
6	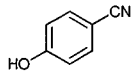	48	>99	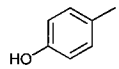	99
7	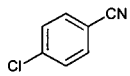	12	>99		93
8	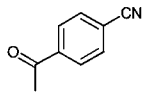	12	>99	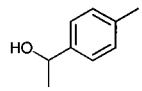	99

[a] Reaction conditions: Pd_2/TiO_2 (10 mg), substrate (10 μmol), ethanol (5 mL), Xe lamp (λ >300 nm), Ar (1 atm), temperature (298 K).

The Hammett plot analysis was carried out to clarify the effect of substituents on the reaction kinetics. Photocatalytic reactions of the above *p*-substituted benzonitriles were carried out with Pd_2/TiO_2 for 1 h, and the first-order rate constants for the decrease in substrate concentration, k (mM h^{-1}), were determined. **Figure 2-5** shows the relationship between log$k$ and the substituent constant, σ.[22] A linear correlation is observed, and the slope of the plot (ρ) is determined to be +0.795. The positive ρ value indicates that stabilization of negative charge in the transition state efficiently promotes the reaction; in other words, the reaction proceeds via a nucleophilic attack by a nucleophile.[23–25] As proposed in **Scheme 2-1**, the reaction of benzonitrile (**1**) would occur via the hydrogenation of –CN group (formation of benzylamine **3**), via the nucleophilic attack by the H–Pd species. The Hammett plot results clearly support this mechanism.

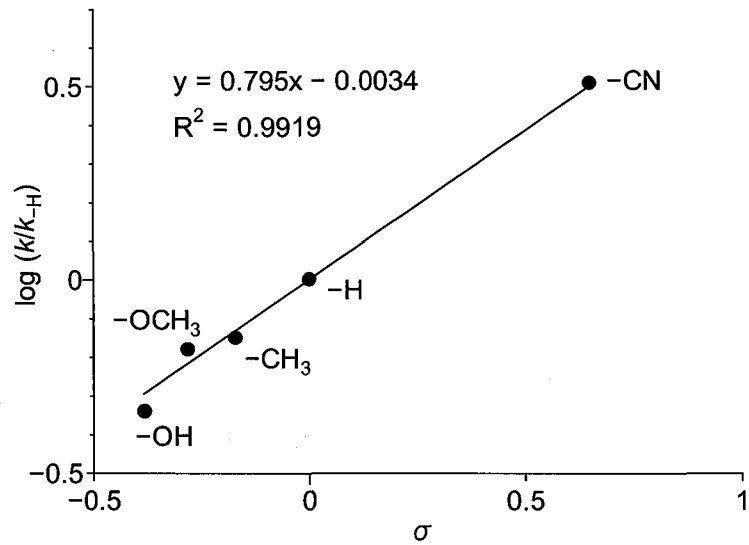

Figure 2-5. Hammett plot for the photocatalytic reaction of *p*-substituted benzonitriles with Pd_2/TiO_2. The k denotes the first-order rate constant for the decrease in substrate concentration (mM h^{-1}) determined by 1 h photoreaction. The reaction conditions are identical to those in **Table 2-4**.

3-5. Effect of Pd amount on the catalytic activity

As shown in **Table 2-2**, the denitrogenation activity depends on the amount of Pd loaded, and Pd_2/TiO_2 shows the highest activity. The H–Pd species are formed on the surface Pd atoms and, hence, the number of surface Pd atoms would strongly affect the denitrogenation activity. As shown in **Figure 2-2**, the high-resolution TEM images of catalysts revealed that the shape of Pd particles is a part of cuboctahedron surrounded by the (111) and (100) facets. The Pd particles on TiO_2 can therefore simply be modeled as a *fcc* cuboctahedron.[26] This structure is generally used as a model for cubic *fcc* metal

nanoparticles. The numbers of surface metal atoms calculated based on this model are often employed for determination of active site in several catalytic systems such as hydrogenation of allyl alcohols with H_2 on Pd particles,[27] steam reforming of methane on Pt particles,[28] and oxidation of cinnamyl alcohols on Au particles.[29] The *fcc* cuboctahedron model therefore allows rough determination of the number of surface Pd atoms on the nanoparticles. Considering the full shell close packing cuboctahedron for Pd particle where one Pd atom is surrounded by twelve others, the number of total Pd atoms per Pd particle (N_{total}*) is expressed by eq. 5 using the number of shells (m). N_{total}* is rewritten with the average diameter of Pd particles (d_{Pd} / nm) and the atomic diameter of Pd (0.274 nm).[30] The number of surface Pd atoms per Pd particle ($N_{surface}$*) is expressed by eq. 6.

$$N_{total}*(-) = \frac{10m^3 - 15m^2 + 11m - 3}{3} = \left(\frac{d_{Pd}}{1.105 \times 0.274}\right)^3 \quad (5)$$

$$N_{surface}*(-) = 10m^2 - 20m + 12 \quad (6)$$

The number of Pd particles per gram catalyst ($n_{particle}$) is expressed by eq. 7, using the percent amount of Pd loaded on the catalyst [x (wt%) = Pd/(Pd + TiO_2) × 100], molecular weight of Pd [M_W (= 106.42 g mol^{-1})], and N_{total}*. The number of surface Pd atoms per gram catalyst ($N_{surface}$) is therefore expressed by eq. 8.

$$n_{particle}\ (\mathrm{mol\,g^{-1}}) = \frac{x}{100 \times M_W \times N_{total}*} \quad (7)$$

$$N_{surface}\ (\mathrm{mol\,g^{-1}}) = N_{surface}* \times n_{particle} \quad (8)$$

The $N_{surface}$ values for respective Pd_x/TiO_2 catalysts can therefore be calculated using their d_{Pd} values determined by the TEM observations (**Figure 2-1**). As shown by the open symbols in **Figure 2-6**, the $N_{surface}$ values increase with an increase in the amount of Pd loaded; the values are 19.8 μmol g^{-1} ($Pd_{0.5}/TiO_2$), 27.8 (Pd_1/TiO_2), 45.5 (Pd_2/TiO_2), and 73.1 (Pd_4/TiO_2), respectively. To clarify the hydrodenitrogenation activity per surface Pd atoms, the turnover number for the reaction per surface Pd atoms on respective catalyst ($TON_{surface}$) was determined based on eq. 9, using the amount of toluene formed (mol) during the photocatalytic reaction of benzonitrile for 6 h in the presence of 10 mg catalyst (**Table 2-2**).

$$TON_{surface}\ (-) = \frac{[\text{toluene formed}]}{N_{surface} \times 10 \times 10^{-3}} \quad (9)$$

As shown by the black symbols in **Figure 2-6**, the $TON_{surface}$ values for $Pd_{0.5}/TiO_2$, Pd_1/TiO_2, and Pd_2/TiO_2 are almost the same. This suggests that these catalysts produce the surface H–Pd species with

similar efficiency. The higher activity of Pd_2/TiO_2 than $Pd_{0.5}/TiO_2$ and Pd_1/TiO_2 (**Table 2-2**) is therefore because larger number of surface H–Pd species is produced due to the larger number of surface Pd atoms ($N_{surface}$).

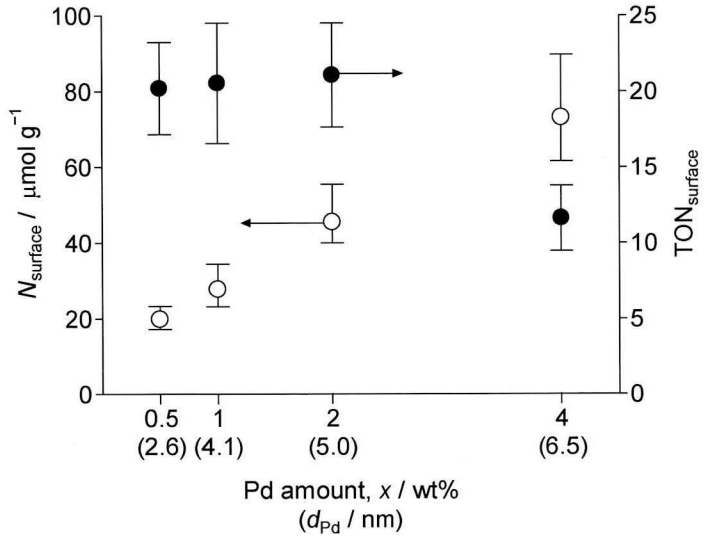

Figure 2-6. (Open symbol) The number of surface Pd atoms per gram Pd_x/TiO_2 catalyst ($N_{surface}$), and (closed symbol) the turnover number for toluene formation per surface Pd atoms on respective catalysts during photocatalytic reaction of benzonitrile ($TON_{surface}$). Reaction conditions for benzonitrile were identical to those in **Table 2-2**.

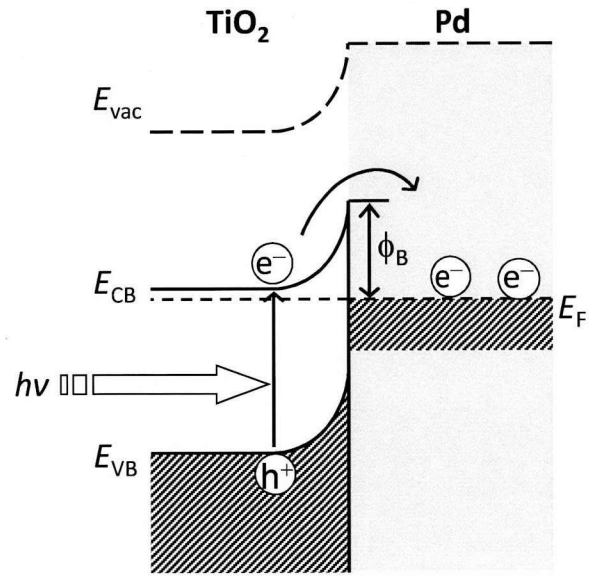

Figure 2-7. Schematic representation of the Schottky barrier created at the Pd/TiO_2 heterojunction.

In contrast, the $TON_{surface}$ value of Pd_4/TiO_2 is much lower than that of lower Pd loading catalysts (**Figure 2-6**), suggesting that the efficiency for H–Pd formation on the catalyst is lower. This is because the photocatalytic oxidation and reduction efficiency is decreased by the amount of Pd loaded. As shown in runs 2–5 (**Table 2-2**), the amounts of acetaldehyde and H_2 produced on Pd_4/TiO_2 are much lower than those on lower Pd loading catalysts. It is well known that, as shown in **Figure 2-7**, the metal/semiconductor heterojunction creates a Schottky barrier (ϕ_B), and the ϕ_B height increases with an increase in the amount of metal loaded.[31] The increased ϕ_B height by the increased Pd loadings therefore suppresses smooth transfer of the conduction band e^- to the Pd particles. This may result in inefficient charge separation between h^+ and e^- and exhibit decreased photocatalytic activity. As a consequence, the H–Pd formation is suppressed, thus resulting in decreased denitrogenation activity. These findings indicate that the Pd_2/TiO_2 catalyst, with relatively low ϕ_B height and large number of surface Pd atoms, exhibits the highest activity for photocatalytic hydrodenitrogenation of aromatic cyanides.

4. Conclusion

TiO_2 loaded with Pd particles (Pd/TiO_2) were used as catalysts for photocatalytic hydrodenitrogenation of aromatic cyanide in ethanol as a hydrogen source. These catalysts, when irradiated by UV light at room temperature, promote denitrogenation and produce the corresponding toluene derivatives and triethylamine with very high selectivity. Photoexcited Pd/TiO_2 produces acetaldehyde and the active H–Pd species. Consecutive reactions involving hydrogenation by H–Pd species and condensation with aldehyde facilitate efficient hydrodenitrogenation. The amount of Pd loaded and the size of Pd particles strongly affect the denitrogenation activity. The Pd/TiO_2 catalyst with a relatively low Schottky barrier height at the Pd/TiO_2 heterojunction and a large number of surface Pd atoms is necessary for efficient denitrogenation.

5. References

[1] Li, T.; Liu, J.; Bai, R.; Ohandja, D.-G.; Wong, F.-S. *Water Res.* **2007**, *41*, 3465.

[2] Marcì, G.; Paola, A. D.; García-López, E.; Palmisano, L. *Catal. Today* **2007**, *129*, 16.

[3] Martínková, L.; Uhnáková, B.; Pátek, M.; Nešvera, J.; Křen, V. *Environ. Int.* **2009**, *35*, 162.

[4] Calza, P.; Pelizzetti, E.; Minero, C. *J. Appl. Electrochem.* **2005**, *35*, 665.

[5] Okamoto, K.; Yamamoto, Y.; Tanaka, H.; Tanaka, M.; Itaya, A. *Bull. Chem. Soc. Jpn.* **1985**, *58*, 2015.

[6] Ohde, H.; Wai, C. M.; Kim, H.; Kim, J.; Ohde, M. *J. Am. Chem. Soc.* **2002**, *124*, 4540.

[7] Silvestre-Albero, J.; Rupprechter, G.; Freund, H.-J. *Chem. Commun.* **2006**, 80.

[8] Ludwig, W.; Savara, A.; Schauermann, S.; Freund, H.-J. *ChemPhysChem* **2010**, *11*, 2319.

[9] Ludwig, W.; Savara, A.; Dostert, K.-H.; Schauermann, S. *J. Catal.* **2011**, *284*, 148.

[10] Yi, D. K.; Lee, S. S.; Ying, J. Y. *Chem. Mater.* **2006**, *18*, 2459.

[11] Huang, X.; Wang, Y.; Liao, X.; Shi, B. *Chem. Commun.* **2009**, 4687.

[12] Wu, H.; Zhuo, L.; He, Q.; Liao, X.; Shi, B. *Appl. Catal. A* **2009**, *366*, 44.

[13] Bakker, J. J. W.; van der Neut, A. G.; Kreutzer, M. T.; Moulijn, J. A.; Kapteijn, F. *J. Catal.* **2010**, *274*, 176.

[14] Sreethawong, T.; Yoshikawa, S. *Catal. Commun.* **2005**, *6*, 661.

[15] Shiraishi, Y.; Takeda, Y.; Sugano, Y.; Ichikawa, S.; Tanaka, S.; Hirai, T. *Chem. Commun.* **2011**, *47*, 7863.

[16] Shiraishi, Y.; Tsukamoto, D.; Sugano, Y.; Shiro, A.; Ichikawa, S.; Tanaka, S.; Hirai, T. *ACS Catal.* **2012**, *2*, 1984.

[17] Tsukamoto, D.; Shiraishi, Y.; Sugano, Y.; Ichikawa, S.; Tanaka, S.; Hirai, T. *J. Am. Chem. Soc.* **2012**, *134*, 6309.

[18] Shiraishi, Y.; Sugano, Y.; Tanaka, S.; Hirai, T. *Angew. Chem. Int. Ed.* **2010**, *49*, 1656.

[19] Tsukamoto, D.; Shiro, A.; Sugano, Y.; Shiraishi, Y.; Ichikawa, S.; Tanaka, S.; Hirai, T. *ACS Catal.* **2012**, *2*, 599.

[20] Shiraishi, Y.; Hirai, T. *J. Photochem. Photobiol. C* **2008**, *9*, 157.

[21] Matsushita, Y.; Ohba, N.; Suzuki, T.; Ichimura, T. *Catal. Today* **2008**, *132*, 153.

[22] Connors, K. A. *Chemcal Kinetics, The Study of Reaction Rates in Solution*, VCH, New York, **1990**.

[23] Yang, X.; Zhao, L.; Fox, T.; Wang. Z.-X.; Berke, H. *Angew. Chem. Int. Ed.* **2010**, *49*, 2058.

[24] Donkers, R. L.; Song, Y.; Murray, R. W. *Langmuir* **2004**, *20*, 4703.

[25] Lu, P.; Toshima, N. *Bull. Chem. Soc. Jpn.* **2000**, *73*, 751.

[26] Benfield, R. E. J. *J. Chem. Soc. Faraday Trans.* **1992**, *88*, 1107.

[27] Wilson, O. M.; Knecht, M. R.; Gareia-Martinez, J. C.; Crooks, R. M. *J. Am. Chem. Soc.* **2006**, *128*, 4510.

[28] Qu, Y.; Sutherland, A. M.; Lien, J.; Suarez, G. D.; Guo, T. *J. Phys. Chem. Lett.* **2010**, *1*, 254.

[29]Abad, A.; Corma, A.; Garcia, H. *Chem. Eur. J.* **2008**, *14*, 212.

[30] Pauling, L. *J. Am. Chem. Soc.* **1947**, *69*, 542.

[31] Uchihara, T.; Matsumura, M.; Yamamoto, A.; Tsubomura, H. *J. Phys. Chem.* **1989**, *93*, 5870.

Chapter III

N-Monoalkylation of Amines with Alcohols on TiO_2 Loaded with Pd Nanoparticles

1. Introduction

Tandem catalysis that enables multistep reactions in one pot has attracted a great deal of attention because it avoids the isolation of unstable intermediates and reduces the production of wastes.[1–3] A variety of one-pot synthetic procedures have been proposed, but many of these employ homogeneous catalysts, which generally suffer from product contamination and limited recyclability.[4–6] Development of heterogeneous catalytic systems that promote efficient one-pot synthetic reactions is currently the focus of attention.[7–11]

Secondary amines are one of the most important classes of chemicals that are widely used for synthesis of pharmaceuticals and agricultural chemicals.[12] Traditionally, these compounds are synthesized by *N*-monoalkylation of primary amines with alkyl halides.[12–14] This method, however, requires stoichiometric or excess amount of inorganic bases, with a concomitant formation of large amounts of inorganic salts as waste.

An alternative environmentally-friendly way for secondary amine synthesis is the *N*-alkylation of primary amines with alcohols as the alkylating reagents in the presence of transition metal catalysts, so-called "borrowing hydrogen (H) strategy".[15–18] The reaction proceeds via three consecutive catalytic steps in one pot: (i) dehydrogenation of an alcohol initially proceeds, producing aldehyde and H atoms on the metal; (ii) catalytic condensation of the formed aldehyde with primary amine produces imine; and, (iii) the imine is hydrogenated by the H atoms, giving the secondary amine. Although many homogeneous catalysts such as Pt-, Ru-, and Ir-complexes, have been proposed so far,[19–24] these methods have shortcomings in the recovery and reuse of expensive catalysts and/or the indispensable use of co-catalysts such as bases and stabilizing ligands. The design of easily recyclable heterogeneous catalytic systems is therefore desirable.

Several heterogeneous systems have also been proposed for one-pot secondary amine synthesis such as Pd oxides supported on Fe_2O_3,[25] Pd particles supported on boehmite nanofibers,[26] Ag clusters supported on Al_2O_3 (in the presence of $FeCl_3{\cdot}6H_2O$ as a homogeneous Lewis acid),[27] Ru or Cu hydroxide supported on Al_2O_3,[28–31] Au particles supported on TiO_2,[32] and Pd particles supported on MgO.[33] All of these systems produce secondary amines selectively, but require relatively high reaction temperatures (>363 K).

The purpose of the present work is to design heterogeneous catalytic systems that promote *N*-monoalkylation of primary amines with alcohols at room temperature. It is well known that photoexcitation of semiconductor TiO_2 loaded with noble metal particles such as Pt,[34] Ag,[35] Au,[36] and Pd[37] under inert gas atmosphere successfully promotes dehydrogenation of alcohols and produces aldehydes at room temperature. The removed H^+ are reduced by the photoformed electrons on the metal particles and are transformed to H atoms (H–metal species), which are finally removed from the metal surface by the formation of H_2.[38] This indicates that TiO_2 loaded with metal particles, when photoactivated in alcohol, produces aldehyde and H atoms at room temperature. The formed aldehyde may react with primary amine on the Lewis acid site on the TiO_2 surface and produce imine.[34,39] The imine may then be hydrogenated by the H atoms formed on the metal surface[40] and converted to secondary amine.

Based on the above scenario, we studied the *N*-alkylation of primary amines with alcohols in the presence of metal-loaded TiO_2 under photoirradiation (λ >300 nm). Here we report that TiO_2 loaded with Pd particles (Pd/TiO_2) successfully promotes *N*-monoalkylation of primary amines at room temperature, via three consecutive steps involving (i) dehydrogenation of alcohols on the photoactivated TiO_2 surface; (ii) catalytic condensation of the formed aldehyde and amine; and, (iii) hydrogenation of the formed imine on the Pd surface. We found that the reaction efficiency strongly depends on the size of Pd particles. The catalyst loaded with 0.3 wt % Pd, containing 2–2.5 nm Pd particles, shows the highest activity.

2. Experimental

2-1. Materials

All reagents were purchased from Wako, Tokyo Kasei, and Sigma-Aldrich and used without further purification. Japan Reference Catalyst JRC-TIO-4 TiO_2 particles were kindly supplied from Catalysis Society of Japan.

Pd_x/TiO_2 [x (wt%) = 0.1, 0.3, 0.5, and 1.0] were prepared as follows: TiO_2 (1.0 g) and $Pd(NO_3)_2$ (2.2, 6.5, 10.9, or 21.9 mg) were added to water (40 mL) and evaporated under vigorous stirring at 353 K for 12 h. The obtained powders were calcined at 673 K under air flow (0.5 L min^{-1}) and then reduced at 673 K under H_2 flow (0.2 L min^{-1}). The heating rate and holding time at 673 K for these treatments were 2 K min^{-1} and 2 h, respectively. $Ag_{0.3}/TiO_2$ and $Pt_{0.3}/TiO_2$ were prepared in a similar manner to those for Pd_x/TiO_2, using $AgNO_3$ (4.7 mg) or $H_2PtCl_6{\cdot}6H_2O$ (8.0 mg) as precursor.

$Au_{0.3}/TiO_2$ was prepared by a deposition-precipitation method as follows: $HAuCl_4{\cdot}4H_2O$ (6.3 mg)

was added to water (50 mL). The pH of the solution was adjusted to 7 by an addition of 1 M NaOH. TiO_2 (1.0 g) was added to the solution and stirred vigorously at 353 K for 3 h. The solids were recovered by centrifugation and washed with water. The obtained solids were dried at 353 K and calcined at 673 K for 2 h under air flow (0.5 L min^{-1}).

2-2. Photoreaction

Each of the respective catalysts (10 mg) was suspended in alcohol (5 mL) containing required amount of amine within a Pyrex glass tube (ϕ10 mm; capacity, 20 mL). The tube was sealed with a rubber septum cap. The catalyst was dispersed by ultrasonication for 5 min, and N_2 was bubbled through the solution for 5 min. The tube was photoirradiated with magnetic stirring at 298 K by a 2 kW Xe lamp (λ >300 nm; Ushio Inc.). The light intensity at 300–400 nm is 18.2 W m^{-2}. After photoirradiation, the gas-phase product was analyzed by GC-TCD (Shimadzu; GC-8A). The resulting solution was recovered by centrifugation and analyzed by GC-FID (Shimadzu; GC-1700), where the substrate and product concentrations were determined with authentic samples. Identification of the products was performed by Shimadzu GC-MS system (GCMS-QP5050A).

2-3. Hydrogenation by H_2

Each of the respective catalysts was suspended in solution (5 mL) containing substrate within a Schlenk tube. The catalyst was dispersed by ultrasonication for 5 min, and H_2 was bubbled through the solution for 5 min, where the H_2 pressure was maintained at 1 atm using a balloon. The tube was placed on the digitally-controlled water bath with magnetic stirring at 298 K.

2-4. Analysis

Total Pd amounts of the catalysts were determined by an X-ray fluorescence spectrometer (Seiko Instruments, Inc.; SEA2110). Diffuse reflectance UV-vis spectra were measured on an UV-vis spectrophotometer (Jasco Corp.; V-550 with Integrated Sphere Apparatus ISV-469) with $BaSO_4$ as a reference.[59,60] TEM observations were carried out using an FEI Tecnai G2 20ST analytical electron microscope operated at 200 kV.[61] The cuboctahedron Pd particles were created on the Crystal Studio Ver. 9.0 software (CrystalSolf. Inc) and used for calculation of the number of Pd atoms.[50] Ab initio calculations were carried out with the Gaussian 03 program, and the geometry optimization was performed with the density functional theory (DFT) using the B3LYP function with the 6–31G* basis set.[62,63]

3. Results and discussion

3-1. Catalytic activity of metal-loaded TiO_2

Table 3-1. Catalyst properties and the results for *N*-alkylation of aniline with benzyl alcohol on various catalysts under photoirradiation.

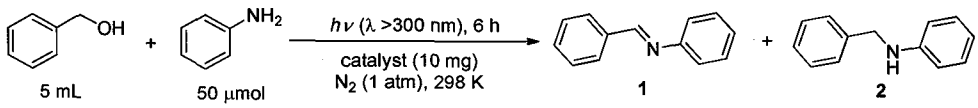

Entry	Catalyst	d_{pd} / nm[a]	Aniline conv. / %[b]	Yields / %[b,c]		Amount of product formed / μmol[b]		
				1	**2**	Benzaldehyde	Toluene	H_2
1	TiO_2		11	10	0	<1	0	<1
2	$Au_{0.3}/TiO_2$		4	4	0	16	0	15
3	$Ag_{0.3}/TiO_2$		9	6	2	4	0	3
4	$Pt_{0.3}/TiO_2$		56	53	3	84	0	98
5	$Pd_{0.1}/TiO_2$	1.6	65	8	49	96	0.9	93
6	$Pd_{0.3}/TiO_2$	2.3	>99	6	92	90	14	79
7	$Pd_{0.5}/TiO_2$	2.6	91	9	81	62	25	18
8	$Pd_{1.0}/TiO_2$	4.1	89	19	64	56	42	6
9[d]	$Pd_{0.3}/TiO_2$		>99	7	92			

[a] Average diameter of Pd particles determined by TEM observations (Figure 1). [b] Determined by GC. [c] d= [product formed] / [initial amount of aniline] × 100. [d] The result obtained by the reuse of catalyst (entry 6) after simple washing with ethanol.

The catalytic activity of metal-loaded TiO_2, M_x/TiO_2 [x (wt %) = M/(M + TiO_2) × 100], was studied for *N*-alkylation of primary amine with alcohol. The catalysts loaded with 0.3 wt % metal particles such as Au, Pt, Ag, and Pd were prepared with JRC-TIO-4 TiO_2 supplied from the Catalyst Society of Japan (equivalent to Degussa P25; anatase/rutile = ca. 80/20; average particle size, 24 nm; BET surface area, 59 m^2 g^{-1}). Metal loadings were carried out by the deposition-precipitation method[41] for Au and by the impregnation-reduction method[34] for Pt, Ag, and Pd, respectively. These catalysts were used for *N*-alkylation of aniline with benzyl alcohol. The reactions were carried out by photoirradiation (λ >300 nm, 6 h) of a benzyl alcohol solution (5 mL) containing aniline (50 μmol) with respective catalyst (10 mg) at room temperature under N_2 atmosphere (1 atm). The conversion of aniline and the yield of N-benzylidenaniline (1) and N-benzylphenylamine (2) (= [product formed] / [initial amount of aniline] ×

100) are summarized in **Table 3-1**. With bare TiO_2 (entry 1), the aniline conversion is only 11% and the imine (*N*-benzylidenaniline: **1**) is formed as the main product, where the secondary amine (*N*-benzylphenylamine: **2**) is scarcely produced. $Au_{0.3}/TiO_2$ and $Ag_{0.3}/TiO_2$ catalysts are also ineffective (entries 2 and 3); their aniline conversions are <10%. In these cases, the amount of benzaldehyde formed is significantly low (<20 μmol). This implies that photocatalytic oxidation of alcohol does not occur effixiently on these catalysts and does not provide enough amount of aldehyde for condensation with aniline. As shown in entry 4, $Pt_{0.3}/TiO_2$ shows relatively high aniline conversion (56%). The **2** yield is however only 3%, and imine (**1**) is produced mainly. This indicates that hydrogenation of imine does noe occur efficiently on the $Pt_{0.3}/TiO_2$ catalyst. In contrast, $Pd_{0.3}/TiO_2$ (entry 6) produces **2** with almost quantitative yield (92%). The results clearly indicate that Pd/TiO_2 catalyst is highly active for *N*-monoalkylation.

3-2. Catalytic activity of Pd/TiO_2

Pd_x/TiO_2 catalysts with different Pd loadings (x = 0.1, 0.3, 0.5, and 1.0 wt %) were prepared to clarify their activity. **Figure 3-1** shows the typical transmission electron microscopy (TEM) images of $Pd_{0.3}/TiO_2$. Highly dispersed Pd nanoparticles were observed for all of the Pd_x/TiO_2 catalysts. As shown in **Figure 3-1**, the size of Pd particles (d_{Pd}) determined by the TEM observations increases with an increase in the Pd loadings; the average diameters for x = 0.1, 0.3, 0.5, and 1.0 catalysts are 1.6, 2.3, 2.6, and 4.1 nm, respectively. In addition, high-resolution TEM image of catalyst (**Figure 3-2**) revealed that the Pd particles can be indexed as *fcc* structure, as well as bulk Pd metal (JCPDS 46-1043). **Figure 3-3** shows the diffuse reflectance UV-vis spectra of respective catalysts. The catalysts with higher Pd loadings show increased absorbance at λ >300 nm due to the light scattering by the Pd particles.

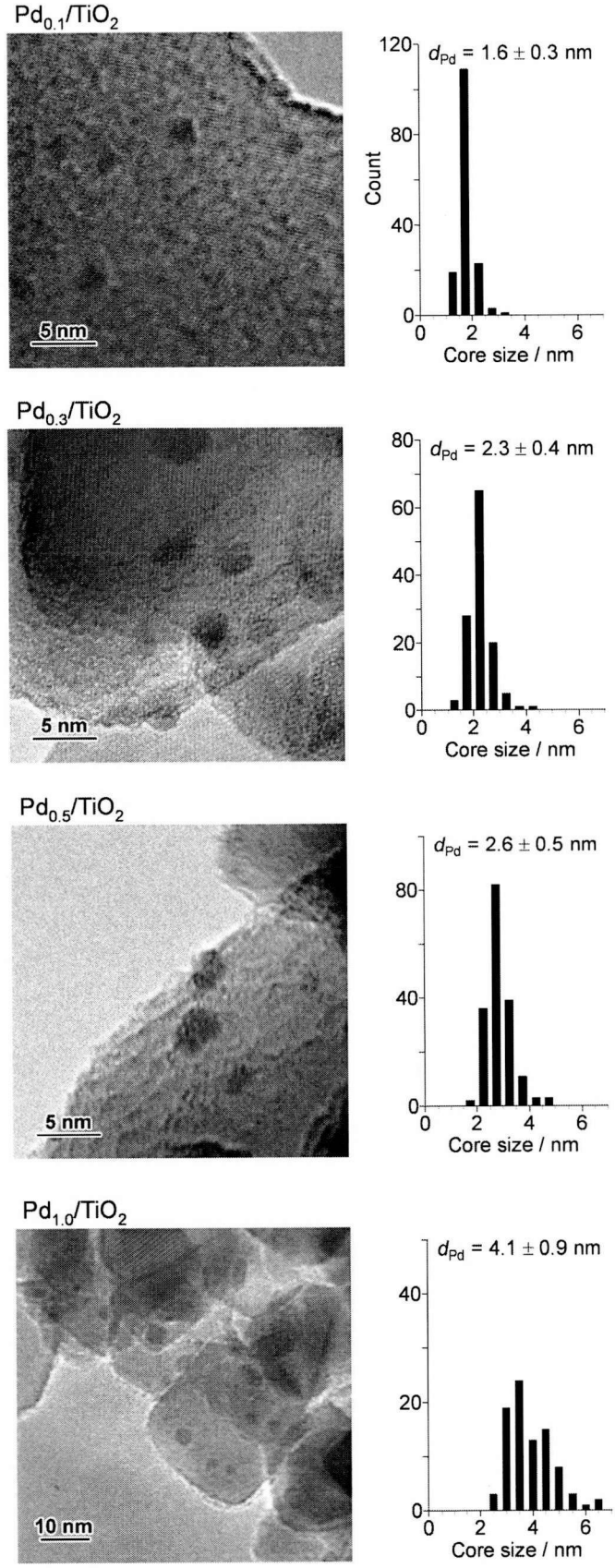

Figure 3-1. Typical TEM image of $Pd_{0.3}/TiO_2$ catalyst, and the size distributions of Pd particles on the respective Pd_x/TiO_2 catalysts.

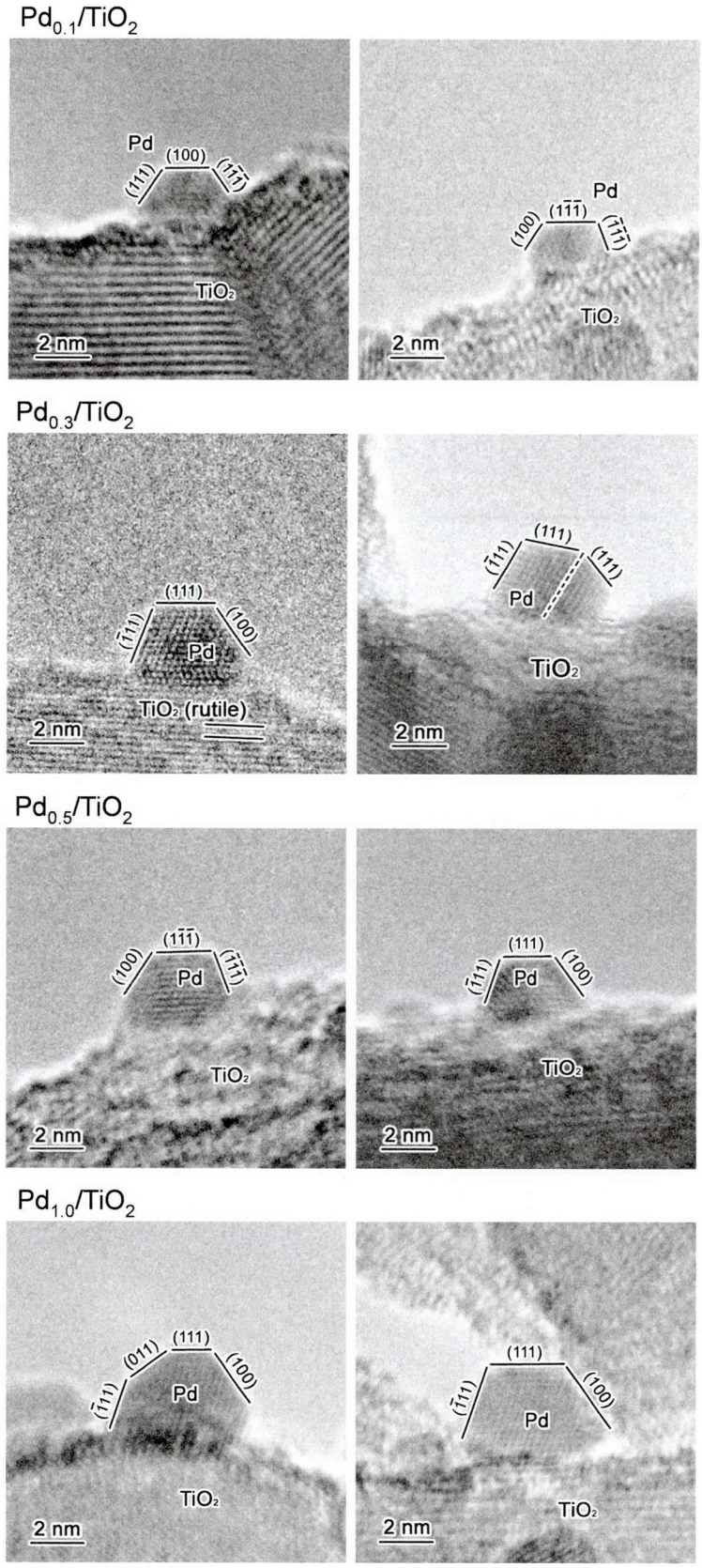

Figure 3-2. High-resolution TEM images of $Pd_{0.3}/TiO_2$. (a) The incident beam direction is [0, –1, 1]. (b) This particle is twinned particle. The incident beam directions are [0, –1, 1] and [0, 1, –1].

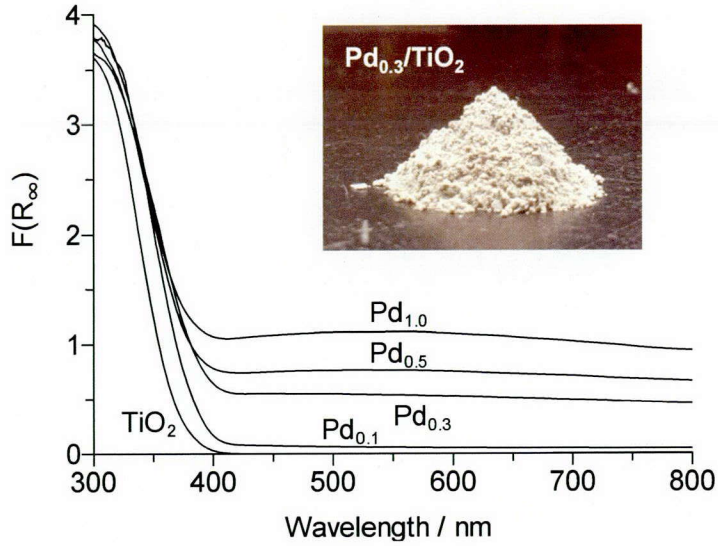

Figure 3-3. Diffuse reflectance UV-vis spectra of Pd_x/TiO_2 catalysts.

Table 3-1 (entries 5–8) summarizes the results for *N*-alkylation of aniline with benzyl alcohol in the presence of Pd_x/TiO_2 catalysts. Among the catalysts, $Pd_{0.3}/TiO_2$ (entry 6) shows the highest aniline conversion (>99%) and the highest **2** yield (92%). The catalysts with lower or higher Pd loadings show decreased activity. These data suggest that $Pd_{0.3}/TiO_2$ shows the best catalytic activity, and the activity strongly depends on the amount of Pd loaded. It is noted that the $Pd_{0.3}/TiO_2$ catalyst is reusable for further reaction. As shown in **Table 3-1** (entry 9), $Pd_{0.3}/TiO_2$, when reused for reaction after simple washing with ethanol, shows the aniline conversions and **2** yield similar to that obtained with the virgin catalyst (entry 6). This indicates that the catalyst is reusable without the loss of activity and selectivity. In addition, $Pd_{0.3}/TiO_2$ is applicable for synthesis of several kinds of secondary amines. As shown in **Table 3-2**, photoirradiation of $Pd_{0.3}/TiO_2$ in alkyl or benzyl alcohols containing several kinds of primary amines produces the corresponding secondary amines with very high yields (>82%).

Table 3-2. *N*-alkylation of various amines with alcohols on the $Pd_{0.3}/TiO_2$ catalyst under photoirradiation.[a]

Entry	Alcohol	Amine	t / h	Amine conv. / %[b]	Product	Yield / %[b]
1		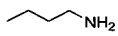	6	>99	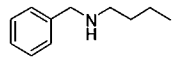	98
2		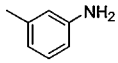	12	>99	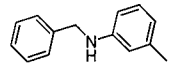	97
3		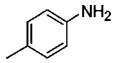	14	98	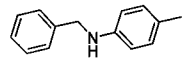	82
4	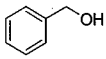	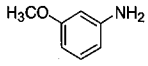	12	>99	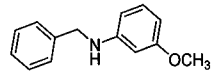	96
5		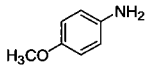	16	94	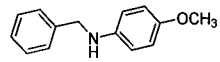	82
6		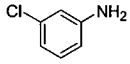	12	>99	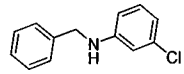	95
7		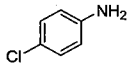	12	>99	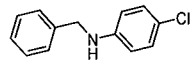	82
8			3	>99	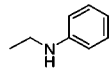	95
9	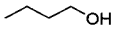		4	>99	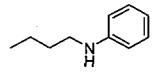	91

[a] Reaction conditions: alcohol, 5 mL; amine, 50 μmol; catalyst, 10 mg; temperature, 298 K; N_2, 1 atm; λ >300 nm; [b] Determined by GCs.

3-3. Mechanism for *N*-alkylation

The Pd/TiO_2 catalysts promote *N*-alkylation of amine with alcohol via tandem photocatalytic and catalytic reactions. The reactions are initiated by photoexcitation of TiO_2, producing the electron (e^-) and positive hole (h^+) pairs.

$$TiO_2 + h\nu \rightarrow h^+ + e^- \quad (1)$$

The h^+ oxidizes alcohol and produces aldehyde and H^+.

$$R_1\text{–}CH_2OH + 2h^+ \rightarrow R_1\text{–}CHO + 2H^+ \quad (2)$$

H^+ is reduced on the surface of Pd particles by the e^- transferred from the TiO_2 conduction band, and transformed to the surface H atom (H–Pd species).

$$H^+ + e^- + Pd \rightarrow H\text{–}Pd \quad (3)$$

Parts of the H atoms are removed from the surface of Pd particles as H_2 gas by coalescence.

$$H\text{–}Pd + H\text{–}Pd \rightarrow H_2\uparrow + 2Pd \quad (4)$$

Condensation of the formed aldehyde with primary amine by the Lewis acid site on the TiO_2 surface produces the imine. The reaction occurs reversibly as follows:[34,39]

$$R_1\text{–}CHO + R_2\text{–}NH_2 \rightleftarrows R_1\text{–}CH{=}N\text{–}R_2 + H_2O \quad (5)$$

The imine is hydrogenated by the H–Pd species and is transformed to secondary amine.[40]

$$R_1\text{–}CH{=}N\text{–}R_2 + 2H\text{–}Pd \rightarrow R_1\text{–}CH_2\text{–}NH\text{–}R_2 + 2Pd \quad (6)$$

Figure 3-4 shows the time-dependent change in the amounts of substrate and products during photocatalytic reaction of aniline with benzyl alcohol in the presence of $Pd_{0.1}/TiO_2$, $Pd_{0.3}/TiO_2$, and $Pd_{1.0}/TiO_2$ catalysts, respectively. As shown in **Figure 3-4b**, photoirradiation of $Pd_{0.3}/TiO_2$ produces benzaldehyde and H_2 at the initial stage. Then, the amount of aniline decreases, and the imine **1** and secondary amine **2** appear. The amount of **1** stays very low and the amount of **2** increases with time; 6 h photoirradiation leads to almost quantitative transformation of aniline to **2**. These substrate and product profiles suggest that the above reaction sequence (eqs 1–6) proceeds efficiently on the $Pd_{0.3}/TiO_2$ catalyst. In contrast, with $Pd_{0.1}/TiO_2$ and $Pd_{1.0}/TiO_2$ (**Figure 3-4a** and **c**), the formation of **2** is much slower than that obtained with $Pd_{0.3}/TiO_2$; quantitative formation of **2** requires more than 10 h. These data suggest that $Pd_{0.3}/TiO_2$ shows the highest activity for *N*-alkylation, and the amount of Pd loaded strongly affects the catalytic activity.

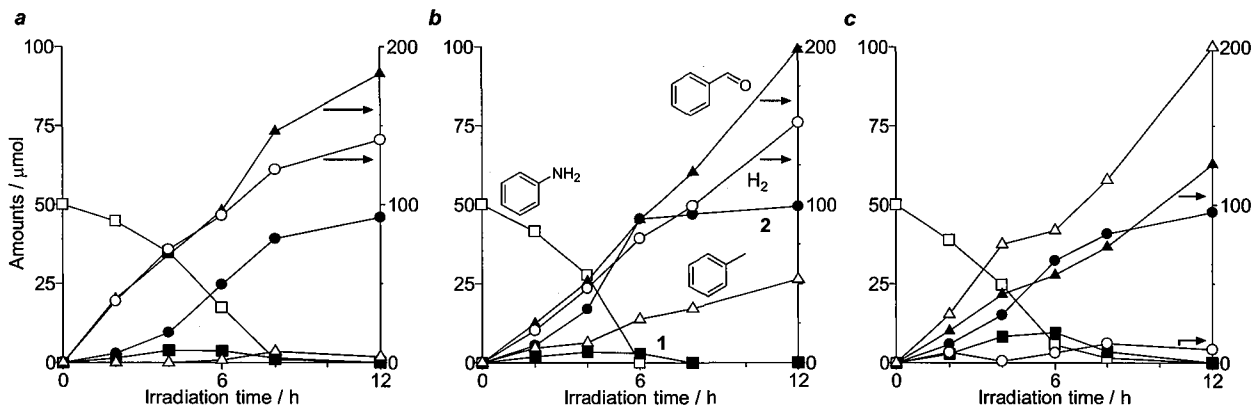

Figure 3-4. Time-dependent change in the amounts of substrate and products during photoreaction of benzyl alcohol and aniline with (a) $Pd_{0.1}/TiO_2$, (b) $Pd_{0.3}/TiO_2$, and (c) $Pd_{1.0}/TiO_2$ catalysts. Reaction conditions are identical to those in Table 1.

3-4. Effect of Pd amount on the reaction steps

The effects of Pd amount on the respective reaction steps (eqs. 2–6) for *N*-alkylation were studied to clarify the reason for high activity of $Pd_{0.3}/TiO_2$. The oxidation of alcohol by the photoformed h^+ (eq. 2) as the first step for reaction was studied by photoirradiation of respective catalysts (10 mg) in benzyl

alcohol (5 mL) without aniline. **Figure 3-5** (white) shows the amount of benzaldehyde formed by 6 h photoirradiation. $Pd_{0.1}/TiO_2$ produces the highest amount of aldehyde and the amount decreases with the Pd loadings. This suggests that lower Pd loading catalysts are more active for photocatalytic oxidation of alcohol. It is well known that a metal/semiconductor heterojunction creates a Schottky barrier.[42] Photoformed conduction band e^- of semiconductor overcomes this barrier and is trapped by metal particles, resulting in enhanced charge separation between h^+ and e^-. The charge separation efficiency therefore strongly depends on the height of Schottky barrier. The increased metal loadings onto semiconductor load to an increase in the height of Schottky barrier due to the electron transfer from semiconductor to metal.[43] The increased barrier height by large Pd loadeings probably suppresses the migration of condection band e^- to Pd particles. This may decrease the charge separation efficiency and result in decreased photocatalytic aldehyde formation (**Figure 3-5**). However, as shown in **Table 3-1** (entries 5–8), all of the Pd_x/TiO_2 catalysts produce benzaldehyde with amounts larger than that of aniline (50 μmol). This suggests that enough amount of aldehyde for condensation with aniline is produced on all of the catalysts, and the photocatalytic alcohol oxidation is not the rate-determining step for *N*-alkylation.

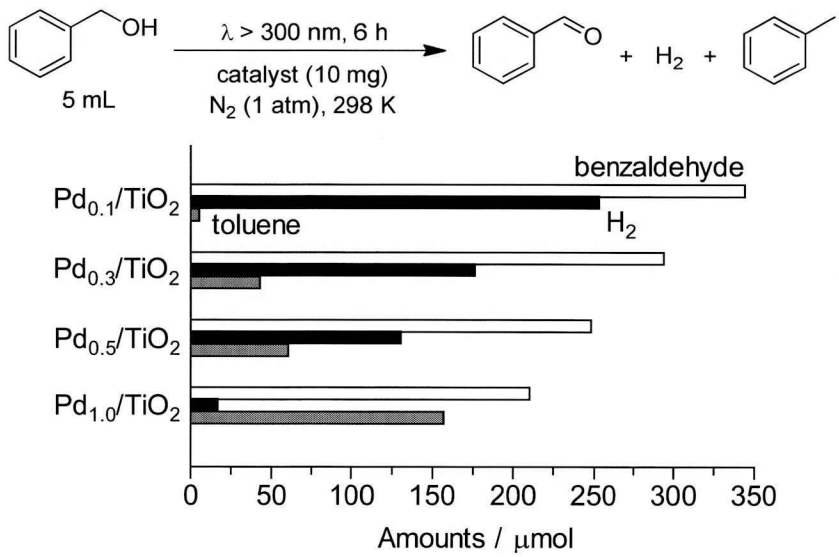

Figure 3-5. Amount of products formed during photoreaction of benzyl alcohol with respective catalysts in the absence of amine.

Condensation of amine with aldehyde (eq. 5) is the next step for *N*-alkylation. The reaction is catalyzed by Lewis acid site on the TiO_2 surface[34,39] and is not affected by the amount of Pd loaded. **Table 3-3** summarizes the results for condensation between aniline and 2 equiv of benzaldehyde in the

presence of respective catalysts for 3 h at 298 K in the dark. The absence of catalyst (entry 1) produces **1** with only 29% yield. In contrast, addition of bare TiO_2 (entry 2) produces **1** with >90% yield. The yield of **1** scarcely changes by the catalysts with different Pd loadings (entries 3–6). These data clearly suggest that the imine formation (eq. 5) is also not the rate-determining step for *N*-alkylation.

Table 3-3. Condensation of benzaldehyde with aniline on the respective catalysts in the dark.[a]

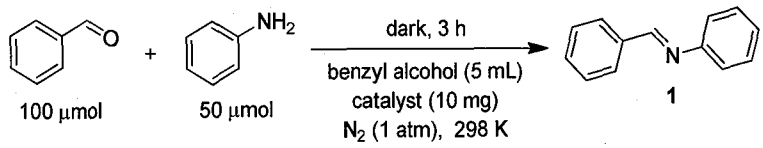

Entry	Catalyst	**1** yield [%][a]
1	none	29
2	TiO_2	90
3	$Pd_{0.1}/TiO_2$	92
4	$Pd_{0.3}/TiO_2$	94
5	$Pd_{0.5}/TiO_2$	92
6	$Pd_{1.0}/TiO_2$	95

[a] Determined by GC.

As a result of the above, the rate-determining step for *N*-alkylation is the hydrogenation of imine by the H atom formed on the surface of Pd particles (eq. 6) as the final step for reaction sequence. The imine hydrogenation is strongly affected by the size of Pd particles loaded. This is confirmed by hydrogenation of imine **1** with molecular hydrogen (H_2) as a hydrogen source. The reaction was performed in MeCN containing **1** with H_2 (1 atm) in the presence of respective Pd_x/TiO_2 catalysts at the constant Pd amount (0.28 μmol) for 2 h in the dark. **Figure 3-6** (black) shows the relationship between the diameter of Pd particles (d_{Pd}) and the yield of secondary amine (**2**) formed. Smaller Pd particles have larger surface area and possess larger number of surface Pd atoms. The **2** yields, however, increase with an increase in the size of Pd particles. This indicates that all of the surface Pd atoms are not the active site, and the Pd atoms on the specific surface site behave as the active site for imine hydrogenation.

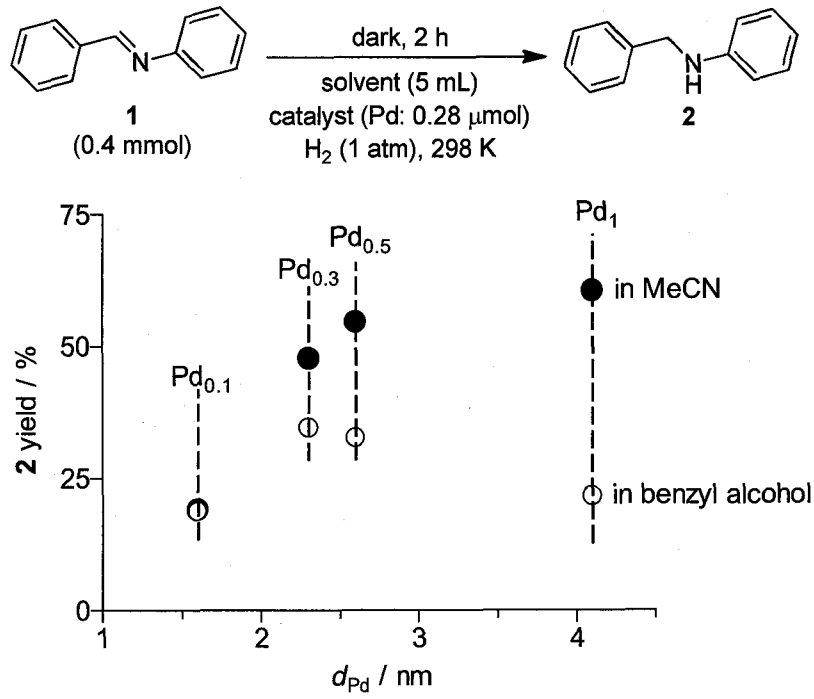

Figure 3-6. The yields of secondary amine **2** obtained during hydrogenation of imine **1** in MeCN or benzyl alcohol with respective Pd_x/TiO_2 catalysts (Pd: 0.28 μmol) under H_2 in the dark condition. The amounts of catalysts used are: 30 mg ($Pd_{0.1}$), 10 mg ($Pd_{0.3}$), 5 mg ($Pd_{0.5}$), and 3 mg (Pd_1), respectively.

3-5. Active site for imine hydrogenation

Specific active site for imine hydrogenation on the Pd particles must be identified. Morphology and size of metal particles strongly affect the catalytic activity due to the electronic and geometric effects.[44–47] Metal particles contain different types of surface atoms located at the vertex, edge, square, and triangle sites. The number of these atoms changes substantially with the size of particles. As shown in **Figure 3-2**, high-resolution TEM images of catalysts revealed that the shape of Pd particle is part of cuboctahedron, which is surrounded by [111] and [100] surfaces. The Pd particles on TiO_2 surface can therefore simply be modeled as a *fcc* cuboctahedron, as shown in **Figure 3-7a**, which is often used for related nanoparticle systems.[48–50] This allows rough determination of the number of Pd atoms on the respective surface sites. Considering the full shell close packing cuboctahedron for Pd particle where one Pd atom is surrounded by twelve others, the number of total Pd atoms per particle (N_{total}*) and the number of surface Pd atoms per particle ($N_{surface}$*) can be expressed by the following equations using the shell number (m).

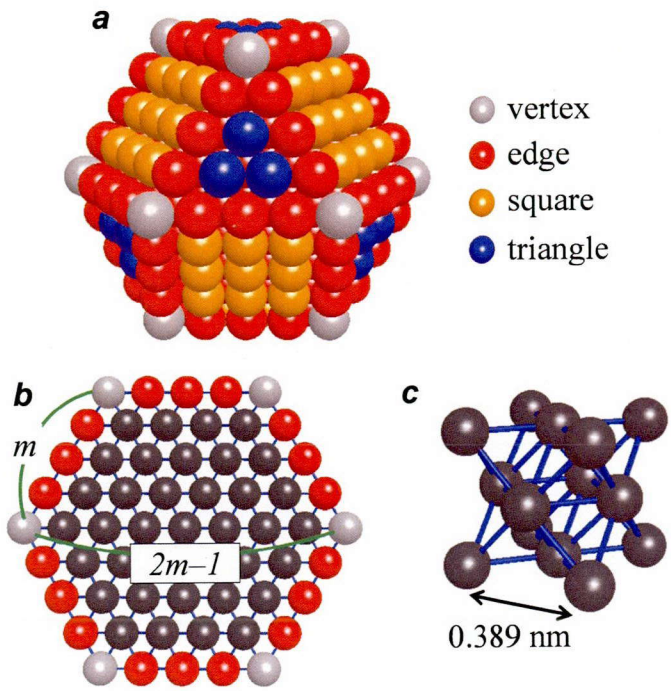

Figure 7. (a) The *fcc* cuboctahedron model for Pd particles. (b) The largest cross-sectional (111) hexagonal facet of the Pd particle. (c) The unit lattice of Pd particle.

$$N_{\text{total}}* = \frac{1}{3}(2m-1)(5m^2-5m+3) \tag{7}$$

$$\begin{aligned} N_{\text{surface}}* &= 10m^2 - 20m + 12 \\ &= N_{\text{vertex}}* + N_{\text{edge}}* + N_{\text{square}}* + N_{\text{triangle}}* \end{aligned} \tag{8}$$

The numbers of Pd atoms on the specific surface sites (N_{specific}*) such as vertex, edge, square, and triangle sites per Pd particles are therefore expressed by the following equations.[51]

$$N_{\text{vertex}}* = 12 \tag{9}$$

$$N_{\text{edge}}* = 24(m-2) \tag{10}$$

$$N_{\text{square}}* = 6(m-2)^2 \tag{11}$$

$$N_{\text{triangle}}* = 4(m-3)(m-2) \tag{12}$$

As shown in **Figure 3-7b**, the number of Pd atoms on the diagonal line of the largest cross-sectional (111) facet of Pd particle is expressed as $2m$–1. The lattice constant of Pd is 0.389 nm (**Figure 3-7c**),[52] and the atomic diameter of Pd is 0.274 nm.[53] The diameter of Pd particle (d_{Pd}) is therefore expressed as follows.

$$d_{\text{Pd}}\ (\text{nm}) = \frac{0.389}{\sqrt{2}}\{(2m-1)-1\} + 0.274 \tag{13}$$

The number of Pd particles per unit weight of Pd (n_{particle}), and the number of Pd atoms on the specific surface site (vertex, edge, square, triangle) per unit weight of Pd (N_{specific}) can therefore be expressed

using the molecular weight of Pd [M_w (= 106.42 g mol^{-1})], as follows.

$$n_{\text{particle}}\ (\text{mol g}^{-1}) = \frac{1}{M_{\text{W}} \times N_{\text{total}}\ *} \tag{14}$$

$$N_{\text{specific}}\ (\text{mol g}^{-1}) = N_{\text{specific}}\ * \times n_{\text{particle}} \tag{15}$$

As shown in **Figure 3-1**, the average diameters of Pd particles (d_{Pd}) for catalysts were determined by TEM observations to be 1.6 nm ($Pd_{0.1}/TiO_2$), 2.3 nm ($Pd_{0.3}/TiO_2$), 2.6 nm ($Pd_{0.5}/TiO_2$), and 4.1 nm ($Pd_{1.0}/TiO_2$), respectively. The shell numbers (m) for Pd particles on the respective catalysts can therefore be calculated using eq 13. The numbers of Pd atoms on the specific surface site per unit weight of Pd ($N_{specific}$) can then be determined using eqs 9–12, 14, and 15. **Figure 3-8** shows the relationship between the diameter of Pd particles and their respective $N_{specific}$ values. The N_{vertex} and N_{edge} values decrease with an increase in the size of Pd particle, and the N_{square} values scarcely change with the Pd particle size. These profiles are completely different from the catalytic activity of Pd particles for imine hydrogenation (Figure 6, black). In contrast, the $N_{tiangle}$ value increases with an increase in the Pd particle size, and the profile is very similar to the imine hydrogenation profile. This calculation result implies that Pd atoms on the triangle site are active for imine hydrogenation.

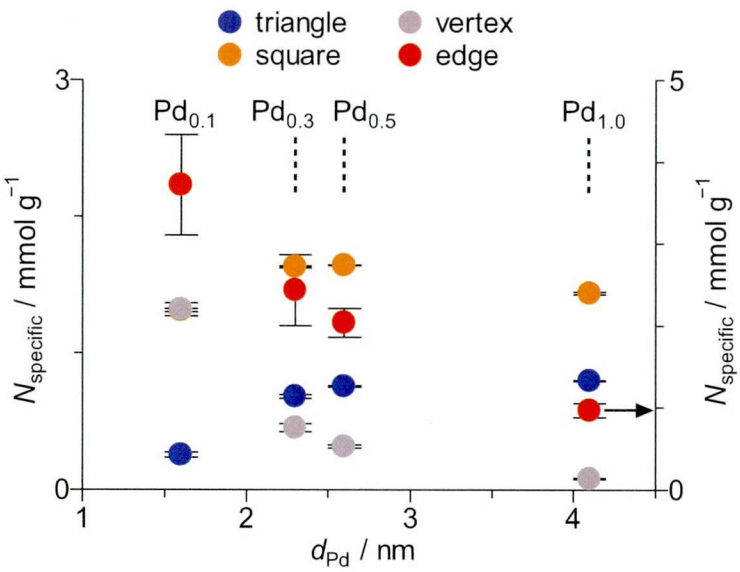

Figure 3-8. Relationship between the diameter of Pd particles on the respective Pd_x/TiO_2 catalyst and the number of Pd atoms on the specific surface site of Pd particle per unit weight of Pd.

This is further confirmed by the turnover number for imine hydrogenation per number of Pd atoms on the specific surface site ($TON_{specific}$). The amount of secondary amine **2** (mol) formed during hydrogenation of imine **1** by H_2 with respective Pd_x/TiO_2 catalysts in the dark (**Figure 3-6**) was divided

by the Pd amount (0.28 μmol) and the respective $N_{specific}$ values, using the following equation.

$$\mathrm{TON}_{specific} = \frac{[\text{amount of product formed}]}{N_{specific} \times (0.28 \times 10^{-6})} \tag{16}$$

Figure 3-9 shows the relationship between the size of Pd particle on the catalysts and respective $\mathrm{TON}_{specific}$ values. The TON_{vertex}, TON_{edge}, and TON_{square} values change with the Pd particle size. In contrast, the $\mathrm{TON}_{triangle}$ values for the respective catalysts are similar and are independent of the Pd particle size. This result clearly indicates that the Pd atoms on the triangle site are the active site for imine hydrogenation.

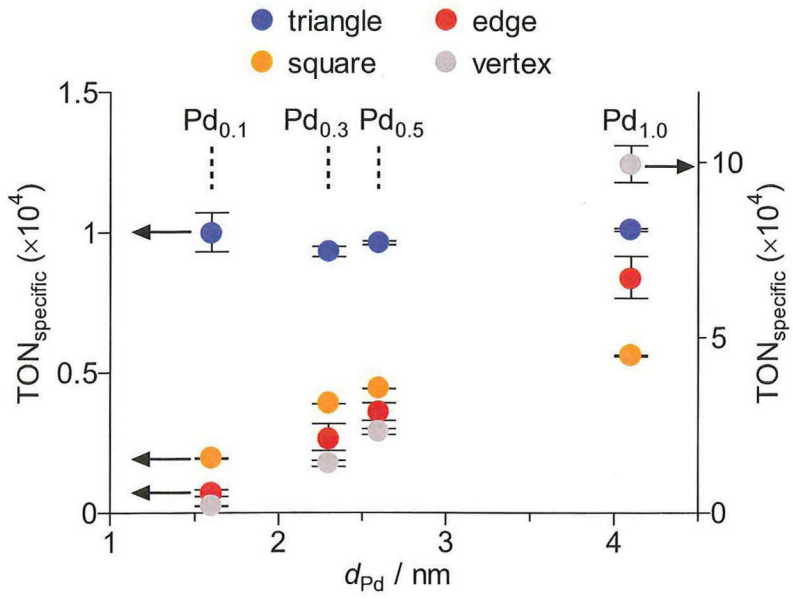

Figure 3-9. Relationship between the Pd particle size and the turnover number for hydrogenation of imine **1** per number of Pd atoms on the specific surface site ($\mathrm{TON}_{specific}$). The $\mathrm{TON}_{specific}$ value was calculated with the results for imine hydrogenation (Figure 6, black) using eq. 16.

The H atoms formed on the Pd particles diffuse around the particle surface,[54] meaning that the H atoms exist randomly on all parts of the Pd particle surface. The strong dependence of the imine hydrogenation activity on the number of Pd atoms on the triangle site is probably due to the adsorption of imine onto the triangle site. The Pd atoms on the triangle site have higher coordination number (9) than those on the other surface sites such as vertex (5), edge (7), and square (8), and are charged more positively. The imine is therefore preferentially adsorbed onto the positively charged triangle site via π electronic interaction with the aromatic ring and C=N bond. This adsorption may promote efficient hydrogenation by the H–Pd species, and result in clear relationship between the imine hydrogenation

activity and the number of Pd atoms on the triangle site. In the hydrogenation of alkyne and diene such as 2-methyl-3-butyn-2-ol[44] and 1,3-butadiene[55] on Pd particle catalysts with H_2, the catalytic activity also depends on the number of Pd atoms on the triangle site, and the dependence is also considered to be due to the adsorption of these olefins onto the positively charged triangle site. These reports support the above mechanism for imine hydrogenation.

3-6. Effect of alcohol on the imine hydrogenation

The above results suggest that the triangle site of Pd particles is the active site for imine hydrogenation. The number of these Pd atoms increases with an increase in the Pd particle size, and the Pd_x/TiO_2 catalyst with higher Pd loadings, which contain larger Pd particles, efficiently promotes imine hydrogenation. However, as shown in **Figure 3-4b** and **c**, photocatalytic reaction of benzyl alcohol and aniline with $Pd_{1.0}/TiO_2$ shows much lower activity for imine hydrogenation than $Pd_{0.3}/TiO_2$. This is inconsistent with the results for imine hydrogenation with H_2 (**Figure 3-6**, black).

The lower imine hydrogenation activity of larger Pd particles is because alcohols are adsorbed onto the larger triangle site more strongly than imines and undergo hydrogenation. **Figure 3-6** (white) shows the results for imine hydrogenation with H_2, when carried out in benzyl alcohol. The hydrogenation activity of smaller Pd particles is similar to that obtained in MeCN (black), but the activity of larger Pd particles is decreased significantly. This data clearly indicates that the imine hydrogenation on larger Pd particles is suppressed by alcohol. In these cases, GC analysis detected the formation of toluene. This indicates that, as reported,[56] Pd particles promote hydrogenation of alcohol by the H–Pd species leading to hydrogenolysis.

Figure 3-10a shows the amount of toluene formed during hydrogenation of benzyl alcohol with H_2 in the dark with respective Pd_x/TiO_2 catalysts at the identical Pd amount (0.28 μmol). The hydrogenation activity increases with the Pd particle size, and the profile is very similar to the imine hydrogenation profile (**Figure 3-6**, black). **Figure 3-10b** shows the turnover number for toluene formation per number of specific surface site ($TON_{specific}$) calculated using eq. 16. The $TON_{triangle}$ values for all of the catalysts are similar as is the case for imine hydrogenation (**Figure 3-9**). These findings indicate that the hydrogenation of alcohol is also promoted on the triangle site of Pd particles, and this suppresses the imine hydrogenation.

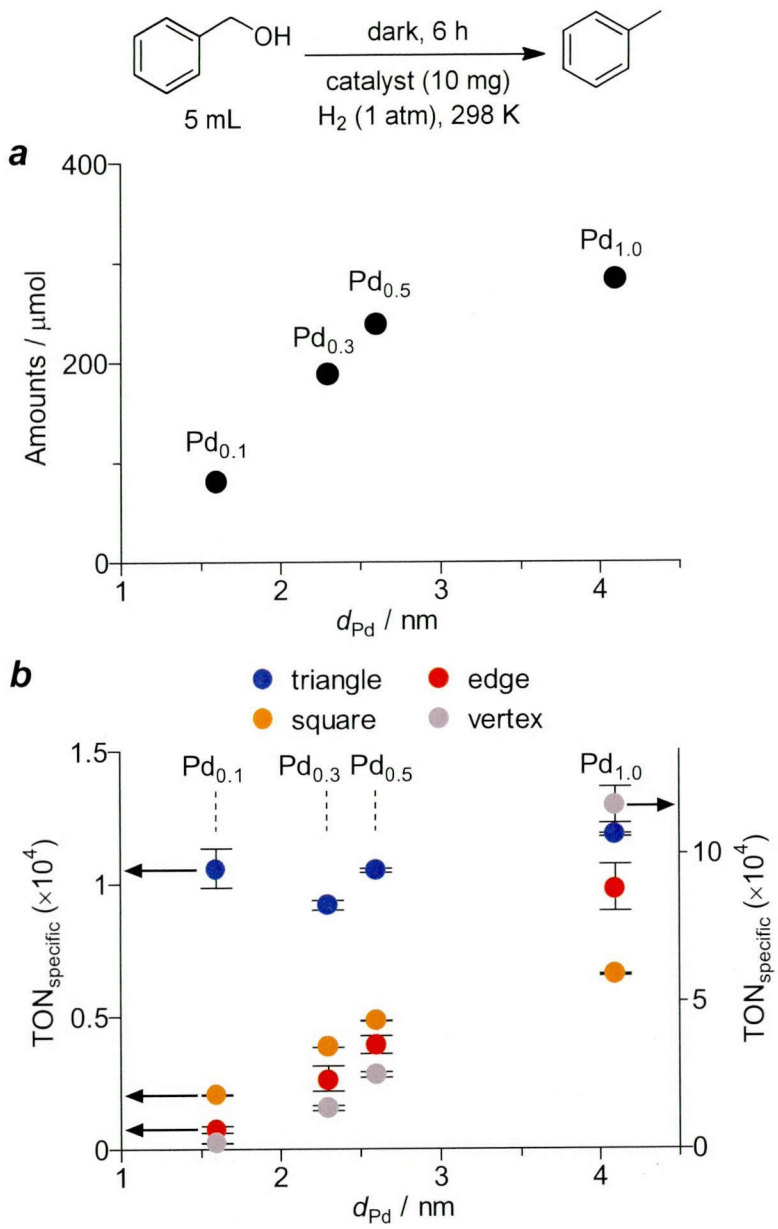

Figure 3-10. (a) Amount of toluene formed during reaction of benzyl alcohol with respective Pd_x/TiO_2 catalysts (Pd: 0.28 μmol) under H_2 in the dark. The amounts of catalysts used are: 30 mg ($Pd_{0.1}$), 10 mg ($Pd_{0.3}$), 5 mg ($Pd_{0.5}$), and 3 mg (Pd_1), respectively. (b) Relationship between the Pd particle size and the turnover number for toluene formation per number of Pd atoms on the specific surface site ($TON_{specific}$). The $TON_{specific}$ values were calculated using eq. 16.

The strongly suppressed imine hydrogenation on larger Pd particles is probably due to the stronger adsorption of alcohol than imine onto larger triangle site by their different adsorption modes. As shown in **Figure 3-11**, benzyl alcohol has a planer structure and is adsorbed very strongly onto the Pd surface via π interaction of aromatic ring and the lone pair electron of oxygen atom.[57] In contrast, the imine has a twisted structure[58] and may be adsorbed more weakly onto the Pd surface. The interaction between

alcohol and the Pd surface is probably strengthened by an increase in the area of triangle site. This probably leads to enhanced alcohol adsorption onto the larger Pd particles and suppresses imine hydrogenation more strongly. As shown in **Figures 3-4** and **5**, larger amount of toluene is produced during photocatalytic reaction of alcohol in the presence of catalysts with larger Pd particle. This indicates that the decreased imine hydrogenation activity of larger Pd particle is due to the strong adsorption of alcohols. These results suggest that the $Pd_{0.3}/TiO_2$ catalyst with 2–2.5 nm Pd particles, which contains relatively larger number of triangle site Pd atoms but does not allow strong adsorption of alcohols, shows the highest activity for imine hydrogenation and promotes efficient *N*-monoalkylation of primary amine with alcohol under photoirradiation.

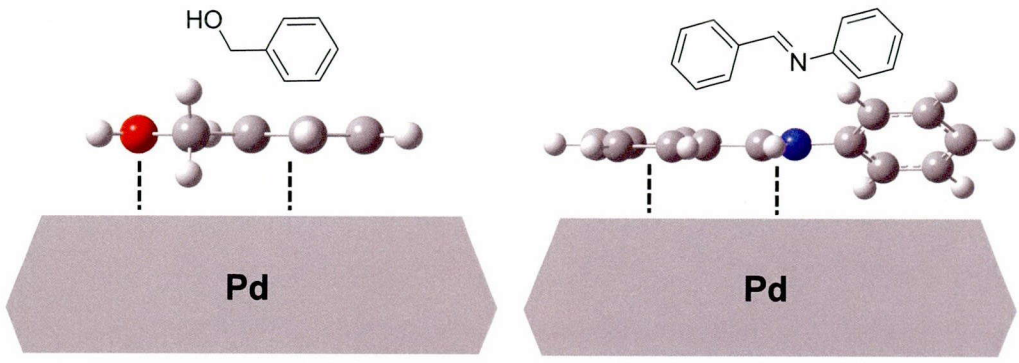

Figure 3-11. Schematic representation of different adsorption modes of benzyl alcohol and imine **1** onto the surface of Pd particle. Geometry optimizations of the molecules were performed with B3LYP/6-31G* basis set.

4. Conclusion

We found that Pd/TiO_2 catalyst promotes *N*-monoalkylation of primary amine with alcohol under photoirradiation at room temperature. Several kinds of secondary amines are successfully produced with high yields. Tandem photocatalytic and catalytic reactions promote three consecutive reactions, consisting of Pd-assisted alcohol oxidation on the photoactivated TiO_2, catalytic condensation of the formed aldehydes with amines on the TiO_2 surface, and hydrogenation of formed imine with H atoms on the Pd particles. The rate-determining reaction is the imine hydrogenation as the final step. The reaction is promoted on the Pd atoms on the triangle site of the Pd particle via an adsorption of imine. The imine adsorption onto the larger triangle site is strongly suppressed by competitive adsorption of alcohol. As a result of this, the catalyst with 2–2.5 nm Pd particles, which contain relatively larger number of triangular Pd atoms and do not promote strong alcohol adsorption, shows the highest activity for imine

hydrogenation and promotes efficient *N*-alkylation of amine with alcohol under photoirradiation. This tandem catalytic system offers significant advantages: (i) no harmful byproduct forms; (ii) the reaction proceeds at room temperature; and, (iii) several secondary amines are successfully produced. The tandem reactions promoted by photocatalytic and catalytic actions, therefore, have a potential to be a powerful method for one-pot synthesis of organic compounds in an environmentally-friendly way.

5. References

[1] Lee, J. M.; Na, Y.; Han, H.; Chang, S. *Chem. Soc. Rev.* **2004**, *33*, 302.

[2] Kolb, H. C.; VanNieuwenhze, M. S.; Sharpless, K. B. *Chem. Rev.* **1994**, *94*, 2483.

[3] Wasilke, J.-C.; Obrey, S. J.; Baker, R. T.; Bazan, G. C. *Chem. Rev.* **2005**, *105*, 1001.

[4] Gunanathan, C.; Ben-David, Y.; Milstein, D. *Science* **2007**, *317*, 790.

[5] Cadierno, V.; Francos, J.; Gimeno, J.; Nebra, N. *Chem. Commun.* **2007**, 2536.

[6] Zweifel, T.; Naubron, J.-V.; Grützmacher, H. *Angew. Chem. Int. Ed.* **2009**, *48*, 559.

[7] Yin, L.; Liebscher, J. *Chem. Rev.* **2007**, *107*, 133.

[8] Motokura, K.; Fujita, N.; Mori, K.; Mizugaki, T.; Ebitani, K.; Kaneda, K. *J. Am. Chem. Soc.* **2005**, *127*, 9674.

[9] Felpin, F.-X.; Fouquet, E. *ChemSusChem* **2008**, *1*, 718.

[10] Kim, J. W.; Yamaguchi, K.; Mizuno, N. *Angew. Chem. Int. Ed.* **2008**, *47*, 9249.

[11] Shiraishi, Y.; Sugano, Y.; Tanaka, S.; Hirai, T. *Angew. Chem. Int. Ed.* **2010**, *49*, 1656.

[12] Salvatore, R. N.; Yoon, C. H.; Jung, K. W. *Tetrahedron* **2001**, *57*, 7785.

[13] Buchwald, S. L.; Mauger, C.; Mignani, G.; Scholz, U. *Adv. Synth. Catal.* **2006**, *348*, 23.

[14] Navarro, O.; Marion, N.; Mei, J.; Nolan, S. P. *Chem. –Eur. J.* **2006**, *12*, 5142.

[15] Hamid, M. H. S. A.; Slatford, P. A.; Williams, J. M. J. *Adv. Synth. Catal.* **2007**, *349*, 1555.

[16] Guillena, G.; Ramón, D. J.; Yus, M. *Chem. Rev.* **2010,** *110,* 1611.

[17] Guillena, G.; Ramón, D. J.; Yus, M. *Angew. Chem. Int. Ed.* **2007**, *46*, 2358.

[18] Nixon, T. D.; Whittlesey, M. K.; Williams, J. M. J. *Dalton Trans.* **2009**, 753.

[19] Tsuji, Y.; Takeuchi, R.; Ogawa, H.; Watanabe, Y. *Chem. Lett.* **1986**, *15*, 293.

[20] Watanabe, Y.; Tsuji, Y.; Ohsugi, Y. *Tetrahedron Lett.* **1981**, *22*, 2667.

[21] Naskar, S.; Bhattacharjee, M. *Tetrahedron Lett.* **2007**, *48*, 3367.

[22] Fujita, K.; Enoki, Y.; Yamaguchi, R. *Tetrahedron* **2008**, *64*, 1943.

[23] Blank, B.; Madalska, M.; Kempe, R.; *Adv. Synth. Catal.* **2008**, *350*, 749.

[24] Michlik, S.; Kempe, R. *Chem. –Eur. J.* **2010**, *16*, 13193.

[25] Zhang, Y.; Qi, X.; Cui, X.; Shi, F.; Deng, Y. *Tetrahedron Lett.* **2011**, *52*, 1334.

[26] Kwon, M. S.; Kim, S.; Park, S.; Bosco, W.; Chidrala, R. K.; Park, J. *J. Org. Chem.* **2009**, *74*, 2877.

[27] Shimizu, K.; Nishimura, M.; Satsuma, A. *ChemCatChem* **2009**, *1*, 497.

[28] Yamaguchi, K.; Mizuno, N. *Synlett* **2010**, 16, 2365.

[29] Kim, J. W.; Yamaguchi, K.; Mizuno, N. *J. Catal.* **2009**, *263*, 205.

[30] Yamaguchi, K.; He, J.; Oishi, T.; Mizuno, N. *Chem. –Eur. J.* **2010**, *16*, 7199.

[31] He, J.; Yamaguchi, K.; Mizuno, N.; *Chem. Lett.*, **2010**, *39*, 1182.

[32] He, L.; Lou, X.-B.; Ni, J.; Liu, Y.-M.; Cao, Y.; He, H.-Y.; Fan, K.-N. *Chem. –Eur. J.* **2010**, *16*, 13965.

[33] Corma, A.; Ródenas, T.; Sabater, M. J. *Chem. –Eur. J.* **2010**, *16*, 254.

[34] Shiraishi, Y.; Ikeda, M.; Tsukamoto, D.; Tanaka, S.; Hirai, T. *Chem. Commun.* **2011**, *47*, 4811.

[35] Sclafani, A.; Mozzanega, M. -N.; Pichat, P. *J. Photochem. Photobiol., A* **59**, *1991*, 181.

[36] Bamwenda, G. R.; Tsubota, S.; Nakamura, T.; Haruta, M. *J. Photochem. Photobiol., A* **1995**, *89*, 177.

[37] Ohtani, B.; Kakimoto, M.; Nishimoto, S.; Kagiya, T. *J. Photochem. Photobiol., A* **1993**, *70*, 265.

[38] Shiraishi, Y.; Takeda, Y.; Sugano, Y.; Ichikawa, S.; Tanaka, S.; Hirai, T. *Chem. Commun.* **2011**, *47*, 7863.

[39] Jennings, W.B.; Lovely, C. J. *Tetrahedron* **1991**, *47*, 5561.

[40] Krupka, J.; Patera, J. *Appl. Catal. A.* **2007**, *330*, 96.

[41] Tsukamoto, D.; Shiraishi, Y.; Sugano, Y.; Ichikawa, S.; Tanaka, S.; Hirai, T. *J. Am. Chem. Soc.* **2012**, *134*, 6309.

[42] Schottky, W. *Z. Phys.* **1939**, *113*, 367.

[43] Uchihara, T.; Matsumura, M.; Yamamoto, A.; Tsubomura, H. *J. Phys. Chem.* **1989**, *93*, 5870.

[44] Semagina, N.; Renken, A.; Laub, D.; Kiwi-Minsker, L. *J. Catal.* **2007**, *246*, 308.

[45] Bars, J. Le.; Specht, U.; Bradlay, J. S.; Blackmond, D. G. *Langmuir* **1999**, *15*, 7621.

[46] Coq, B.; Figueras, F. *J. Mol. Catal. A* **2001**, *173*, 117.

[47] Molnár, A.; Sárkány, A.; Varga, M. *J. Mol. Catal. A* **2001**, *173*, 185.

[48] Wilson, O. M.; Knecht, M. R.; Garcia-Martinez, J. C.; Crooks, R. M. *J. Am. Chem. Soc.* **2006**, *128*, 4510.

[49] Arruda, T. M.; Shyam, B.; Zeigelbauer, J. M.; Mukerjee, S.; Ramaker, D. E. *J. Phys. Chem. C* **2008**, *112*, 18087.

[50] Shiraishi, Y.; Tsukamoto, D.; Sugano, Y.; Shiro, A.; Ichikawa, S.; Tanaka, S.; Hirai, T. *ACS Catal*

2012, *2*, 1984.

[51] Benfield, R. E. *J. Chem. Soc. Faraday Trans.* **1992**, *88*, 1107.

[52] Fornander, H.; Hultman, L.; Birch, J.; Sundgren, J.-E. *J. Cryst. Growth* **1998**, *186*, 189.

[53] Pauling, L. *J. Am. Chem. Soc.* **1947**, *69*, 542.

[54] Parambhath, V. B.; Nagar, R.; Sethupathi, K.; Ramaprabhu, S. *J. Phys. Chem.* **2011**, *115*, 15679.

[55] Silvestre-Albero, J.; Rupprechter, G.; Freund, H. J. *Chem. Commun.* **2006**, 80.

[56] Keresszegi, C.; Ferri, D.; Mallat, T.; Baiker, A. *J. Phys. Chem. B* **2005**, *109*, 958.

[57] Souto, R. M.; Rodríguez, J. L.; Pastor, E. *Langumuir* **2000**, *16*, 8456.

[58] Traetteberg, M.; Hilmo, I. *J. Mol. Struct.* **1978**, *48*, 395.

[59] Shiraishi, Y.; Saito, N.; Hirai, T. *J. Am. Chem. Soc.* **2005**, *127*, 8304.

[60] Shiraishi, Y.; Saito, N.; Hirai, T. *J. Am. Chem. Soc.* **2005**, *127*, 12820.

[61] Tsukamoto, D.; Shiro, A.; Shiraishi, Y.; Sugano, Y.; Ichikawa, S.; Tanaka, S.; Hirai, T. *ACS Catal* **2012**, *2*, 599.

[62] Shiraishi, Y.; Ichimura, C.; Sumiya, S.; Hirai, T. *Chem. –Eur. J.* **2011**, *17*, 8324.

[63] Shiraishi, Y.; Sumiya, S.; Hirai, T. *Chem. Commun.* **2011**, *47*, 4953.

Chapter IV

Dehalogenation of Organic Halides on TiO_2 Loaded with Bimetallic Pd-Pt Alloy Nanoparticles

1. Introduction

The dehalogenation of organic halides is a significant process for the removal of halogenated organic pollutants and the synthesis of fine chemicals.[1] The reaction is currently carried out via the hydrodehalogenation processes with catalysts containing Pd particles using molecular hydrogen (H_2) as the hydrogen source,[2] which inevitably holds explosion risks. Alternative methods with safe hydrogen sources such as alcohols are therefore desirable.

Recently, a H_2-free dehalogenation method with alcohol as the hydrogen source was proposed by Fuku et al.[3] They employed a photocatalytic reaction using TiO_2 loaded with 1 wt% Pd particles (Pd/TiO_2). Photoirradiation (λ >300 nm) of a 2-PrOH solution containing chlorobenzene with Pd/TiO_2 and a base (NaOH) produces the corresponding benzene quantitatively. The reactions are initiated by photoexcitation of TiO_2, producing the electron (e^-) and positive hole (h^+) pairs (eqn (1)). The h^+ oxidizes 2-PrOH and produces acetone and protons (eqn (2)).[4] The H^+ is activated by the reduction with e^- on the Pd particles (eqn (3)), and the formed hydrides species (H^-–Pd) promote dehalogenation (eqn (4)). The removed Cl^- is solidified as NaCl by the reaction with NaOH (eqn (5)). The overall reaction is expressed as eqn (6).

$$TiO_2 + h\nu \rightarrow h^+ + e^- \quad (1)$$

$$(CH_3)_2CHOH + 2h^+ \rightarrow (CH_3)_2CO + 2H^+ \quad (2)$$

$$H^+ + 2e^- + Pd \rightarrow H^- - Pd \quad (3)$$

$$Ar-C + H^- - Pd \rightarrow Ar-H + Cl^- + Pd \quad (4)$$

$$H^+ + Cl^- + NaOH \rightarrow H_2O + NaCl\downarrow \quad (5)$$

$$Ar\text{-}Cl + (CH_3)_2CHOH + NaOH \xrightarrow{h\nu,\ TiO_2} Ar\text{-}H + (CH_3)_2CO + H_2O + NaCl\downarrow \quad (6)$$

These reactions proceed at room temperature with alcohol as the hydrogen source, and have a potential to be a safe and sustainable dehalogenation process. The reactions, however, proceed very slowly when compared to the conventional method with H_2. The activity improvement is therefore necessary.

Herein, we report that TiO_2 loaded with bimetallic Pd-Pt alloy particles ($PdPt/TiO_2$) promotes highly efficient photocatalytic dehalogenation. The activity is more than three times that of Pd/TiO_2 and

higher than the conventional method with H_2. The high activity is due to the enhanced consumption of photoformed e^- on the Pt site by H^+ reduction and efficient transfer of the formed hydrogen atom to the adjacent Pd site within the alloy particles.

2. Experimental

2-1. Materials

All reagents were purchased from Wako, Tokyo Kasei, and Sigma-Aldrich and used without further purification. Japan Reference Catalyst JRC-TIO-4 TiO_2 particles were kindly supplied from Catalysis Society of Japan.

Pd_1Pt_y/TiO_2 catalysts [y (wt%) = Pt/(Pt + TiO_2) × 100; y = 1, 3, 5, 7, 10] were prepared as follows: TiO_2 (0.5 g), $Pd(NO_3)_2$ (11 mg), and H_2PtCl_6 (13, 27, 70, 94, 147 mg) were added to water and evaporated with vigorous stirring at 353 K for 12 h. The obtained powders were calcined at 673 K for 3 h under air flow and then reduced under H_2 at 473 K for 2 h.

Pd_1+Pt_5/TiO_2 catalyst was prepared as follows: TiO_2 (0.5 g) and $Pd(NO_3)_2$ (11 mg) were added to water and evaporated with vigorous stirring at 353 K for 12 h. The obtained powders were calcined at 673 K for 3 h under air flow and then reduced under H_2 at 473 K for 2 h. The obtained powders and H_2PtCl_6 (70 mg) were added to water and evaporated at 353 K for 12 h under vigorous stirring. The resultant was calcined at 673 K for 3 h under air flow and reduced under H_2 at 473 K for 2 h.

2-2. Photoreaction procedure

Photoreactions were performed within a Pyrex glass tube (capacity, 20 mL) using a 2 kW Xe lamp (λ >300 nm; Ushio Inc.) with magnetic stirring at 298 K. The light intensity was determined by a spectroradiometer to be 192.7 W m^{-2} at 300–800 nm. The light intensity at 300–400 nm, which mainly contributes to the photocatalytic reaction, is therefore calculated from the spectral irradiance to be 18.2 W m^{-2}. The reactant and product concentrations were determined by GC-FID or -TCD, using authentic samples as standards.

2-3. Analysis

The total Pd and Pt amounts of the catalysts were analyzed by an inductively-coupled argon plasma atomic emission spectrophotometer (Seiko Instruments, Inc.; SPS7800) after dissolution of the catalysts to an aqua regalia. Diffuse reflectance UV-vis spectra were measured on UV-vis spectrophotometer (Jasco Corp.; V-550 with Integrated Sphere Apparatus ISV-469) with $BaSO_4$ as a reference. TEM

observations were carried out using an FEI Tecnai G2 20ST analytical electron microscope operated at 200 kV, which is equipped with an Energy Dispersive X-ray Spectroscopy (EDX) detector. EDX spectra from a metallic particle were taken under Scanning Transmission Electron Microscopy (STEM) mode. XPS measurements were performed using a JEOL JPS-9000MX spectrometer using Mg Kα radiation as the energy source.

3. Results and discussion

3-1. Synthesis and characterization of catalysts

Pd_1Pt_y/TiO_2 with Pd-Pt alloy consisting of 1 wt% Pd [= Pd/(Pd + TiO_2) × 100] and different amounts of Pt [y (wt%) = Pt/(Pt + TiO_2) × 100] were prepared with Japan Reference Catalyst JRC-TIO-4 TiO_2 (equivalent to Degussa P25) by simultaneous impregnation of $Pd(NO_3)_2$ and H_2PtCl_6 followed by reduction with H_2).[5] A transmission electron microscopy (TEM) image of Pd_1Pt_5/TiO_2 showed spherical metal particles with an average diameter of 2.9 nm (**Figure 4-1**). The lower or higher Pt loadings create smaller or larger particles; $Pd_1Pt_1$and Pd_1Pt_{10} contain 2.5 and 3.4 nm particles, respectively. An X-ray photoelectron spectroscopy (XPS) of catalysts confirmed the presence of both Pd and Pt (**Figure 4-2**). An energy dispersive X-ray spectroscopy (EDX) of metal particles on Pd_1Pt_5/TiO_2 (**Figure 4-3**) determined the average Pt/Pd ratio as 4.95 (wt/wt), which is close to the ratio of the total amount of Pt and Pd (4.96) determined by ICP analysis. An X-ray diffraction (XRD) pattern of Pd_1Pt_5/TiO_2 (**Figure 4-4**) shows a (111) diffraction of the Pd-Pt alloy at 39.9°, which is located between the Pt(111) and Pd(111) diffractions (39.81 and 40.21). The lattice parameter of the alloy calculated from the XRD data (a = 0.391 nm) agrees with that calculated with the Vegard's law[6] (0.391 nm). In addition, the d-value calculated from the lattice spacing of the alloy in the TEM image (d_{111} = 0.225 nm, **Figure 4-5**) is in between the standard Pt (d_{111} = 0.2265 nm, JCPDS 04-0802) and Pd (d_{111} = 0.2246 nm, JCPDS 46-1043). These indicate that Pd-Pt alloy particles are indeed loaded on TiO_2. Diffuse reflectance UV-vis spectra (**Figure 4-6**) revealed that Pd_1Pt_y/TiO_2 with higher Pt loadings show increased absorbance at >300 nm due to light scattering by the Pt particles.

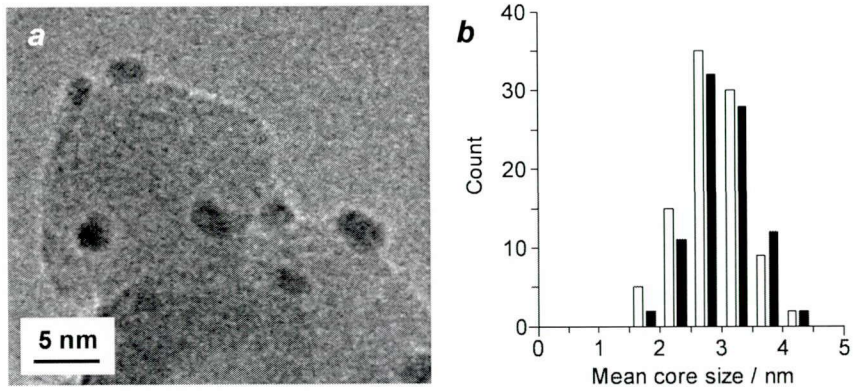

Figure 4-1. (a) TEM image of Pd_1Pt_5/TiO_2 and (b) size distribution of metal particles on (white) the fresh catalyst and (black) the catalyst recovered after 2nd reuse in reaction (**Table 1**, run 16).

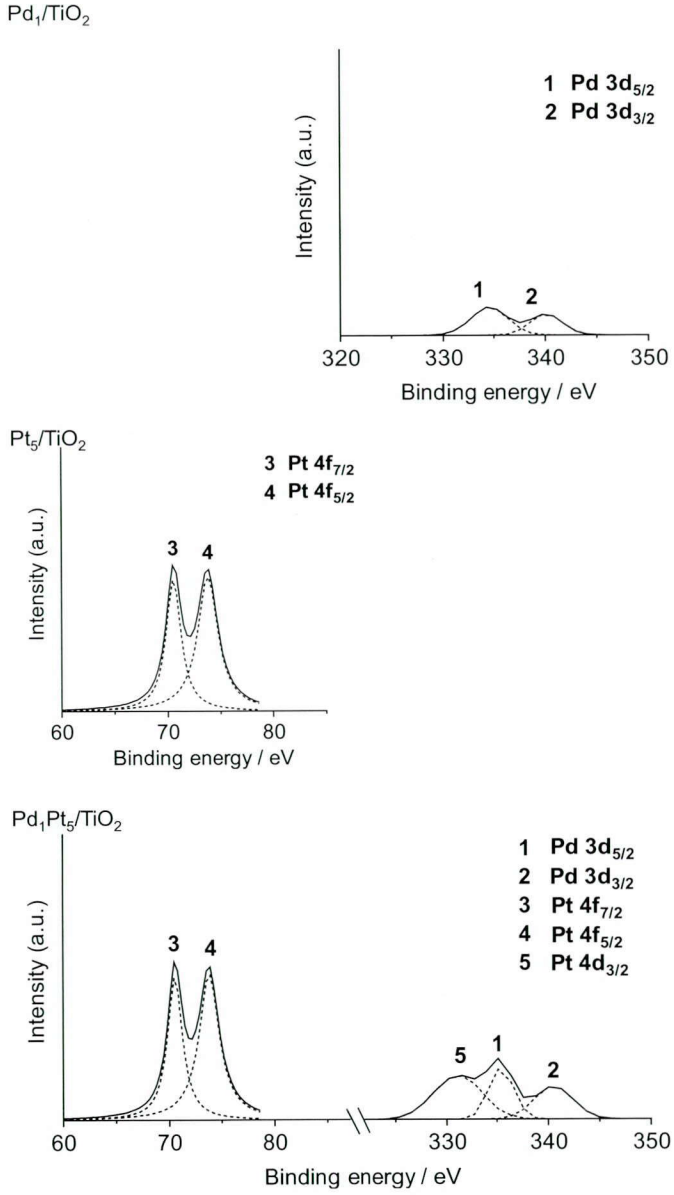

Figure 4-2. XPS results for respective catalysts.

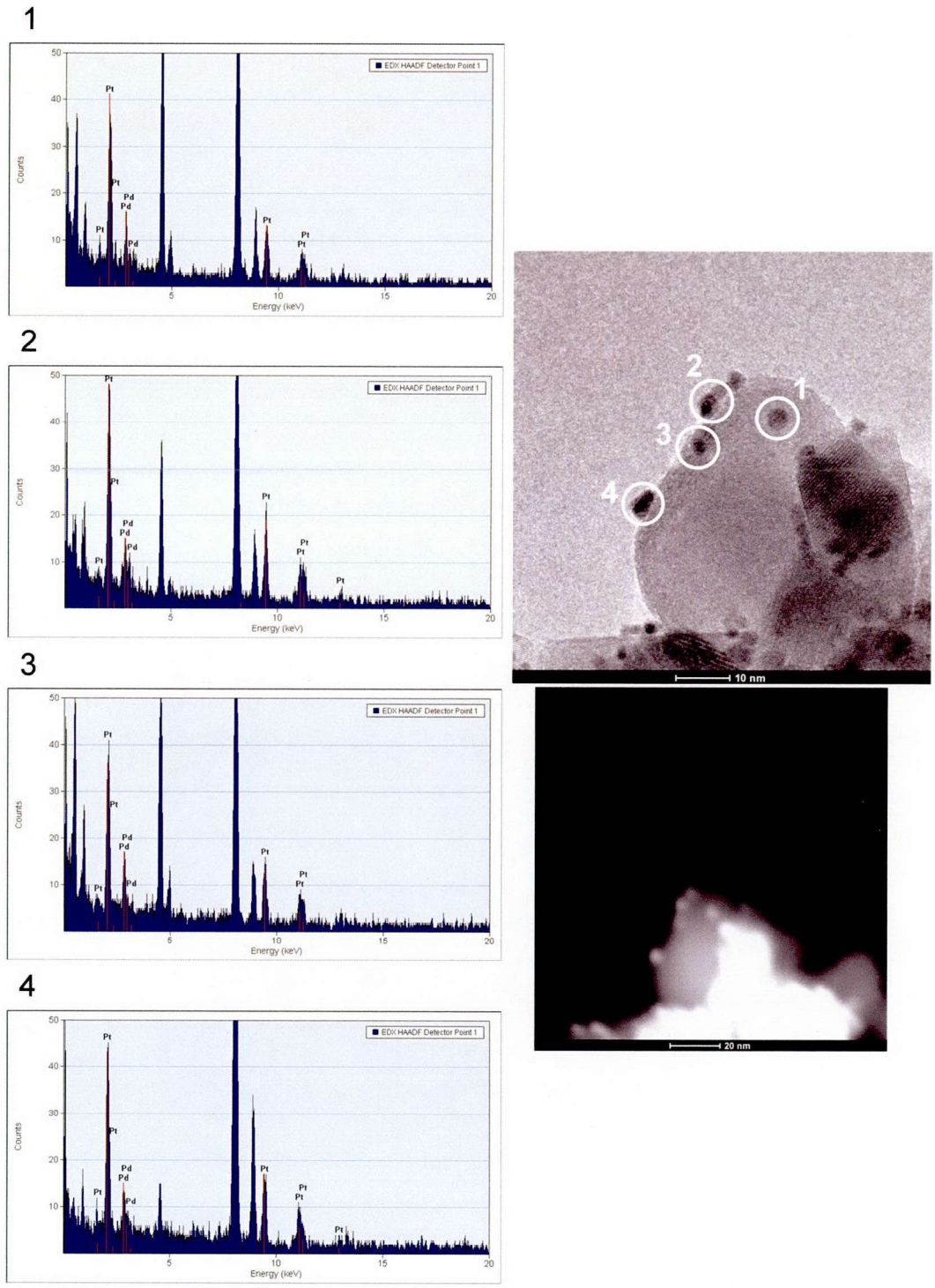

Figure 4-3. TEM and STEM-HAADF images of Pd_1Pt_5/TiO_2 and EDX spectra for respective metal particles.

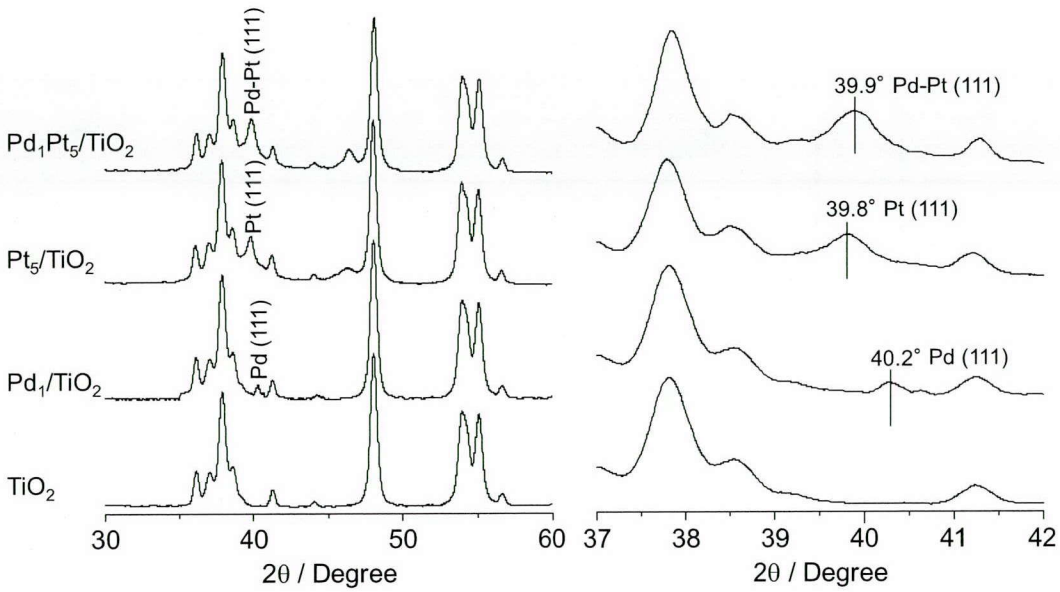

Figure 4-4. XRD patterns of respective catalysts.

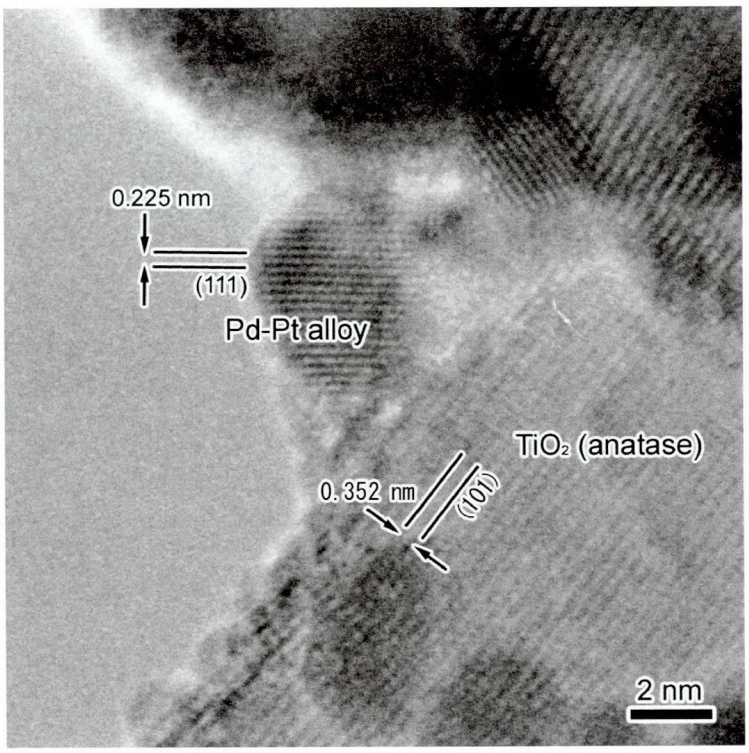

Figure 4-5. High-resolution TEM image of Pd_1Pt_5/TiO_2.

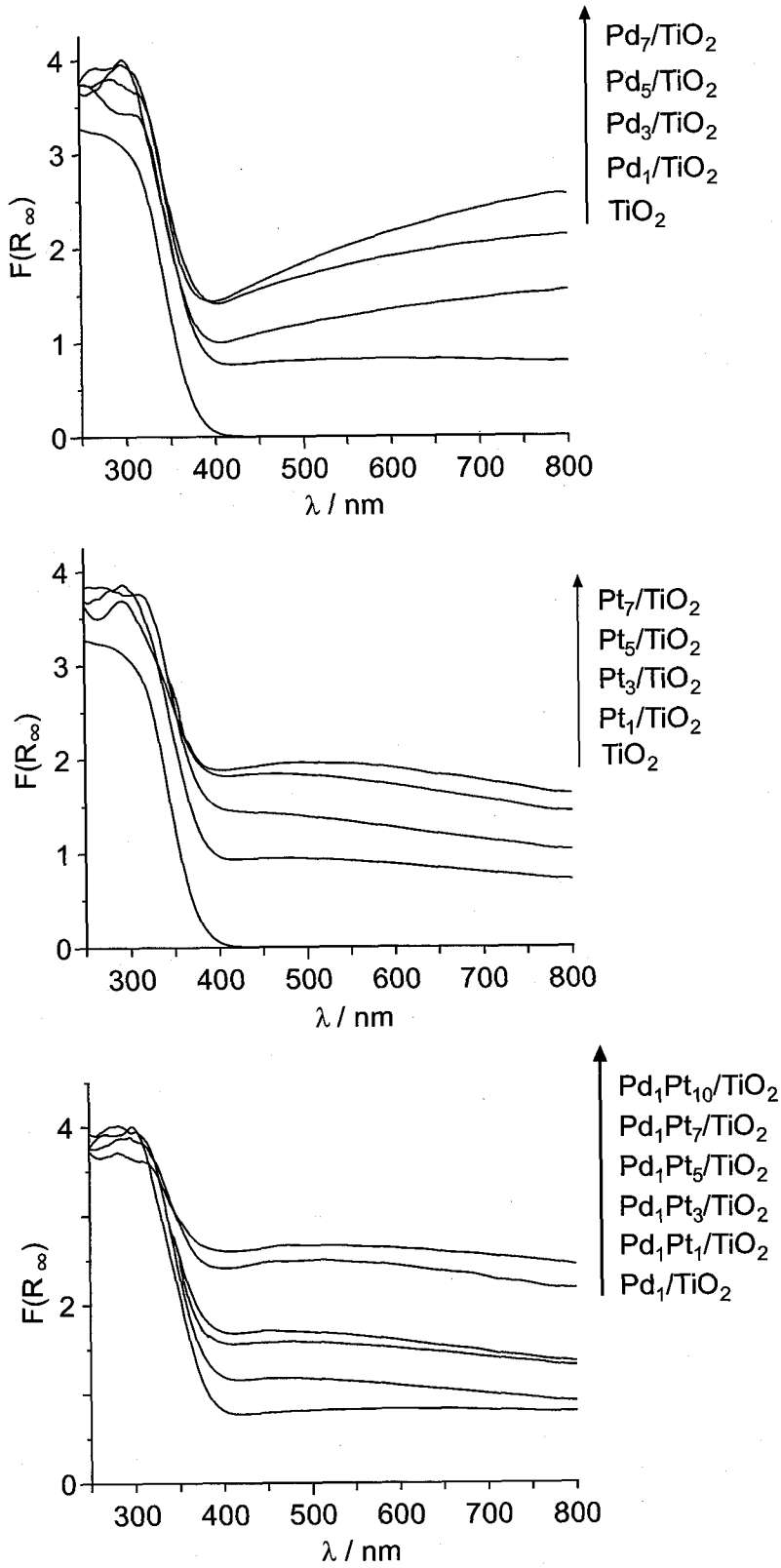

Figure 4-6. Diffuse reflectance UV-vis spectra of respective catalysts.

3-2. Photocatalytic activity of $PdPt/TiO_2$ catalysts

Table 4-1. Results of dechlorination of *p*-chlorotoluene in the photocatalytic and H_2 system.[a]

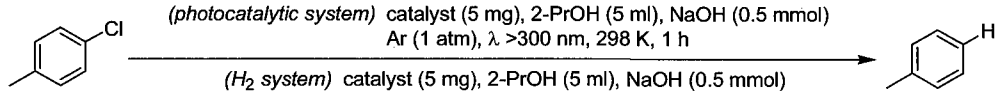

Run	Catalyst	Metal particle size[b] / nm	Photocatalytic system				H_2 system	
			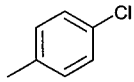 conv. / %	yield / %	formed / μmol	H^+ balance[c]	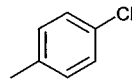 conv. / %	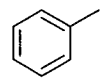 yield / %
1	Pd_1/TiO_2	5.3	20	19	42	0.92	56	54
2	Pd_3/TiO_2		21	20	43	0.96	56	54
3	Pd_5/TiO_2		19	18	41	0.88	52	51
4	Pd_7/TiO_2		14	13	29	0.90	35	34
5	Pd_1Pt_1/TiO_2	2.5	28	27	55	0.97	32	31
6	Pd_1Pt_3/TiO_2		45	43	88	0.97	26	23
7	Pd_1Pt_5/TiO_2	2.9	76	76	155	0.98	21	20
8	Pd_1Pt_7/TiO_2		39	38	80	0.95	15	13
9	Pd_1Pt_{10}/TiO_2	3.4	36	35	79	0.90	12	11
10	Pt_1/TiO_2	2.2	0	0	43		0	0
11	Pt_3/TiO_2		0	0	65		0	0
12	Pt_5/TiO_2	3.9	0	0	102		0	0
13	Pt_7/TiO_2		0	0	79		0	0
14	Pd_1+Pt_5/TiO_2		27	26	118	0.44	26	25
15[d]	Pt_1Pd_5/TiO_2		75	75				
16[e]	Pt_1Pd_5/TiO_2	3.1[f]	75	75				

[a] The results obtained with Pd_1Pt_5/TiO_2 in other solvents are summarized in **Table 4-2**. [b] Average diameter of metal nanoparticles determined by TEM observation (**Figure 5-1**). [c] Determined by eqn (8). [d] 1st reused after washing with 2-PrOH. [e] 2nd reuse. [f] Measured after 2nd reuse.

Table 4-1 summarizes the results of photocatalytic reaction (λ >300 nm) of *p*-chlorotoluene (0.2 mmol) in 2-PrOH (5 mL) with catalysts (5 mg) and NaOH (0.5 mmol) for 1 h at 298 K under Ar. The results obtained using H_2 (1 atm) in the dark at 298 K are also shown for comparison. Both

photocatalytic and H_2 systems (runs 1–9) selectively produce toluene. The toluene yields in the photocatalytic system with the catalysts containing Pd alone, Pd_x/TiO_2 [x (wt%) = Pd/TiO_2 × 100], are less than 21% (runs 1–4). In contrast, the yields in the H_2 system with Pd_x/TiO_2 are ca. 50%, indicating that the photocatalytic system is indeed inefficient.

The loading of Pd-Pt alloy particles significantly enhances the photocatalytic dechlorination (runs 5–9): Pd_1Pt_y/TiO_2 show increased toluene yields with an increase in the Pt amount of the particles, where Pd_1Pt_5/TiO_2 shows the highest yield (76%), which is more than three times that of Pd_x/TiO_2. In contrast, such alloying effect is not observed in the H_2 system (runs 5–9); the toluene yields decrease monotonically with the Pt loadings (<56%).

It is noted that the catalysts containing Pt alone, Pt_y/TiO_2 [y (wt%) = Pt/TiO_2 × 100], do not promote dechlorination (runs 10–13). This indicates that, on the alloy catalysts, the Pd site is active for dehalogenation. It is also noted that the Pd-Pt alloy site is necessary for efficient dehalogenation: a Pd_1+Pt_5/TiO_2 catalyst (run 14), prepared by a step-by-step deposition of respective Pd and Pt particles, scarcely enhances dehalogenation.

Table 4-2. Results of photocatalytic dechlorination of *p*-chlorotoluene in various solvent.[a]

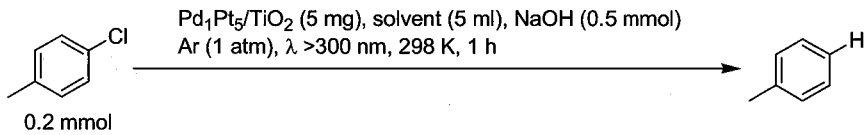

Run	Solvent	*p*-chlorotoluene conv. / %	Toluene yield / %	Aldehyde or ketone formed / μmol
1	MeCN	2	0	
2	Water/MeCN (1/1 v/v)	2	0	
3	EtOH	8	7	18
4	2-PrOH	76	76	155
5	*n*-butanol	5	4	12
6	*n*-hexanol	2	<1	<1

[a] the reaction conditions are identical to those of **Table 4-1**.

3-3. Reaction mechanism

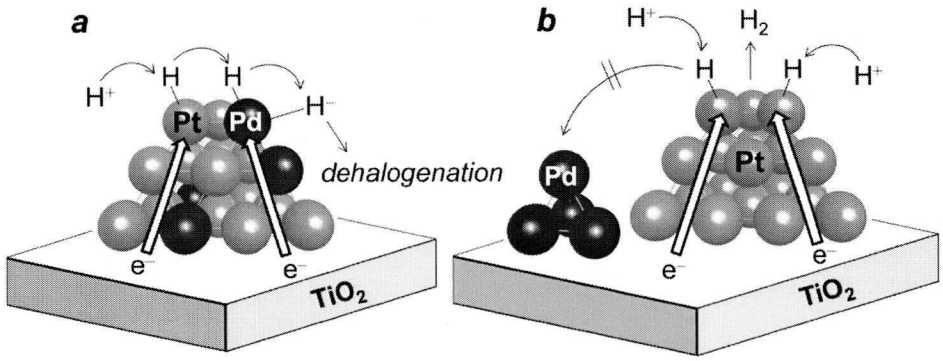

Scheme 4-1. The reaction sequence for protons on the metal particles of (a) Pd_1Pt_5/TiO_2 and (b) Pd_1+Pt_5/TiO_2 catalysts.

The high activity of the alloy catalyst is due to the efficient consumption of photoformed e^- by H^+ reduction on the Pt site and efficient transfer of the formed H atom to the adjacent Pd site (**Scheme 4-1a**). The efficient e^- consumption on Pt is confirmed by the amount of formed acetone (**Table 4-1**). Pd_x/TiO_2 produce <45 μmol acetone (runs 1–4), whereas Pt_y/TiO_2 produce larger amounts (runs 10–13). This is because e^- is efficiently trapped by Pt due to the larger work function[7] and consumed by H^+ reduction, facilitating efficient alcohol oxidation by h^+. As shown in run 12, Pt_5/TiO_2 produces the largest amount of acetone among Pt_y/TiO_2 and higher Pt loadings decrease the production. A similar tendency is observed for Pd_1Pt_y/TiO_2 :Pd_1Pt_5 produces the largest amount of acetone. The higher activity of Pd_1Pt_5/TiO_2 than Pd/TiO_2 is thus because the photoformed e^- is efficiently consumed by H^+ reduction on the Pt site, producing a H atom.[8]

$$H^+ + e^- + Pt \rightarrow H\text{–}Pt \qquad (7)$$

The H atom on Pt within the alloy particles is efficiently used for dehalogenation. This is confirmed by the H^+ balance, defined as the ratio of the formed dehalogenation product to that of the formed H^+. As shown by eqn (6), two H^+ formed by photooxidation of 2-PrOH are consumed by dehalogenation (eqn (3) and (4)) and reaction with NaOH (eqn (5)), respectively. The H^+ balance is therefore expressed by the ratio of the amount of formed toluene to that of formed acetone,

$$H^+ \text{ balance} = [\text{toluene formed}]/[\text{acetone formed}] \qquad (8)$$

Table 4-1 summarizes the H^+ balance for the respective systems obtained by photoreaction for 1 h. The values for Pd_x/TiO_2 are almost 1 (runs 1–4), indicating that H^+ formed by alcohol oxidation are

consumed quantitatively by dehalogenation on Pd (eqn (6)).[3] The values for $PdPt/TiO_2$ are also almost 1 (runs 5–9), suggesting that H^+ are also consumed quantitatively although H^+ are reduced on Pt (eqn (7)). The results suggest that, as shown in **Scheme 4-1a**, the H atom formed on Pt is transferred to the adjacent Pd site (H–Pd formation), which is probably due to the stronger H–Pd interaction.[9]

$$\text{H–Pt} \rightarrow \text{H–Pd} \tag{9}$$

The H atom is reduced to the hydride species (H^-–Pd) by e^-, which promotes dechlorination (eqn (4))

$$\text{H–Pd} + e^- \rightarrow H^-\text{–Pd} \tag{10}$$

As shown in run 14, the H^+ balance for the Pd_1+Pt_5/TiO_2 system is only 0.44. This is because the absence of Pd around the Pt site suppresses the H transfer from Pt to Pd and results in removal of H atoms by H_2 formation (**Scheme 4-1b**).[10]

$$\text{H– Pt} + \text{H– Pt} \rightarrow H_2\uparrow + 2\text{Pt} \tag{11}$$

Change in H_2 amount during reaction confirms this (**Figure 4-7**). Pd_1+Pt_5/TiO_2 promotes H_2 formation and dechlorination simultaneously; however, Pd_1Pt_5/TiO_2 scarcely produces H_2 until *p*-chlorotoluene disappears. The alloy sites are therefore necessary for efficient H transfer from the Pt to Pd sites.

The above results reveal that, on the alloy site (**Scheme 4-1a**), efficient reduction of H^+ by e^- on Pt, smooth H transfer to Pd, and reduction of H by e^- occur sequentially. This sequence produces a large amount of H^-–Pd species and promotes efficient dehalogenation. It must be noted that, as shown in runs 15 and 16 (**Table 4-1**), the alloy catalyst is reusable for dehalogenation at least two times without loss of activity and selectivity. In addition, as shown in **Figure 4-1b**, the size of Pd-Pt alloy particles scarcely changes even after the reaction.

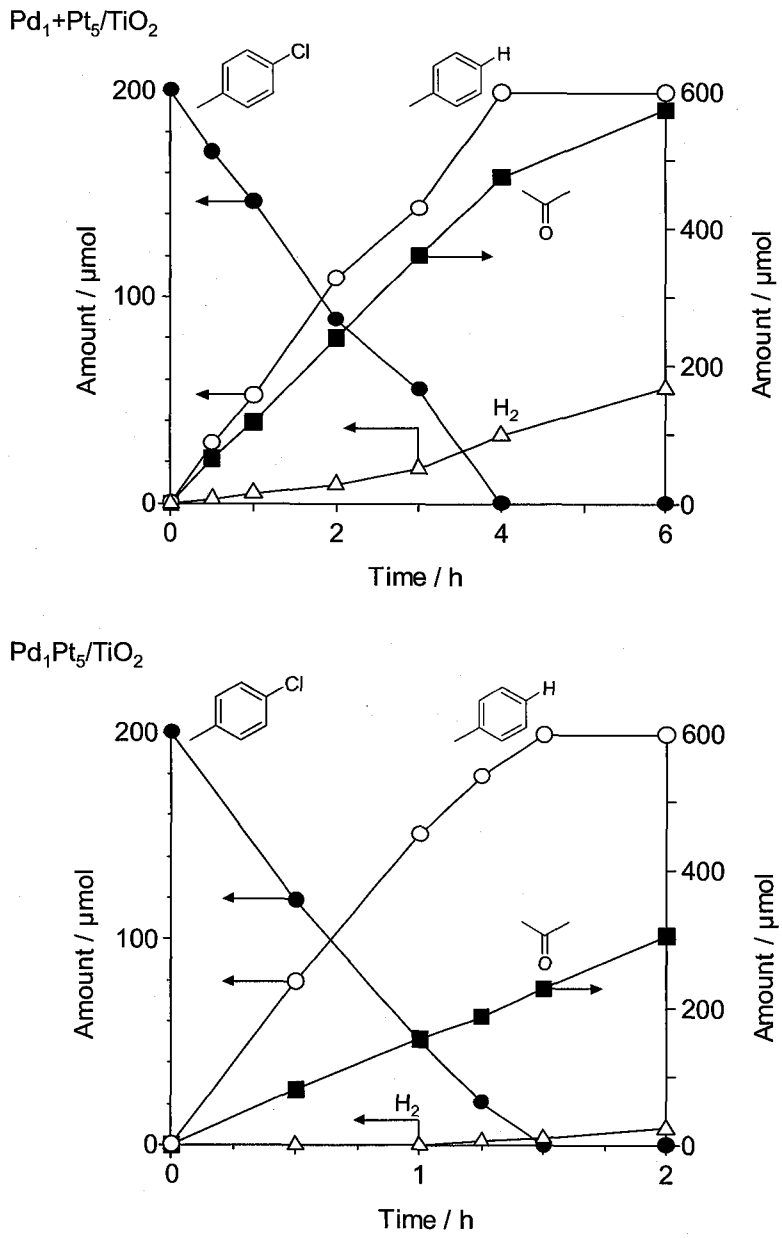

Figure 4-7. Time-dependent change in the amounts of substrate and products during photoirradiation of a 2-PrOH solution containing *p*-chlorotoluene with Pd_1+Pt_5/TiO_2 or Pd_1Pt_5/TiO_2 catalyst. The reaction conditions are identical to those in **Table 4-1**.

3-4. Dehalogenation of various aromatic halides

Table 4-3. Dehalogenation of various aromatic halides.

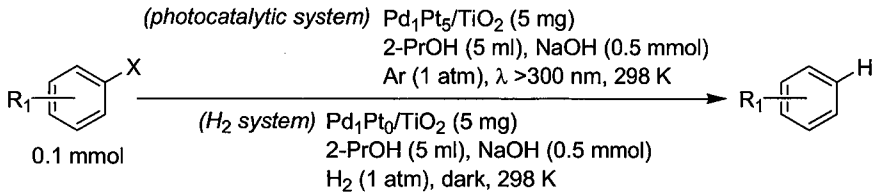

Run	Substrate	System	Time / h	Conv. / %	Yield / %
1		Photo	1.5	99	97
2		H_2	1.5	74	72
3		Photo	1	>99	99
4		H_2	1	52	51
5	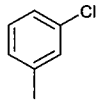	Photo	1	>99	99
6		H_2	1	58	57
7	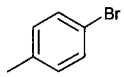	Photo	1	>99	99
8		H_2	1	77	76
9	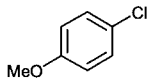	Photo	1	>99	97
10		H_2	1	76	75
11	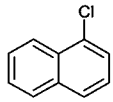	Photo	2	97	96
12		H_2	2	51	49
13	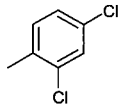	Photo	2	92	87 (toluene)
14		H_2	2	60	37 (toluene)

The alloy catalyst is tolerant for photocatalytic dehalogenation of various aromatic halides (**Table 4-3**). Pd_1Pt_5/TiO_2 produces the corresponding dehalogenation compounds with very high yield, and the catalytic activities are much higher than those obtained with Pd_1/TiO_2 using H_2.

4. Conclusion

In summary, we found that UV irradiation of TiO_2 loaded with Pd-Pt alloy promotes efficient dehalogenation. This offers crucial advantages: (i) safe alcohols can be used as a hydrogen source; and, (ii) the reaction proceeds much faster. The alloy catalyst that facilitates efficient production of active species (H^-–Pd) may also promote other hydrogenation reactions, and the work along these lines is currently in progress.

5. References

[1] (a) Alonso, F.; Beletskaya, I. P.; Yus, M. *Chem. Rev.* **2002**, *102*, 4009. (b) Grushin, V. V.; Alper, H.; *Chem. Rev.* **1994**, *94*, 1047. (c) Pinder, A. R. *Synthesis*, **1980**, 425. (d) Hitchman, M. L.; Spackman, R. A.; Agra, C. *Chem. Soc. Rev.* **1995**, *95*, 423.

[2] (a) Kaneda, K.; Hara, T.; Kaneta, T.; Mori, K.; Mitsudome, T.; Mizugaki, T.; Ebitani, K. *Green Chem.* **2007**, *9*, 1246. (b) Lapierre, R. B.; Guczi, L.; Kranich, W. L.; Weiss, A. H. *J. Catal.* **1978**, *52*, 230. (c) Yuan, G.; Keane, M. A. *Ind. Eng. Chem. Res.* **2007**, *46*, 705.

[3] Fuku, K.; Hashimoto, K.; Kominami, H. *Chem. Commun.* **2010**, *46*, 5118.

[4] Shiraishi, Y.; Sugano, Y.; Tanaka, S.; Hirai, T. *Angew. Chem. Int. Ed.* **2010**, *49*, 1656.

[5] Legawiec-Jarzyna, M.; Srebowata, A.; Juszczyk, W.; Karpinski, Z. *Catal. Today* **2004**, *88*, 93.

[6] Vegard, L. *Z. Phys.* **1921**, *5*, 17.

[7] Herbert, B.; Michaelson, J. *J. Appl. Phys.* **1977**, *48*, 4728.

[8] (a) Yang, Y. Z.; Chang, C.-H.; Idriss, H. *Appl. Catal. B* **2006**, *67*, 217. (b) Strataki, N.; Antoniadou, M.; Dracopoulos, V.; Lianos, P. *Catal. Today* **2010**, *151*, 53.

[9] Yamauchi, M.; Kobayashi, H.; Kitagawa, H. *ChemPhysChem* **2009**, *10*, 2566.

[10] Ohtani, B.; Iwai, K.; Nishimoto, S.; Sato, S. *J. Phys. Chem. B* **1997**, *101*, 3349.

Chapter V

Partial Oxidation of Cyclohexane on WO_3 Loaded with Pt Nanoparticles under Visible Light Irradiation

1. Introduction

The partial oxidation of cyclohexane (CHA) to cyclohexanol (CHA-ol) and cyclohexanone (CHA-one) has attracted much attention because these products are the intermediates in ε-caprolactam synthesis.[1] Of particular interest is the catalytic CHA oxidation in heterogeneous systems with molecular oxygen (O_2).[2] Photocatalytic CHA oxidation with O_2 has also been studied extensively with various catalysts such as TiO_2,[3] Fe porphyrin-modified TiO_2,[4] polyoxotungstate-modified SiO_2,[5] and V_2O_5-impregnated Al_2O_3.[6] Some of these systems promote partial oxidation of CHA with high selectivity (>89%).[3b,f,g,4a,5] All of these systems, however, require UV light for catalyst activation. Earlier, we reported that Cr-containing silica with highly dispersed chromate species catalyzes partial oxidation of CHA under visible light with high selectivity (>99%).[7] Cr species are, however, very toxic to living organisms;[8] therefore, an alternative Cr-free photo-catalytic system is desirable for clean production of CHA-ol and CHA-one.

Photocatalytic oxidation of CHA on TiO_2 proceeds via the following mechanism.[3c,f,g] Photoexcitation of TiO_2 produces the electron (e^-) and positive hole (h^+) pairs. The h^+ oxidizes CHA (C_6H_{12}) and produces a cyclohexyl radical ($C_6H_{11}\bullet$). This radical reacts with O_2 and produces a peroxy radical ($C_6H_{11}OO\bullet$).

$$TiO_2 + h\nu \rightarrow h^+ + e^- \quad (1)$$

$$C_6H_{12} + h^+ \rightarrow C_6H_{11}\bullet + H^+ \quad (2)$$

$$C_6H_{11}\bullet + O_2 \rightarrow C_6H_{11}OO\bullet \quad (3)$$

Combination of the peroxy radicals produces CHA-ol ($C_6H_{11}OH$) and CHA-one ($C_6H_{10}O$).

$$C_6H_{11}OO\bullet + C_6H_{11}OO\bullet \rightarrow C_6H_{11}OH + C_6H_{10}O + O_2 \quad (4)$$

The e^- on TiO_2 is consumed by a single-electron reduction of O_2, producing a superoxide anion ($O_2\bullet^-$). This reacts with $C_6H_{11}\bullet$ and produces CHA-one.

$$O_2 + e^- \rightarrow O_2\bullet^- \ (-0.13 \text{ V vs. NHE}) \quad (5)$$

$$C_6H_{11}\bullet + O_2\bullet^- \rightarrow C_6H_{10}O + OH^- \quad (6)$$

Selective production of CHA-ol and CHA-one on TiO_2 is, however, difficult. One of the reasons is that CHA is decomposed simultaneously during the reactions: the formed peroxy radical ($C_6H_{11}OO\bullet$) reacts with h^+ and is decomposed to CO_2 via the C–C bond cleavage.[9]

$$C_6H_{11}OO\bullet + h^+ \rightarrow \text{decomposition } (CO_2 \text{ formation}) \quad (7)$$

Another reason is that the formed CHA-ol and CHA-one are decomposed subsequently by photocatalytic reactions, producing CO_2.[10] Although he detailed mechanism for decomposition has not been clarified, it is considered that the oxidation of these compounds by h^+ (radical formation) and the reaction with $O_2\bullet^-$ are involved in the mechanism.

$$C_6H_{11}OH \text{ (or } C_6H_{10}O) + h^+ + O_2\bullet^- \rightarrow \text{decomposition } (CO_2 \text{ formation}) \quad (8)$$

This suggests that $O_2\bullet^-$, produced via the reduction of O_2 by the conduction band e^- on TiO_2 (eqn (5)), promotes decomposition of CHA-ol and CHA-one. Therefore, if the formation of $O_2\bullet^-$ is suppressed, the decomposition of these partial oxidation products would be inhibited.

WO_3 is a semiconductor material that is excited by visible light irradiation ($\lambda < 443$ nm). There are, however, only a few reports of photocatalytic reactions on WO_3 because of its low a ctivity.[11] As shown in **Scheme 5-1**, the conduction band potential of WO_3 (+0.5 V vs.NHE) is more positive than the potential for single-electron reduction of O_2 (eqn (5), −0.13 V). The photoformed e^- on WO_3 is therefore not consumed efficiently by O_2, resulting in low catalytic activity. A recent report,[12] however, revealed that the WO_3 loaded with Pt particles (Pt/WO_3) exhibits enhanced catalytic activity for degradation of acetic acid and acetaldehyde under visible light. This is because the conduction band e^- of WO_3 is consumed efficiently on the Pt particles by the promotion of a multi-electron reduction of O_2,as follows.

$$O_2 + 2H^+ + 2e^- \rightarrow H_2O_2 \text{ (+0.68 V } vs. \text{ NHE)} \quad (9)$$

$$O_2 + 4H^+ + 4e^- \rightarrow 2H_2O \text{ (+1.23 V } vs. \text{ NHE)} \quad (10)$$

On the Pt/WO_3 system, the formation of $O_2\bullet^-$ that promotes subsequent decomposition of CHA-ol and CHA-one (eqn (8)) is unfavorable. This system, if employed for CHA oxidation, would promote partial oxidation under visible light.

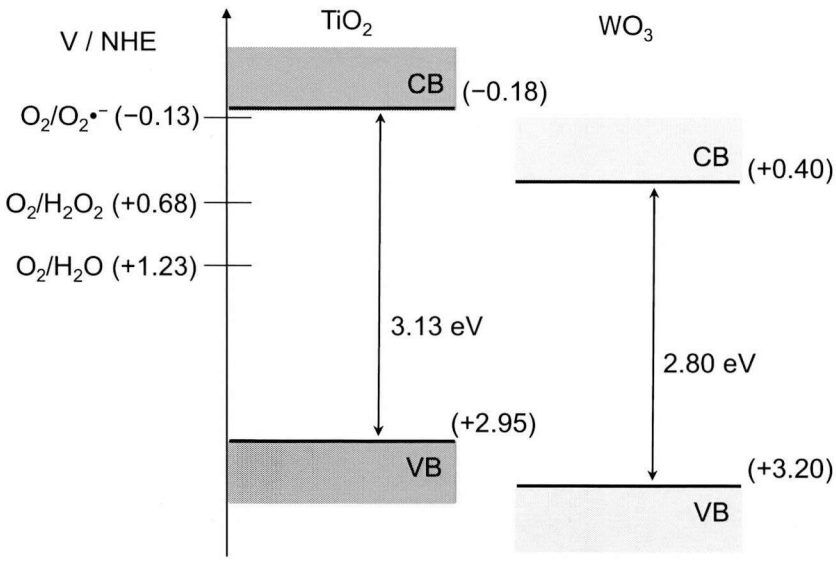

Scheme 5-1. Redox potentials of TiO_2 and WO_3 (pH 0).

In the present work, the Pt/WO_3 catalysts were employed for photocatalytic oxidation of CHA with O_2 under visible light. The catalysts successfully promote partial oxidation with ca. 93% selectivity. The ESR measurements with a spin trapping reagent and the photocatalytic reactions with an $O_2\bullet^-$ scavenger indicate that selective oxidation of CHA on Pt/WO_3 is indeed achieved due to the decreased formation of $O_2\bullet^-$.

2. Experimental

2-1. Materials

WO_3 particles were supplied from Kojundo Chem. Lab. Co. (diameter, 128.0 nm; BET surface area, 3.1 $m^2\ g^{-1}$). JRC-TIO-4 TiO_2 particles (equivalent to Degussa P25, diameter, 25.8 nm, BET surface area; 54.0 $m^2\ g^{-1}$) were kindly supplied from the Catalysis Society of Japan. Other reagents were purchased from Wako, Tokyo Kasei, and Sigma-Aldrich and used without further purification. Water was purified by the Milli Q system.

2-2. Catalyst preparation

Pt_x/WO_3 catalysts with different Pt loadings [x (wt%) = Pt/(Pt + WO_3) × 100; x = 0.1, 0.2, 0.3, 0.6, 1.3] were prepared as follows: WO_3 particles (0.1 g) and H_2PtCl_6 (0.34, 0.42, 0.61, 1.31, 2.77 mg) were added to a water/MeOH (24/1 v/v) mixture (10 mL) in a Pyrex glass tube (20 cm^3; φ 10 mm). The tubes were purged with N_2 gas and photoirradiated using a high-pressure Hg lamp (300 W; Eikohsha Co. Ltd.; light intensity at 300–500 nm, 32.9 W m^{-2}) with magnetic stirring at 303 K for 30 min. The catalysts

were recovered by filtration, washed with water, and dried in vacuo at 353 K for 12 h.

2-3. Photoreaction

The catalysts (10 mg) were added to a CHA/MeCN (1/9 v/v, 10 mL) mixture in a Pyrex glass tube (20 cm^3; φ 10 mm). The tubes were purged with O_2 gas and photoirradiated with magnetic stirring by a Xe lamp (2 kW; Ushio Inc.), filtered through an aqueous $NaNO_2$ (20 wt%) solution to give light wavelengths of λ >420 nm. The temperature of solution during irradiation was 303 K. After the reaction, the gas phase product was analyzed by GC-TCD (Shimadzu; GC-14B). The resulting solution was recovered by centrifugation and analyzed by GC-FID (Shimadzu; GC-1700).

2-4. ESR measurement

ESR spectra were recorded at the X-band using a Bruker EMX-10/12 spectrometer with a 100 kHz magnetic field modulation at a microwave power level of 1.0 mW, where the microwave power saturation of the signals does not occur. The magnetic field was calibrated using 1,1'-diphenyl-2-picrylhydrazyl (DPPH) as a standard. CHA/MeCN (1/9 v/v, 10 mL) mixture, catalyst (10 mg), and 5,5'-dimethyl-1-pyrroline-*N*-oxide (DMPO, 25 mM) were added to a Pyrex glass tube (20 cm^3).The tube was purged with O_2 and photoirradiated using a Xe lamp for 3 min under magnetic stirring at 303 K. The solution was recovered by filtration, and ESR measurement was carried out at 298 K.

2-5. Analysis

The Pt amount on the catalysts was determined by an X-ray fluorescence spectrometer (Seiko Instruments Inc.; SEA2110). Diffuse reflectance UV-vis absorption spectra were measured on a JASCO V-550 spectrophotometer. The light intensity was measured with a spectroradiometer (USR-40, Ushio Inc.). The H_2O_2 amount in solution was determined by an iodometric titration;[13] the reaction mixture recovered by filtration was treated with an excess amount of NaI and the amount of I_3^- formed was determined with UV-vis analysis at 361 nm ($\varepsilon = 2.0 \times 10^3$ M^{-1} cm^{-1} in CHA/MeCN (1/9 v/v) mixture) using an UV-visible spectrophotometer (Shimadzu; Multispec-1500).

3. Results and discussion

3-1. Catalyst properties

The Pt_x/WO_3 catalysts with different Pt loadings [x (wt%) = Pt/(Pt + WO_3) × 100] were prepared by

a photodeposition method (**Table 5-1**).[12] UV irradiation of a water/MeOH mixture containing WO_3 particles and different amounts of H_2PtCl_6 produces dark yellow powders of catalysts. As shown in **Figure 5-1a**, the high resolution transmission electron microscopy (HRTEM) image of the $Pt_{0.2}/WO_3$ catalyst reveals that isolated hemispherical Pt nanoparticles are supported on WO_3. The mean diameter of the Pt particles was determined to be 4.7 nm. The size of Pt particles is scarcely affected by the Pt loadings; $Pt_{1.3}/WO_3$ contains 4.8 nm Pt particles (**Figure 5-1b**). **Figure 5-2** shows the diffuse reflectance UV-vis absorption spectra of catalysts. The Pt/WO_3 catalysts with larger Pt loadings show increased absorbance at λ >400 nm due to the light scattering by the Pt particles,[14] although the band gap energies of catalysts are similar (2.6–2.8 eV).

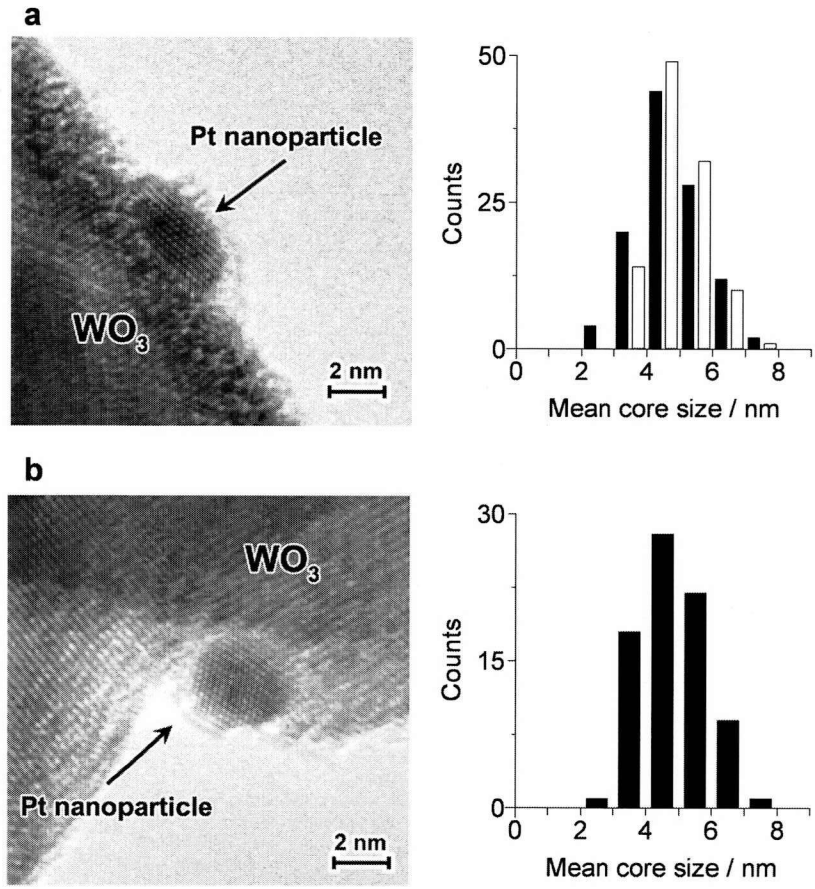

Figure 5-1. Typical cross-sectional HRTEM image and size distribution of Pt particles on (a) $Pt_{0.2}/WO_3$ and (b) $Pt_{1.3}/WO_3$. The black bars are the data for fresh catalysts and the white bars are the data for catalysts after the reuse reactions (**Table 5-1**, run 11).

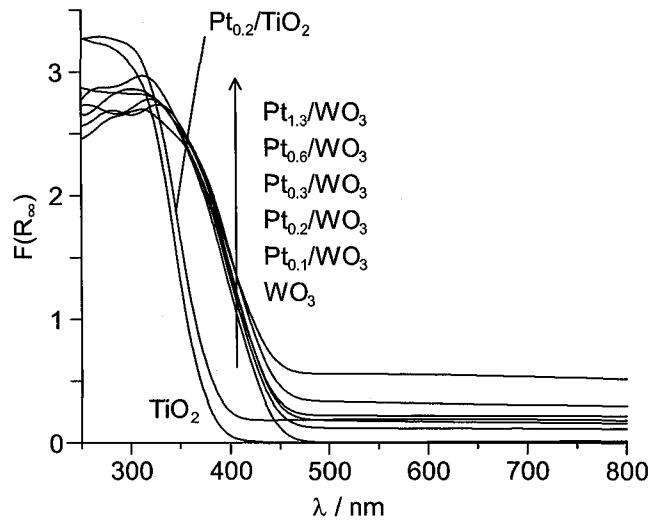

Figure 5-2. Diffuse reflectance UV-vis absorption spectra of catalysts.

3-2. Photocatalytic activity

Table 5-1. Results of photooxidation of cyclohexane (CHA) with various catalysts.[a]

run	catalyst	Pt particle size[b] / nm	yields / μmol			selectivity for partial oxidation[c] / %	H_2O_2 formed / μmol
			CHA-ol	CHA-one	CO_2		
1	WO_3		0.7	0.7	0.7	92	1.8
2	$Pt_{0.1}/WO_3$		4.3	3.8	3.9	93	3.0
3	$Pt_{0.2}/WO_3$	4.7	4.3	4.4	4.2	93	3.3
4	$Pt_{0.3}/WO_3$		3.7	3.3	2.9	94	2.6
5	$Pt_{0.6}/WO_3$		3.4	3.1	2.9	93	2.4
6	$Pt_{1.3}/WO_3$	4.8	3.2	2.7	2.5	93	2.3
7	TiO_2		1.4	2.6	11.6	67	0.5
8	$Pt_{0.2}/TiO_2$[d]	2.0	1.8	3.4	12.9	71	
9	1st reuse[e]		4.3	4.6	4.3	93	
10	2nd reuse[e]		4.0	4.4	4.0	93	
11	3rd reuse[e]	4.8[f]	4.3	3.8	3.9	93	

[a] Reaction conditions: CHA/MeCN (1/9 v/v, 10 mL), catalyst (10 mg), λ >420 nm, O_2 (1 atm), photoirradiation time, 12 h. [b] determined by TEM analysis. [c] = [(CHA-ol + CHA-one)/(CHA-ol + CHA-one + (1/6)CO_2)] × 100 (refs. 3d and 6b). [d] prepared by a photodeposition method similar to Pt/WO_3. [e] $Pt_{0.2}/WO_3$ reused after simple washing with MeCN. [f] Determined after the reaction.

Table 5-1 summarizes the results of photocatalytic oxidation of CHA. The reactions were performed by visible light irradiation (λ >420 nm) of a CHA/MeCN (1/9 v/v) mixture with catalyst and O_2 for 12 h. As shown in run 1, pure WO_3 is inactive for oxidation, where only a small amount of CHA-ol and CHA-one is produced (both 0.7 μmol). The Pt loadings onto WO_3 enhance oxidation. As shown in runs 2–6, the Pt/WO_3 catalysts produce larger amounts of CHA-ol and CHA-one (>2.7 μmol). The selectivity for these products is ca.93%. Run 7 shows the results obtained with a common TiO_2 catalyst (anatase/rutile = 8/2); the CHA-ol and CHA-one yields are much lower than those obtained with Pt/WO_3, although the amount of CO_2 formed is much higher. The partial oxidation selectivity is 67%, which is lower than that obtained with Pt/WO_3. In addition, as shown in run 8, the Pt loading onto TiO_2 does not enhance the selectivity and yields. These findings indicate that the Pt/WO_3 system promotes selective and efficient photooxidation of CHA.

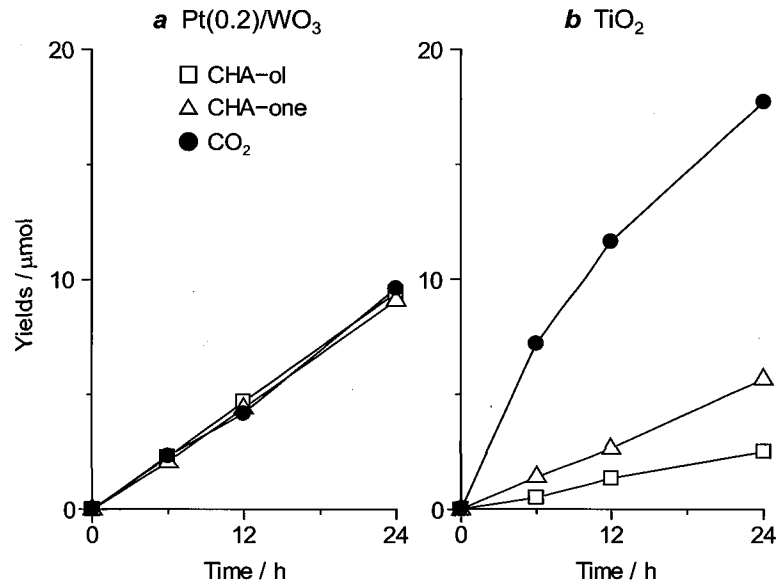

Figure 5-3. Time-dependent change in the yields of CHA-ol, CHA-one, and CO_2 formed during photooxidation of CHA (1 mL, 9.3 mmol) in MeCN with (a) $Pt_{0.2}/WO_3$ and (b) TiO_2. Reaction conditions are identical to those in **Table 5-1**.

Figure 5-3 shows the time-dependent change in the amounts of CHA-ol, CHA-one, and CO_2 produced during the photocatalytic oxidation of CHA with $Pt_{0.2}/WO_3$ or TiO_2 catalyst. With TiO_2 (**Figure 5-3b**), the amount of CO_2 formed is much larger than those of CHA-ol and CHA-one. In contrast, with $Pt_{0.2}/WO_3$ (**Figure 5-3a**), the CO_2 amount is comparable to those of CHA-ol and CHA-one. This again suggests that Pt/WO_3 indeed produces CHA-ol and CHA-one selectively, while suppressing

CO_2 formation.

Among the Pt/WO_3 catalysts (runs 2–6), $Pt_{0.2}/WO_3$ (run 3) shows the highest yields of CHA-ol (4.3 μmol) and CHA-one (4.4 μmol). The catalysts with larger Pt loadings show decreased yields. This is probably because excess amount of Pt increases the absorbance at λ >400 nm, as shown in **Figure 5-2**, and suppresses the incident light absorption by WO_3.[14] It is noted that the catalyst is reusable for reactions. As shown in runs 9–11, the $Pt_{0.2}/WO_3$ catalyst, when reused for further reactions, shows the selectivity and yields similar to those of the virgin catalyst (run 3). In addition, HRTEM analysis of the catalyst recovered after the reuse revealed that the Pt particle size scarcely changes during reactions (**Figure 5-1a**). These indicate that the catalyst is reusable without loss of activity and selectivity.

3-3. Multi-electron reduction on WO_3

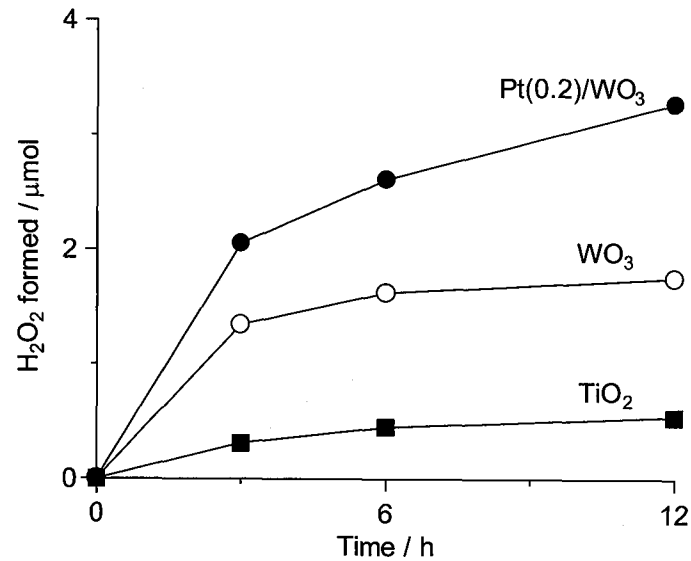

Figure 5-4. Time-dependent change in the amount of H_2O_2 formed during photooxidation of CHA (1 mL, 9.3 mmol) in MeCN with TiO_2, WO_3, or $Pt_{0.2}/WO_3$ catalyst. Reaction conditions are identical to those in **Table 5-1**.

On the photoexcited TiO_2, the conduction band e^- is mainly consumed by single-electron reduction of O_2 ($O_2\bullet^-$ formation, eqn (5)).[10] In contrast, on Pt/WO_3, this reduction is difficult because the conduction band potential of WO_3 is more negative than the potential of single-electron reduction of O_2 (**Scheme 5-1**).[11] The enhanced oxidation of CHA by the Pt loadings on WO_3 (**Table 5-1**) is due to the efficient consumption of e^- on WO_3 by a multi-electron reduction of O_2, producing H_2O_2 or H_2O (eqn (9) and (10)).[12] This is confirmed by the amount of H_2O_2 formed during photooxidation of CHA. As shown in **Figure 5-4**, the amount of H_2O_2 formed after 12 h photoirradiation with $Pt_{0.2}/WO_3$ is 3.3 μmol,

whereas pure WO_3 and TiO_2 produce smaller amounts. As summarized in **Table 5-1** (final column), the H_2O_2 amount increases with the Pt loadings on WO_3, but the catalysts with >0.2 wt% Pt produce decreased amount of H_2O_2. This tendency is consistent with the oxidation activity of CHA (**Table 5-1**). These data clearly indicate that the multi-electron reduction of O_2 promoted on the Pt particles efficiently consumes the conduction band e^- of WO_3 and enhances CHA oxidation.

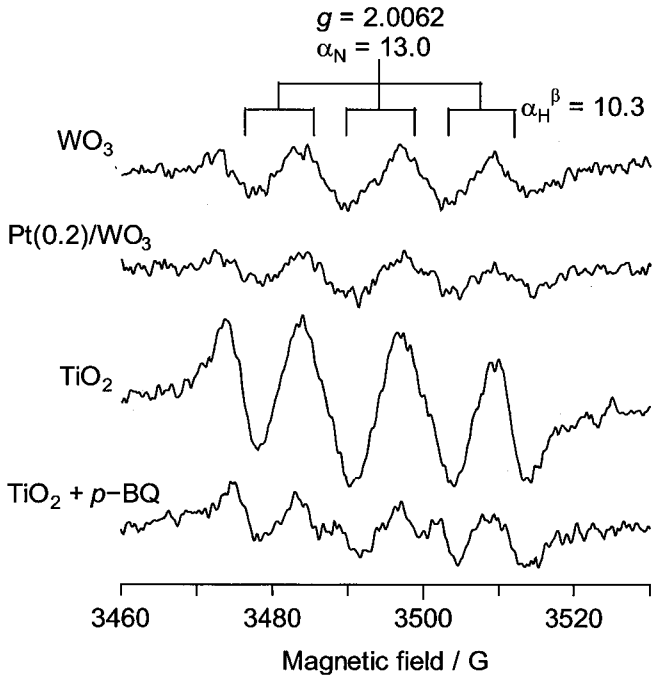

Figure 5-5. ESR spectra for DMPO–$O_2^{\bullet-}$ spin adduct signals obtained by photoirradiation of O_2-saturated CHA/MeCN (1/9 v/v) mixture containing DMPO with WO_3, $Pt_{0.2}/WO_3$, or TiO_2 in the absence and presence of *p*-BQ (0.05 mmol). Reaction conditions: catalyst (10 mg), DMPO (0.25 mmol), CHA/MeCN (1/9 v/v, 10 mL), O_2 (1 atm), irradiation time (3 min).

On the Pt/WO_3 catalyst, the single-electron reduction of O_2 is indeed difficult. This is confirmed by ESR analysis. **Figure 5-5** shows the spectra obtained after photoirradiation of an O_2-saturated CHA/MeCN (1/9 v/v) mixture with catalysts in the presence of DMPO, a spin-trapping reagent.[15] All of the catalysts show distinctive signals assigned to the DMPO–$O_2^{\bullet-}$ spin adduct (α_N = 13.0 G; α_H^{β} = 10.3 G, g = 2.0062).[15] The spin adduct signal is observed on WO_3, although its conduction band potential is more positive than the potential of single-electron reduction of O_2 (**Scheme 5-1**). As also observed for the related WO_3 system,[16] this is probably attributable to the negative shift of particle charge due to the effect of electrical potential floating in non-aqueous media or the energy level spreading due to the distribution of reduction potential of O_2. The intensity of the spin adduct signal observed on $Pt_{0.2}/WO_3$ is

much weaker than that on TiO_2. This clearly indicates that the single-electron reduction of O_2 is indeed unfavorable on Pt/WO_3 and a lower amount of $O_2^{\bullet -}$ is produced.

3-4. Suppression of subsequent decomposition of products

The selective formation of partial oxidation products on Pt/WO_3 is because the catalyst suppresses subsequent photocatalytic decomposition of the CHA-ol and CHA-one produced. In contrast, TiO_2 decomposes these products and produces CO_2, as denoted by eqn (8). **Figure 5-6** shows the time-dependent change in the amount of CO_2 formed during photoreaction of 0.1 mmol of CHA, CHA-ol, or CHA-one as the starting material. With TiO_2 (white circle), CO_2 is scarcely formed from CHA (**Figure 5-6a**), but is produced significantly from CHA-ol and CHA-one (**Figure 5-6b** and **c**). This indicates that, in the CHA photooxidation on TiO_2 (**Figure 5-3b**), the formed CHA-ol and CHA-one are subsequently decomposed, resulting in small amounts of CHA-ol and CHA-one and a large amount of CO_2. In contrast, on $Pt_{0.2}/WO_3$ (**Figure 5-6b** and **c**; black circle), the CO_2 production from CHA-ol and CHA-one is much suppressed. This indicates that, in the CHA photooxidation on $Pt_{0.2}/WO_3$ (**Figure 5-3a**), further decomposition of the products is suppressed, resulting in large amounts of CHA-ol and CHA-one and a relatively small amount of CO_2.

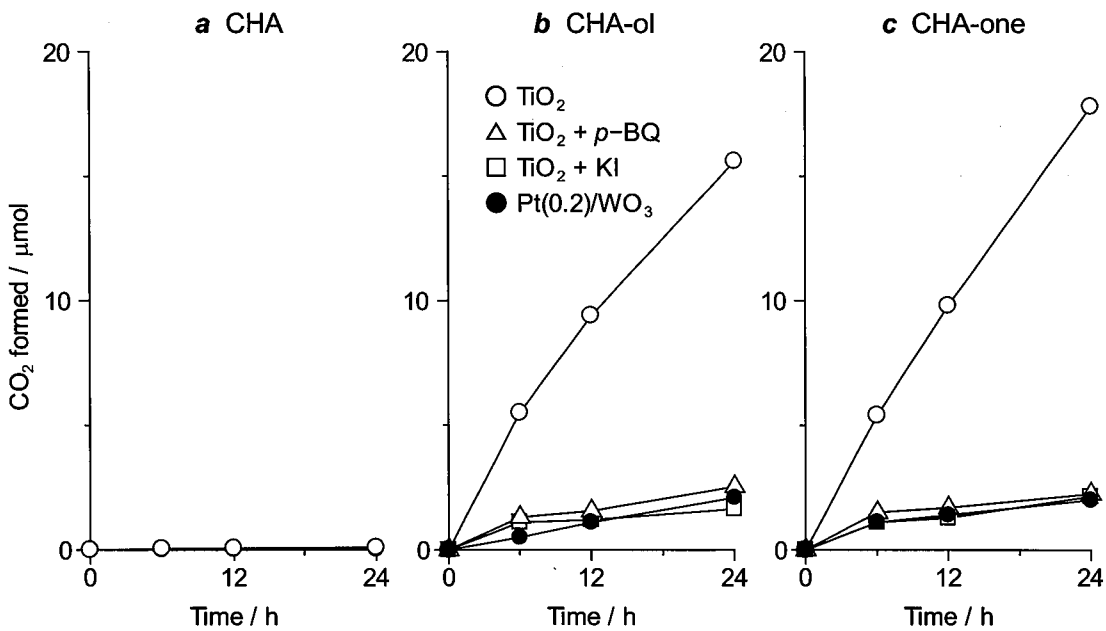

Figure 5-6. The amount of CO_2 formed during photooxidation of 0.1 mmol of (a) CHA, (b) CHA-ol, and (c) CHA-one with TiO_2 or $Pt_{0.2}/WO_3$ in the absence/presence of *p*-BQ (0.05 mmol) or KI (0.05 mmol). Reaction conditions: catalyst (10 mg), substrate (0.1 mmol), MeCN (10 mL), λ >420 nm, O_2 (1 atm). The light intensity at 420–500 nm is 26.9 W m^{-2}.

The decreased decomposition of CHA-ol and CHA-one on Pt/WO_3 is due to the suppression of $O_2\bullet^-$ formation. To clarify this, the effect of *p*-benzoquinone (*p*-BQ), an $O_2\bullet^-$ quencher,[17] on the photocatalytic decomposition of CHA-ol and CHA-one with TiO_2 was studied. As shown in **Figure 5-5**, the ESR signal for the DMPO–$O_2\bullet^-$ adduct obtained with TiO_2 in the presence of *p*-BQ is much weaker than that obtained with TiO_2 alone, indicating that *p*-BQ indeed quenches $O_2\bullet^-$. **Figure 5-6b** and **c** show the amount of CO_2 formed during photoreaction of CHA-ol and CHA-one with TiO_2 in the presence of *p*-BQ. The addition of *p*-BQ decreases the CO_2 formation. This indicates that the decomposition of partial oxidation products is indeed promoted by $O_2\bullet^-$.

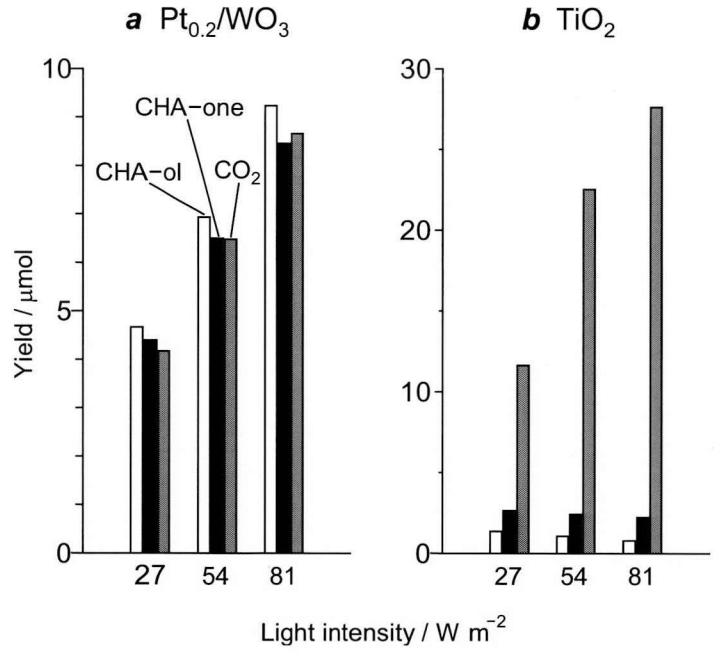

Figure 5-7. The yields of products formed by photooxidation of CHA (1 mL, 9.3 mmol) for 12 h with (a) $Pt_{0.2}/WO_3$ and (b) TiO_2 catalysts at different light intensities (420–500 nm). Reaction conditions are identical to those in **Table 5-1**.

The involvement of $O_2\bullet^-$ in the decomposition of partial oxidation products is confirmed by photooxidation of CHA at different light intensities. **Figure 5-7** shows the product yields after 12 h photoirradiation. With $Pt_{0.2}/WO_3$ (**Figure 5-7a**), the yields of all products increase with the intensity increase, and the product selectivity is unchanged. This indicates that, under the suppressed $O_2\bullet^-$ formation condition, the decomposition of CHA-ol and CHA-one is not accelerated even by an increase in the amount of h^+ formed on the catalyst; in other words, CO_2 formation is not promoted by the decomposition of CHA-ol and CHA-one but by the decomposition of a peroxy radical ($C_6H_{11}OO\bullet$) with

h^+ (eqn (7)). In contrast, with TiO_2 (**Figure 5-7b**), the intensity increase enhances CO_2 formation while decreasing the formation of CHA-ol and CHA-one. The increase in light intensity enhances $O_2\bullet^-$ formation (eqn (5)). This accelerates the decomposition of CHA-ol and CHA-one by $O_2\bullet^-$, as proposed in eqn (8).[10] These data clearly indicate that $O_2\bullet^-$ is involved in the decomposition of partial oxidation products.

Effect of h^+ on the decomposition of partial oxidation products was studied. Potassium iodide (KI), a h^+ scavenger,[18] was added to a MeCN solution containing CHA-ol or CHA-one together with TiO_2 and used for the photocatalytic reaction. As shown in **Figure 5-6b** and **c**, the addition of KI decreases CO_2 formation as compared to that obtained with TiO_2 alone. This suggests that the photoformed h^+ is also involved in the mechanism for decomposition of CHA-ol and CHA-one. These findings indicate that, as proposed in eqn (8),[10] the decomposition of partial oxidation products is promoted by the combination of $O_2\bullet^-$ and h^+. The decreased $O_2\bullet^-$ formation on the Pt/WO_3 catalyst, therefore, suppresses the decomposition and promotes selective formation of CHA-ol and CHA-one. As denoted by eqn (7), CHA is inevitably decomposed via the reaction of a peroxy radical with h^+. Further improvement is therefore necessary for more selective CHA oxidation. Nevertheless, the results presented here suggest that the suppression of $O_2\bullet^-$ formation is one of the efficient ways for selective production of CHA-ol and CHA-one by photocatalysis.

4. Conclusion

WO_3 loaded with Pt particles (Pt/WO_3) were used as catalysts for oxidation of CHA with O_2 under visible light. These catalysts successfully promote partial oxidation (formation of CHA-ol and CHA-one) with ca. 93% selectivity. The high selectivity for CHA oxidation on Pt/WO_3 is due to the decreased $O_2\bullet^-$ formation. This suppresses the photocatalytic decomposition of partial oxidation products occurring via the combination of h^+ and $O_2\bullet^-$.

5. References

[1] (a) Schuchardt, U.; Cardoso, D.; Sercheli, R.; Pereira, R.; de Cruz, R. S.; Guerreiro, M. C.; Mandelli, D.; Spinacé, E. V.; Pires, E. L. *Appl. Catal. A* **2001**, *211*, 1. (b) Bellussi, G.; Perego, C. *CATTECH* **2000**, *4*, 4.

[2] For example: (a) Zhao, R.; Ji, D.; Lv, G.; Qian, G.; Yan, L.; Wang, X.; Suo, J. *Chem. Commun.* **2004**, 904. (b) Raja, R.; Sankar, G.; Thomas, J. M. *J. Am. Chem. Soc.* **1999**, *121*, 11926.

[3] (a) Giannotti, C.; Le Greneur, S.; Watts, O. *Tetrahedron Lett.***1983**, *24*, 5071. (b) Lu, G.; Gao, H.; Suo, J.; Li, S. *J. Chem. Soc.Chem. Commun.* **1994**, 2423. (c) Boarini, P.; Carassiti, V.; Maldotti, A.;

Amadelli, R. *Langmuir* **1998**, *14*, 2080. (d) Sclafani, A.; Herrmann, J. M. *J. Phys. Chem.* **1996**, *100*, 13655. (e) Shimizu, K.-I.; Kaneko, T.; Fujishima, T.; Kodama, T.; Yoshida, H.; Kitayama, Y. *Appl. Catal. A* **2002**, *225*, 185. (f) Almquist, C. B.; Biswas, P. *Appl. Catal. A* **2001**, *214*, 259. (g) Brusa, M. A.; Grela, M. A. *J. Phys. Chem. B* **2005**, *109*, 1914. (h) Gonzalez, M . A.; Howell, S. G.; Sikdar, S. K. *J. Catal.* **1999**, *183*, 159.

[4] (a) Amadelli, R.; Bregola, M.; Polo, E.; Carassiti, V.; Maldotti, A. *J. Chem. Soc. Chem. Commun.* **1992**, 1355. (b) Molinari, A.; Amadelli, R.; Antolini, L.; Maldotti, A.; Battioni, P.; Mansuy, D. *J. Mol. Catal. A* **2000**, *158*, 521.

[5] (a) Molinari, A.; Amadelli, R.; Andreotti, L.; Maldotti, A. *J. Chem. Soc. Dalton Trans.* **1999**, 1203. (b) Maldotti, A.; Molinari, A.; Varani, G.; Lenarda, M.; Storaro, L.; Bigi, F.; Maggi, R.; Mazzacani, A.; Sartori, G. *J. Catal.* **2002**, *209*, 210.

[6] (a) Teramura, K.; Tanaka, T.; Yamamoto, T.; Funabiki, T. *J. Mol. Catal. A* **2001**, *165*, 299. (b) Teramura, K.; Tanaka, T.; Kani, M.; Hosokawa, T.; Funabiki, T. *J. Mol.Catal. A* **2004**, *208*, 299.

[7] (a) Shiraishi, Y.; Teshima, Y.; Hirai, T. *Chem. Commun.* **2005**, 4569. (b) Shiraishi, Y.; Ohara, H.; Hirai, T. *J. Catal.* **2008**, *254*, 365. (c) Shiraishi, Y.; Ohara, H.; Hirai, T. *New J. Chem.* **2010**, *34*, 2841. (d) Tsukamoto, D.; Shiro, A.; Shiraishi, Y.; Hirai, T. *J. Phys. Chem. C* **2011**, *115*, 19782.

[8] Cervantes, C.; Campos-García, J.; Devars, S.; Gutiérrez-Corona, F.; Loza-Tavera, H.; Torres-Guzmán, J. C.; Moreno-Sá nchez, R. *FEMS Microbiol. Rev.* **2001**, *25*, 335.

[9] Schwizgebel, J.; Ekerdt, J. G.; Gerischer, H.; Heller, A. *J. Phys.Chem.* **1995**, *99*, 5633.

[10] (a) Mills, A.; Hunte, S. L. *J. Photochem. Photobiol. A* **1997**, *108*, 1. (b) Du, P.; Moulijn, J. A.; Mul, G. *J. Catal.* **2006**, *238*, 342.

[11] (a) Arai, T.; Horiguchi, M.; Yanagida, M.; Gunji, T.; Sugihara, H.; Sayama, K. *Chem. Commun.* **2008**, 5565. (b) Abe, R.; Sayama, K.; Sugihara, H. *J. Phys. Chem. B* **2005**, *109*, 16052. (c) Sclafani, A.; Palmisano, L.; Marcí, G.; Venezia, A. M.; *Sol. Energy Mater. Sol. Cells* **1998**, *51*, 203. (d) Kim, J.; Lee, C. W.; Choi, W. *Environ. Sci. Technol.* **2010**, *44*, 6849. (e) Arai, T.; Yanagida, M.; Konishi, Y.; Ikura, A.; Iwasaki, Y.; Sugihara, H.; Sayama, K. *Appl. Catal. B* **2008**, 84, 42.

[12] Abe, R.; Takami, H.; Murakami, N.; Ohtani, B. *J. Am. Chem. Soc.* **2008**, *130*, 7780.

[13] Ohkubo, K.; Mizushima, K.; Iwata, R.; Souma, K.; Suzuki, N.; Fukuzumi, S. *Chem. Commun.* **2010**, *46*, 601.

[14] Shiraishi, Y.; Sugano, Y.; Tanaka, S.; Hirai, T. *Angew. Chem. Int. Ed.* **2010**, *49*, 1656.

[15] Harbour, J. R.; Hair, M. L. *J. Phys. Chem.* **1978**, *82*, 1397.

[16] Noda, H.; Oikawa, K.; Ohya-Nishiguchi, H.; Kamada, H. *Bull. Chem. Soc. Jpn.* **1993**, *66*, 3542.

[17] Yang, J.; Chen, C.; Ji, H.; Ma, W.; Zhao, J. *J. Phys. Chem. B* **2005**, *109*, 21900.

[18] Beranek, R.; Neumann, B.; Sakthivel, S.; Janczarek, M.; Dittrich, T.; Tributsch H.; Kisch, H. *Chem. Phys.* **2007**, *339*, 11.

Chapter VI

Aerobic Oxidation by Platinum Nanoparticle Supported on Anatase Titanium Dioxide under Visible Light Irradiation

1. Introduction

Aerobic oxidation by heterogeneous catalysts with molecular oxygen (O_2) as an oxidant is an essential process for the synthesis of various chemicals.[1] Photocatalytic oxidation with O_2 has also been studied extensively with semiconductor materials such as titanium dioxide (TiO_2);[2–6] several types of substrates such as alcohols, amines, hydrocarbons, and sulfides are successfully oxidized at atmospheric pressure and room temperature. One of the critical issues for practical application of photocatalytic processes is the low catalytic activity under irradiation of visible light (λ >400 nm), the main component of solar irradiance. Several TiO_2 materials doped with nitrogen,[7,8] sulfur,[9,10] carbon,[11,12] or boron atoms[13] have been proposed to extend the absorption edge of catalysts into the visible region. These doped catalysts, however, suffer from low quantum yields for reaction (<0.5%), because they inherently contain a large number of crystalline lattice that acts as a charge recombination center.[14] Development of visible-light-driven catalysts that promote highly efficient aerobic oxidation is still a challenge.

Nanosized noble metals such as gold (Au) and silver (Ag) absorb light in the visible region due to a resonant oscillation of free electrons coupled by light, known as localized surface plasmon resonance (SPR).[15] Application potentiality of SPR to photocatalysis was first discovered by Tian et al.[16] Visible light irradiation of Au particles loaded on a TiO_2 film that is coated on an indium tin oxide electrode generates an anodic photocurrent in the presence of Fe^{2+}. This occurs via a collective oscillation of electrons (e^-) on the Au particles induced by visible light and a subsequent transfer of e^- to the TiO_2 conduction band. Simultaneously, the positively charged Au particles receive e^- from the electron donor (Fe^{2+}). This suggests that visible light irradiation successfully creates the charge-transferred state at the metal/semiconductor heterojunction and would promote catalytic oxidation and reduction reactions, *i.e.* plasmonic photocatalysis.[17,18]

Very recently, we found that visible-light-induced plasmonic photocatalysis successfully promotes aerobic oxidation of alcohols at the Au/semiconductor interface.[19] This is achieved by Au particles loaded on a mixture of anatase/rutile TiO_2 (Degussa, P25). The activity of Au/P25 catalyst critically depends on its architecture; Au particles with ca. 4 nm diameter located at the interface of anatase/rutile TiO_2 are necessary. The plasmonic reaction on Au/P25 proceeds via the multistep e^- transfer, as summarized in Scheme 1. The photoactivated Au particles transfer e^- to rutile (a). The e^- is then

transferred to the adjacent anatase (b). O_2 is reduced on the anatase surface by e^- and produces a peroxo-type oxygen anion ($O–O^-$) (c). Alcohol is adsorbed onto the positively charged Au particles via the interaction of its H atom with the $O–O^-$ species, producing an Au–alcoholate species (d).[20] Subsequent removal of H atom from the species produces the corresponding aldehydes or ketones (e). The apparent quantum yield for this reaction is 3.8% by the irradiation of 550 nm monochromatic light, which is much higher than that obtained with the doped photocatalysts (<0.5%).[7–13] The metal/semiconductor system is chemically stable under aerated condition as compared to the doped photocatalysts.[17] The plasmonic photocatalysis therefore has a potential for visible-light-induced aerobic oxidation.

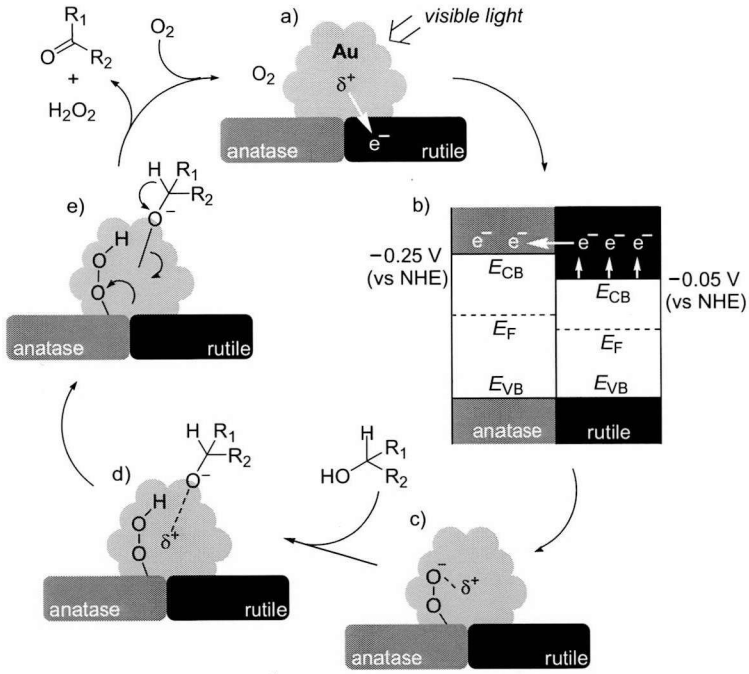

Scheme 6-1. Aerobic oxidation of alcohol on the Au/P25 catalyst activated by visible light.

The next challenge is further activity improvement of the plasmonic photocatalysts. In the plasmonic reaction, the charge separation is facilitated by the reduction of O_2 on the semiconductor surface with the e^- transferred from the photoactivated metal particles. The anatase surface is active for O_2 reduction, whereas rutile surface is inactive.[21] In contrast, photoactivated Au particles scarcely transfer e^- to anatase, probably due to the weak Au/anatase interaction, but the e^- transfer to rutile does occur.[19] Therefore, as shown in **Scheme 6-1**, the Au/P25 system requires the Au→rutile→anatase multistep e^- transfers for reaction. This circuitous process may suppress smooth e^- transfer and decrease the reaction efficiency. In particular, the rutile→anatase e^- transfer (**Scheme 6-1b**) is probably the

rate-determining step. This is because the conduction band potential (E_{CB}) of rutile is more positive than E_{CB} of anatase, and the rutile→anatase e^- transfer requires a negative shift of rutile E_{CB} by the accumulation of e^- on its conduction band.[22,23] Development of more efficient plasmonic photocatalysts therefore requires the creation of metal/anatase heterojunction that enables direct e^- transfer to anatase.

Pt particles also exhibit absorption band in the visible region, which is assigned to the intraband transition of electrons from sp band to the sp-conduction band (SPR absorption) and the interband transition of electrons from d band to sp-conduction band.[24] The intensity of this absorption is much weaker than that of Au particles.[15] There is only one report of photocatalysis driven by visible light activation of Pt particles; Zhai et al.[25] reported that Pt particles loaded on a TiO_2 thin film promote dehydrogenation of alcohols by visible light (λ >420 nm) under N_2 atmosphere. Herein, we report that Pt particles with 3–4 nm diameter loaded on anatase TiO_2, when used for aerobic oxidation under visible light, facilitate direct e^- transfer to anatase and promote the reaction highly efficiently. The Pt/anatase catalysts promote aerobic oxidation of alcohols with an apparent quantum yield 7.1% (550 nm), which is much higher than that obtained with the Au/P25 catalyst (3.8%).[19] In addition, the catalyst successfully promotes the reaction even under irradiation of sunlight.3

2. Experimental

2-1. Preparation of catalysts

$Pt_{x(y)}/TiO_2$ catalysts [x (wt %) = 0.5, 1, 2, 3, 4; y (K) = 473, 573, 673, 773, 823, 873] were prepared as follows. TiO_2 (1.0 g) was added to water (20 mL) containing $H_2PtCl_6 \cdot 6H_2O$ (13.3, 26.8, 54.2, 82.1, or 110.6 mg). The solvents were removed by evaporation at 353 K with vigorous stirring. The obtained powders were calcined under air flow and then reduced under H_2 flow at the identical temperature (y). The heating rate was 2 K min^{-1} and the holding time at the designated temperature was 2 h, respectively. $Pt_{2(673)}/SiO_2$ was prepared in a similar manner.

Au_2/P25 was prepared by the deposition-precipitation method as described previously.[19] P25 TiO_2 (1.0 g) was added to water (50 mL) containing $HAuCl_4 \cdot 4H_2O$ (45.8 mg). The pH of solution was adjusted to ca. 7 with 1 mM NaOH, and the solution was stirred at 353 K for 3 h. The particles were recovered by centrifugation, washed with water, and dried at 353 K for 12 h. The powders were calcined under air flow, where the heating rate was 2 K min^{-1} and the holding time at 673 K was 2 h.

2-2. Reaction procedure

Catalyst (5 mg) was added to toluene (5 mL) containing an alcohol within a Pyrex glass tube (φ 10

mm; capacity, 20 mL), and the tube was sealed with a rubber septum cap. The catalyst was dispersed well by ultrasonication for 5 min, and O_2 was bubbled through the solution for 5 min. The tube was immersed in a temperature-controlled water bath (298 ± 0.5 K)[61] and photoirradiated at λ >450 nm with magnetic stirring using a 2 kW Xe lamp (USHIO Inc.),[62] filtered through a CS3-72 glass (Kopp Glass Inc.). The light intensity at 450–800 nm was 16.8 mW cm^{-2}. Sunlight reactions were performed on 30th January, 2012 at 10:00–14:00 at the top of the laboratory building (north latitude 34.7°, east longitude 135.5°). The light intensity at 300–800 nm was 8.1 mW cm^{-2} (**Figure S6**). The highest temperature of solution during the sunlight exposure was 293 K, and the dark experiments were carried out at 293 K. After the reactions, the catalyst was recovered by centrifugation, and the solution was subjected to GC-FID analysis, where the concentrations of substrates and products were calibrated with authentic samples.

2-3. Action spectra analysis

The photoreactions were carried out in a toluene solution (2 mL) containing **1** (0.4 mmol) with $Pt_{2(673)}$/anatase or Au_2/P25 catalyst (8 mg) using a Pyrex glass tube. After ultrasonication and O_2 bubbling, the tube was photoirradiated using a 2 kW Xe lamp, where the incident light was monochromated by band pass glass filters (Asahi Techno Glass Co.). The full-width at half-maximum (FWHM) of the light was 11–16 nm. The photon number entered into the reaction vessel was determined with a spectroradiometer USR-40 (USHIO Inc.).

2-4. ESR measurement

The measurements were carried out at the X-band using a Bruker EMX-10/12 spectrometer with a 100 kHz magnetic field modulation at a microwave power level of 10.0 mW.[63] The magnetic field was calibrated using 1,1′-diphenyl-2-picrylhydrazyl (DPPH) as standard. Catalyst (20 mg) was placed in a quartz ESR tube, and the tube was evacuated at 423 K for 3 h and cooled to room temperature. O_2 (20 Torr) was introduced to the tube and kept for 10 min. The tube was photoirradiated at 298 K using a Xe lamp at λ >450 nm. The tube was then evacuated for 10 min to remove the excess amount of O_2 and analyzed at 77 K.

2-5. Analysis

Total amount of Pt in the catalysts was analyzed by an inductively-coupled argon plasma atomic emission spectrometer (ICAP-AES; SII Nanotechnology, SPS 7800), after dissolution of catalysts in an

aqua regia. TEM observations were carried out using an FEI Tecnai G2 20ST analytical electron microscope operated at 200 kV. XPS analysis was performed using a JEOL JPS-9000MX spectrometer with Mg Kα radiation as the energy source. Diffuse reflectance UV-vis spectra were measured on an UV-vis spectrophotometer (Jasco Corp.; V-550 with Integrated Sphere Apparatus ISV-469) with $BaSO_4$ as a reference.[64]

3. Results and discussion

3-1. Preparation and properties of catalysts

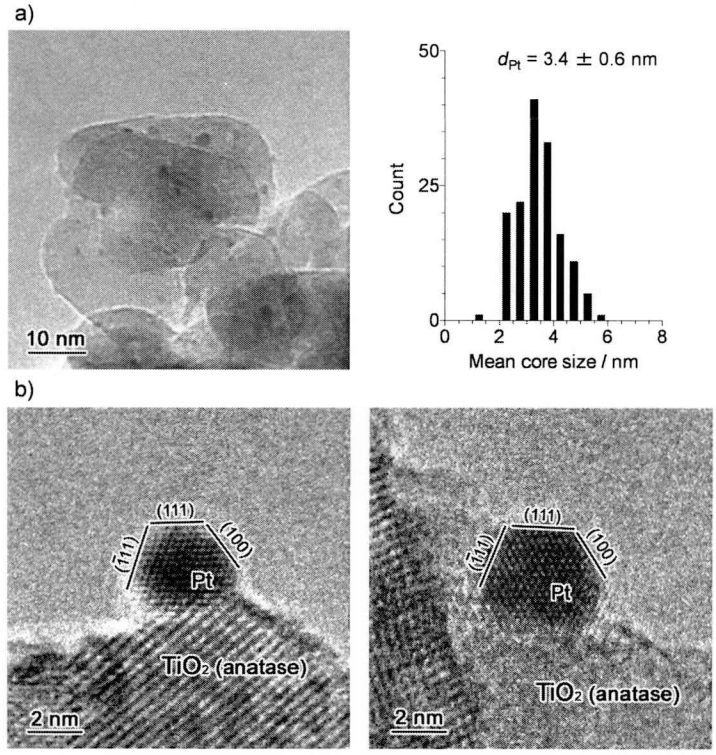

Figure 6-1. (a) TEM image of $Pt_{2(673)}$/anatase catalyst and size distribution of the Pt particles. (b) High-resolution TEM images.

The Pt/TiO_2 catalysts were prepared by impregnation of Pt precursors followed by reduction with H_2,[26,27] using anatase (Japan Reference Catalyst, JRC-TIO-1; average particle size, 21 nm; BET surface area, 81 $m^2\ g^{-1}$), P25 (JRC-TIO-4; 24 nm; 57 $m^2\ g^{-1}$; anatase/rutile = ca. 83/17), and rutile TiO_2 particles (JRC-TIO-6; 15 nm; 104 $m^2\ g^{-1}$), supplied from the Catalyst Society of Japan. TiO_2 was added to water containing H_2PtCl_6, and the water was removed by evaporation with vigorous stirring. The resultant was calcined in air for 2 h and reduced with H_2 for 2 h at the identical temperature, affording $Pt_{x(y)}/TiO_2$ as brown powder. The x is the amount of Pt loaded [x (wt %) = Pt/(Pt + TiO_2) × 100], and y is the

temperature (K) for calcination and reduction treatments.

As shown in **Figure 6-1a**, the transmission electron microscopy (TEM) images of $Pt_{2(673)}$/anatase catalysts exhibit monodispersed Pt particles; the average diameter of particles (d_{Pt}) is 3.4 nm. In addition, the high-resolution TEM images of catalysts (**Figure 6-1b**) reveal that the Pt particles can be indexed as *fcc* structures, as is the case for bulk Pt (JCPDS 04-0802). $Pt_{2(673)}$/P25 and $Pt_{2(673)}$/rutile also contain Pt particles with similar d_{Pt} (3.1 and 2.9 nm). X-ray photoelectron spectroscopy (XPS) of the catalysts shows distinctive Pt 4f peaks at 71 and 74 eV (**Figure 6-2**), indicating that Pt atoms exist as metallic state.[28] As shown in **Figure 6-3a**, diffuse reflectance UV-vis spectra of the catalysts containing 2 wt % Pt exhibit broad absorption band at λ >400 nm, assigned to the intraband and interband transitions of Pt particles.[29] Their absorption intensities are much lower than those of Au particles on the Au_2/P25 catalyst containing 2 wt % Au.[19]

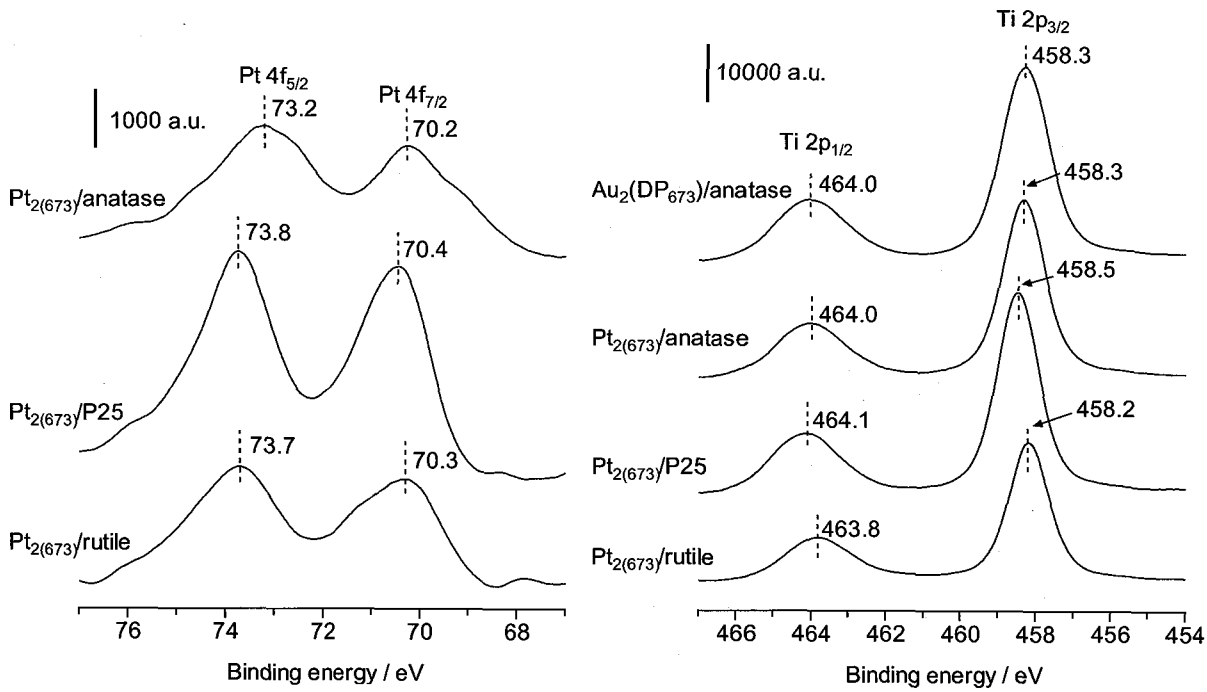

Figure 6-2. XPS chart for Pt/TiO_2 catalysts.

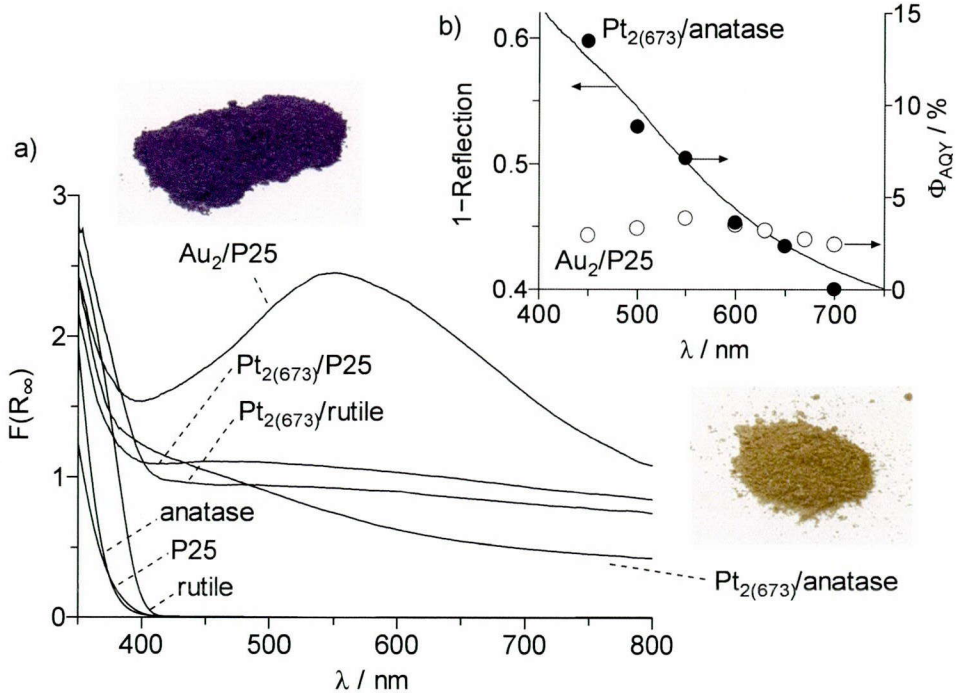

Figure 6-3. (a) Diffuse reflectance UV-vis spectra of catalysts. (b) Action spectra for photocatalytic oxidation of **1** on (black) $Pt_{2(673)}$/anatase and (white) Au_2/P25 catalysts. The apparent quantum yield for the **2** formation was calculated with the following equation: Φ_{AQY} (%) = [{(Y_{vis}–Y_{dark}) × 2}/(photon number entered into the reaction vessel)] × 100, where Y_{vis} and Y_{dark} are the amounts of **2** formed (μmol) under light irradiation and dark conditions, respectively.

3-2. Catalytic activity

The activity of Pt/TiO_2 catalysts was studied by oxidation of benzyl alcohol (**1**) to benzaldehyde (**2**), a typical aerobic oxidation.[30] The reactions were performed by stirring a toluene solution (5 mL) containing **1** (0.1 mmol) and catalyst (5 mg) under O_2 atmosphere (1 atm). The temperature of solution was kept rigorously at 298 ± 0.5 K. **Figure 6-4** summarizes the amount of **2** produced by 12 h reaction in the dark (black bars) or visible light irradiation by a Xe lamp (λ >450 nm, white bars). It is noted that both reactions selectively produced **2** (mass balance: >99%). With bare anatase TiO_2, almost no reaction occurred in the dark, and visible light irradiation produced only 2 μmol **2**. In contrast, the dark reaction with $Pt_{2(673)}$/anatase produced 12 μmol **2** due to the high catalytic activity of Pt particles for aerobic oxidation.[31–33] Light irradiation further enhanced the reaction; twice amount of **2** (25 μmol) was produced. This suggests that visible light irradiation of Pt/anatase catalyst indeed enhances aerobic oxidation.[34] It is noted that the activity of Pt/anatase catalyst is much higher than that of Au_2/P25 catalyst;[19] Au_2/P25 produced only 7.8 μmol **2** even under photoirradiation. Zhai et al.[25] reported that

Pt/TiO_2 catalyst promotes oxidation of alcohols by visible light (λ >420 nm) under N_2 atmosphere; however, as shown in **Figure 6-4**, photoirradiation of $Pt_{2(673)}$/anatase under N_2 produced very small amount of aldehyde. This indicates that aerobic oxidation is much more efficient for alcohol oxidation.

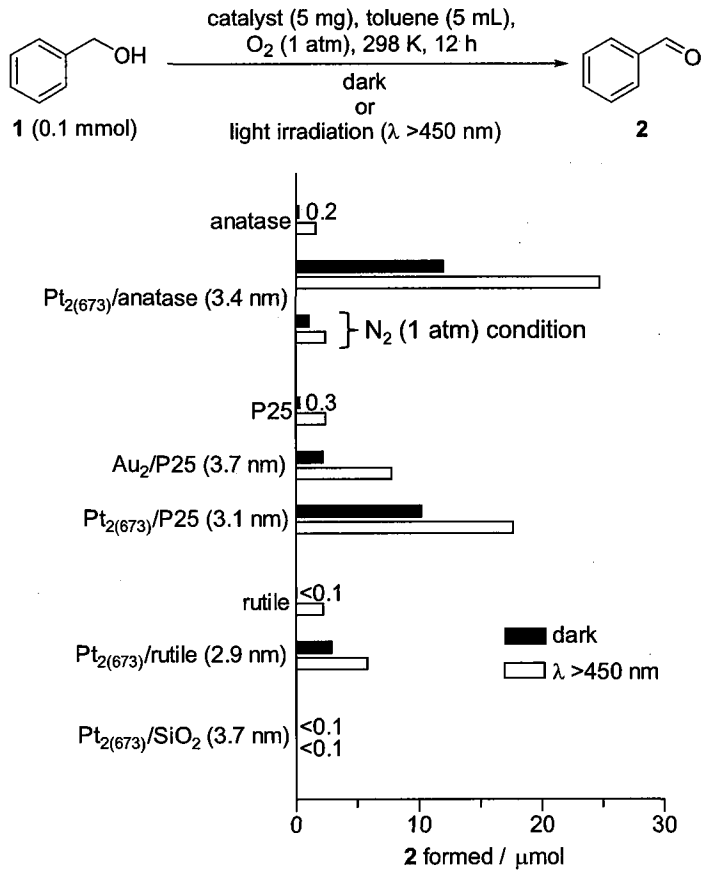

Figure 6-4. The amount of **2** formed during aerobic oxidation of **1** with respective catalysts, (black) in the dark or (white) visible light irradiation (λ >450 nm; light intensity at 450–800 nm, 16.8 mW cm^{-2}). The data obtained under N_2 (1 atm) condition were also shown in the figure. Average diameter of metal particles on the catalysts is denoted in the parenthesis. The detection limit of **2** is 0.02 μmol (4 μM) and the range of calibration is 0.004–20 mM.

Semiconductor support is necessary for the reaction enhancement by visible light irradiation. As shown in **Figure 6-4**, $Pt_{2(673)}/SiO_2$ catalyst with SiO_2 support (Aldrich; average particle size, 16 nm; BET surface area, 625 m^2 g^{-1}) shows almost no reaction enhancement even by photoirradiation. Visible light irradiation of $Pt_{2(673)}$/P25 also enhances the reaction, but the enhancement is lower than that of $Pt_{2(673)}$/anatase. In addition, $Pt_{2(673)}$/rutile is almost inactive for reaction. As shown in **Figure 6-5**, other anatase TiO_2 loaded with Pt particles also enhance aerobic oxidation under visible light irradiation. These data clearly suggest that Pt particles loaded on anatase TiO_2 promote efficient aerobic oxidation

under visible light. As shown in **Figure 6-6**, the Pt/anatase catalyst maintains its activity even after prolonged photoirradiation (~36 h), indicating that the catalyst is stable under photoirradiation.

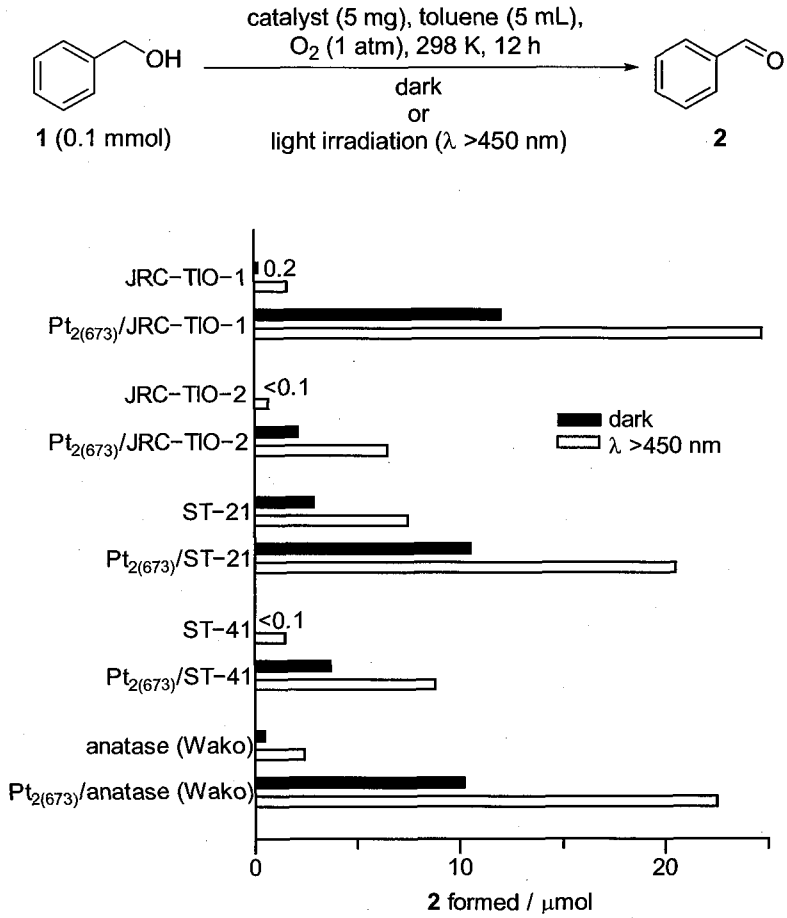

Catalyst	Supplier	S_{BET} / m^2 g^{-1}	Particle size / nm	pzc / pH
JRC-TIO-1	Catalysis Society of Japan	81	21	2.4
JRC-TIO-2	Catalysis Society of Japan	18	400	6.7
ST-21	Ishihara Sangyo Co., Ltd.	69	25	7.1
ST-41	Ishihara Sangyo Co., Ltd.	11	200	6.9
anatase (Wako)	Wako	59	29	4.6

Figure 6-5. The amount of **2** formed during aerobic oxidation of **1** with various anatase TiO_2 catalysts loaded with Pt particles, (black) in the dark or (white) under visible light irradiation (λ >450 nm). The reaction conditions are identical to those in Figure 3 in the manuscript.

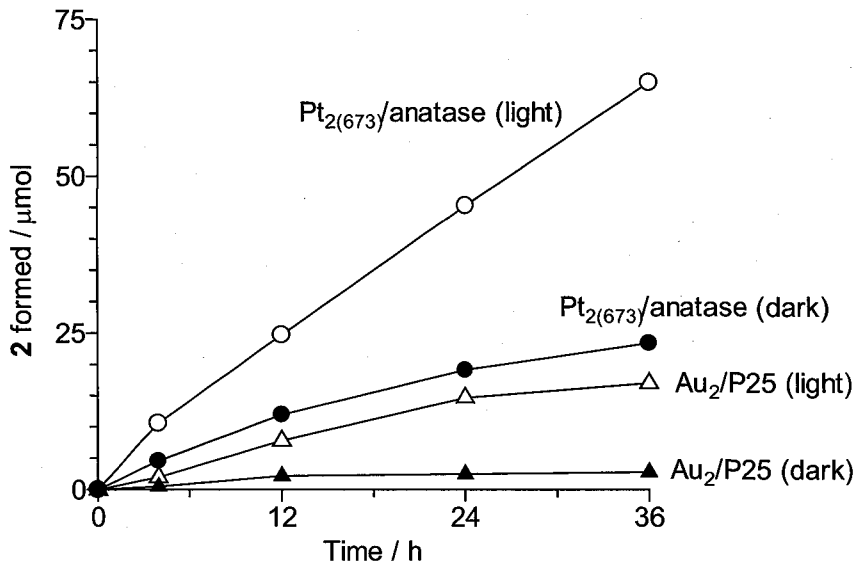

Figure 6-6. Time-dependent change in the amount of **2** formed during aerobic oxidation of **1** with respective catalysts in the dark or under visible light irradiation (λ >450 nm). The reaction conditions are identical to those in Figure 3 in the manuscript.

3-3. Electron transfer at the Pt/anatase heterojunction

The enhanced aerobic oxidation on the Pt/anatase catalyst under visible light is initiated by the intraband or interband transition of Pt particles. Some literatures[35,36] reported that Pt/TiO_2 promotes photocatalytic reaction under visible light (λ >400 nm), although TiO_2 itself scarcely absorbs light at this wavelength range. This was explained by the narrowed bandgap of TiO_2 by the Pt loadings. In the present case, as shown in **Figure 6-3b**, the action spectrum analysis revealed that the absorption band of $Pt_{2(673)}$/anatase correlates well with the apparent quantum yield (Φ_{AQY}) for photocatalytic oxidation of **1** (black circle). This data clearly suggests that the enhanced aerobic oxidation on the Pt/anatase catalyst is triggered by the activation of Pt particles. It is also noted that Φ_{AQY} for $Pt_{2(673)}$/anatase is higher than that for Au_2/P25 (white circle)[19] at the broad wavelength range of incident light, especially at λ <600 nm. The Φ_{AQY} values for $Pt_{2(673)}$/anatase at 450 nm and 550 nm are 13.7% and 7.1%, respectively, which are much higher than those for Au_2/P25 (2.9% and 3.8%).

In the Pt/anatase system, photoactivated Pt particles transfer e^- to anatase, and the e^- reduces O_2 on its surface. This is confirmed by ESR analysis of the catalysts at 77 K, after treatment of the sample with O_2 at room temperature in the dark or visible light irradiation (λ >450 nm). As shown in **Figure 6-7** (blue), bare anatase TiO_2 treated with O_2 in the dark shows weak signals (g = 2.029, 2.001), which are assigned to O^- formed via a dissociative adsorption of O_2 onto the oxygen vacancy sites of TiO_2 surface.[37,38] Photoirradiation of this sample does not create any new signal (**Figure 6-7a**, black). As

shown in **Figure 6-7b**, $Pt_{2(673)}$/anatase treated with O_2 in the dark also shows O^- signal, but photoirradiation creates strong signals assigned to a superoxide-type oxygen anion (O_2^-; g_{xx} = 2.002, g_{yy} = 2.009, g_{zz} = 2.028), which is stabilized on TiO_2 surface.[39] This suggests that photoactivated Pt particles indeed transfers e^- to anatase and promotes the reduction of O_2 on its surface. As shown in **Figure 6-7c** and **d**, photoirradiation of $Pt_{2(673)}$/P25 and $Pt_{2(673)}$/rutile samples creates much weaker O_2^- signals. This means that the O_2 reduction does not occur efficiently on these catalysts, and the data agree with their photocatalytic activities (**Figure 6-4**). It is noted that, as shown in **Figure 6-7b** (green), the Pt/anatase catalyst, when treated with O_2 at high temperature (353 K) in the dark, does not create O_2^- signal. This indicates that photo-thermal conversion[40] on the Pt particles, even if occurs in the present system,[41–44] does not promote O_2 reduction. This again suggests that electronic excitation of Pt particles by visible light enables e^- transfer to anatase and promotes O_2 reduction.

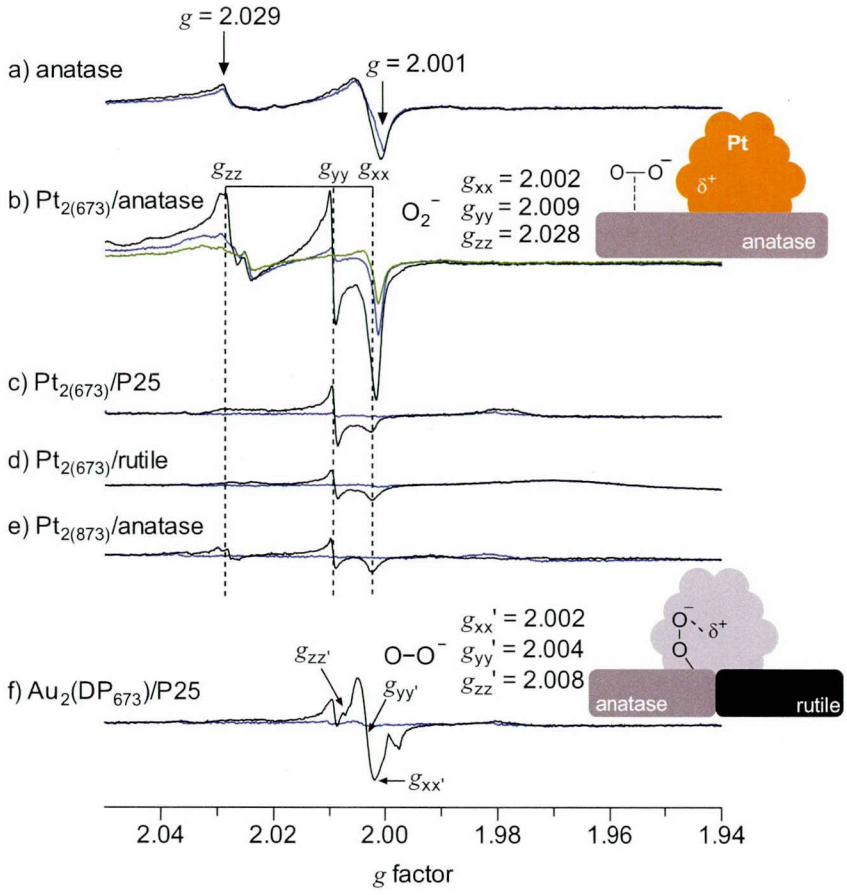

Figure 6-7. ESR spectra of respective catalysts. The catalysts were treated with 20 Torr O_2, (blue) in the dark at 298 K, (black) under visible light irradiation at 298 K, or (green) in the dark at 353 K. After evacuation, the samples were measured at 77 K.

In the Au/P25 system,[19] photoactivated Au particles scarcely transfer e^- to anatase. However, in the Pt/anatase system, the Pt→anatase e^- transfer occurs successfully. This is probably due to the strong affinity between Pt particles and anatase surface. Gong et al.[45] studied the adsorption properties of Pt and Au clusters onto the anatase (101) surface by means of scanning tunneling microscopy and *ab initio* calculations. They clarified that Pt clusters are strongly adsorbed onto the anatase surface via the association with the steps, terraces, and oxygen vacancy sites, and the adsorption energy for Pt/anatase is ten-fold higher than that for Au/anatase. The strong Pt/anatase interaction, therefore, probably enables the Pt→anatase e^- transfer.

As shown in **Figure 6-7b**, photoirradiation of $Pt_{2(673)}$/anatase with O_2 produces superoxide-type oxygen anion (O_2^-). In contrast, Au_2/P25[19] (**Figure 6-7f**) generates peroxide-type oxygen anion (O–O$^-$; $g_{xx}' = 2.002$, $g_{yy}' = 2.004$, $g_{zz}' = 2.008$), associated with the residual positive charge on Au particles.[46] The formation of O_2^- species on Pt/anatase is explained by the high e^- diffusivity in the anatase conduction band. Sun et al.[47] reported that the e^- diffusivity in anatase is two-fold higher than that in rutile. This may allow smooth e^- diffusion in anatase and promote O_2 reduction at the surface spatially separated from the Pt particles (**Figure 6-7b**). In contrast, on Au/P25, the Au→rutile→anatase multistep e^- transfers (**Scheme 6-1**) suppress smooth e^- diffusion and promote O_2 reduction at the surface near to the Au particles. This thus produces O–O$^-$ species associated with the residual positive charge on Au particles (**Figure 6-7f**).

Mechanism for photocatalytic reaction on Pt/anatase can be depicted as Scheme 2B, similar to the mechanism in the dark (**Scheme 6-2A**). It is considered that the dark reaction is initiated by activation of O_2 on the anionic site of metal particles.[20] The activated species removes H atom of alcohol and produces hydroperoxide and alcoholate species on the Pt surface.[48] Subsequent removal of H atom from the species affords the product. In the photocatalytic reaction (**Scheme 6-2B**), photoactivated Pt particles transfer e^- to anatase (a). The e^- reduces O_2 and produces O_2^- species (b). The O_2^- species attracts H atom of alcohol and produces the hydroperoxide and alcoholate species (c). These species give rise to the product (d). These mechanisms suggest that both dark and photocatalytic reactions are initiated by the activation of O_2, leading to the formation of hydroperoxide and alcoholate species. Although it is unclear whether the dark and photocatalytic reactions affect each other, the O_2 reduction on anatase surface promoted by e^- transfer from photoactivated Pt particles is the crucial step facilitating efficient aerobic oxidation.

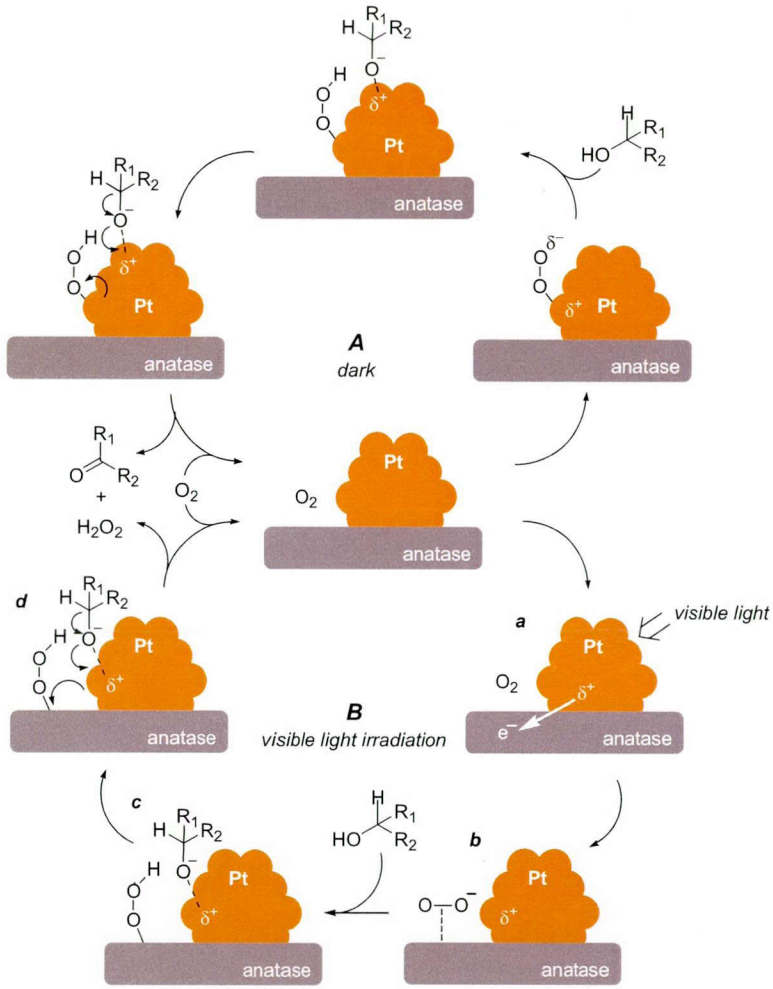

Scheme 6-2. Proposed Mechanism for Aerobic Oxidation of Alcohol on the Pt/anatase Catalyst under (A) Dark and (B) Visible Light Irradiation Conditions.

3-4. Effect of Pt amount

Photocatalytic activity of Pt/anatase catalysts depends on the amount of Pt loaded. This is confirmed by the reaction using $Pt_{x(673)}$/anatase catalysts with different Pt loadings [x (wt %) = Pt/(Pt + TiO_2) × 100]. As shown in **Figure 6-8a** (orange), d_{Pt} of the catalysts are similar (3.3–3.4 nm). In contrast, as shown in **Figure 6-9a**, absorbance of the catalysts in the visible region increases with the Pt loadings due to the increase in the number of Pt particles. The bar graphs in **Figure 6-8a** show the results for aerobic oxidation of **1** obtained with respective catalysts. The dark activity (black bar) increases with the Pt loadings due to the increase in the number of surface Pt atoms that are active for aerobic oxidation.[30] Visible light irradiation (white bar) further enhances the reaction, but the enhancement depends on the Pt loadings; 2 wt % Pt shows the largest enhancement, and higher loading catalysts are ineffective despite their stronger absorbance. As schematically shown in **Scheme 6-3**, the metal/semiconductor heterojunction creates a Schottky barrier (ϕ_B).[49] Visible light irradiation leads to a collective oscillation

of sp band or d band electrons on the metal particles and promotes the intraband or interband excitation to the sp-conduction band. This provides energy to the electrons to overcome ϕ_B and facilitates e^- transfer to semiconductor conduction band.[50,51] The height of ϕ_B, therefore, strongly affects the e^- transfer efficiency. As reported,[52] the increase in the amount of metal loaded onto the semiconductor leads to an increase in ϕ_B, due to the decrease in Fermi level of semiconductor. The decreased photocatalytic activity for larger Pt loading catalysts (**Figure 6-8a**) is therefore probably because the increased ϕ_B suppresses e^- transfer from photoactivated Pt particles to anatase.

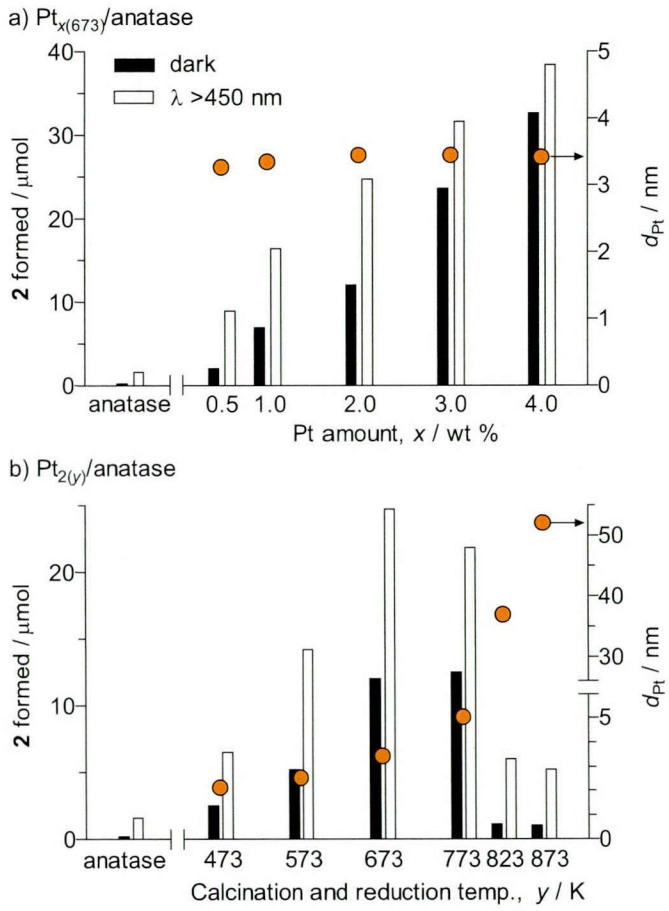

Figure 6-8. The amount of **2** formed during aerobic oxidation of **1** with (a) $Pt_{x(673)}$/anatase and (b) $Pt_{2(y)}$/anatase catalysts in the dark or under visible light irradiation. Orange keys denote d_{Pt} of catalysts. The reaction conditions are identical to those in **Figure 6-3**.

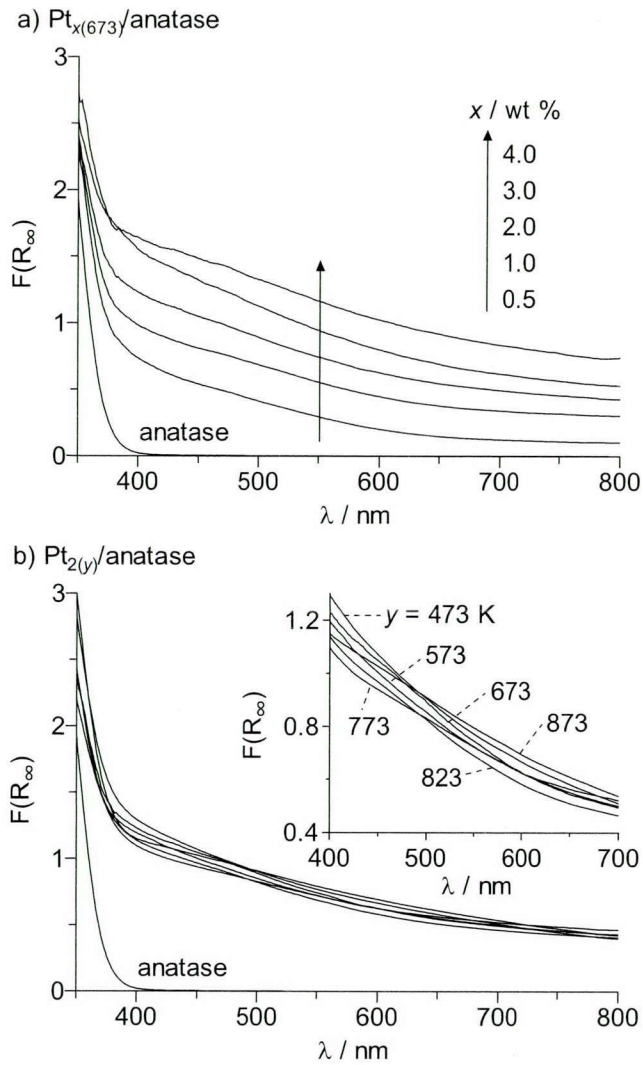

Figure 6-9. Diffuse reflectance UV-vis spectra of (a) $Pt_{x(673)}$/anatase and (b) $Pt_{2(y)}$/anatase catalysts.

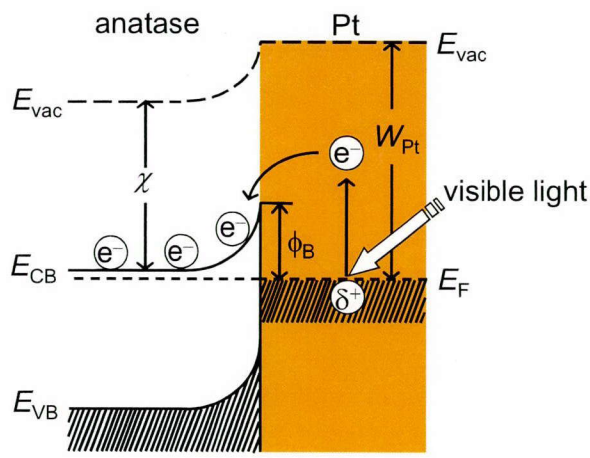

Scheme 6-3. Proposed Mechanism for Electron Transfer from the Photoactivated Pt Particles to Anatase. E_{vac}, E_F, W_{Pt}, ϕ_B, and χ denote the vacuum level, Fermi level, work function of Pt, Schottky barrier height (= $W_{Pt}-\chi$), and electron affinity of anatase conduction band, respectively.

3-5. Effect of Pt particle size

The size of Pt particles also affects the photocatalytic activity. To clarify this, the $Pt_{2(y)}$/anatase catalysts with 2 wt % Pt were prepared at different calcination and reduction temperature, y (K). As shown in **Figure 6-8b** (orange), d_{Pt} of the catalysts increase with the temperature increase due to the sintering of Pt particles; d_{Pt} for $Pt_{2(473)}$, $Pt_{2(573)}$, $Pt_{2(673)}$, $Pt_{2(773)}$, $Pt_{2(823)}$, and $Pt_{2(873)}$ catalysts are 2.1, 2.5, 3.4, 5.0, 39.1, and 52.8 nm, respectively. X-ray diffraction patterns of the catalysts indicate that the anatase-to-rutile phase transition scarcely occurs (**Figure 6-10**). As shown by the black bars in **Figure 6-8b**, in the dark condition, the $Pt_{2(673)}$ catalyst shows the highest activity, and the catalysts with smaller or larger Pt particles show decreased activity. The low activity of smaller Pt particles is due to the decreased density of low-coordination Pt sites that are active for oxidation.[53] In contrast, larger Pt particles contain decreased number of surface Pt atoms and, hence, show decreased activity.[30]

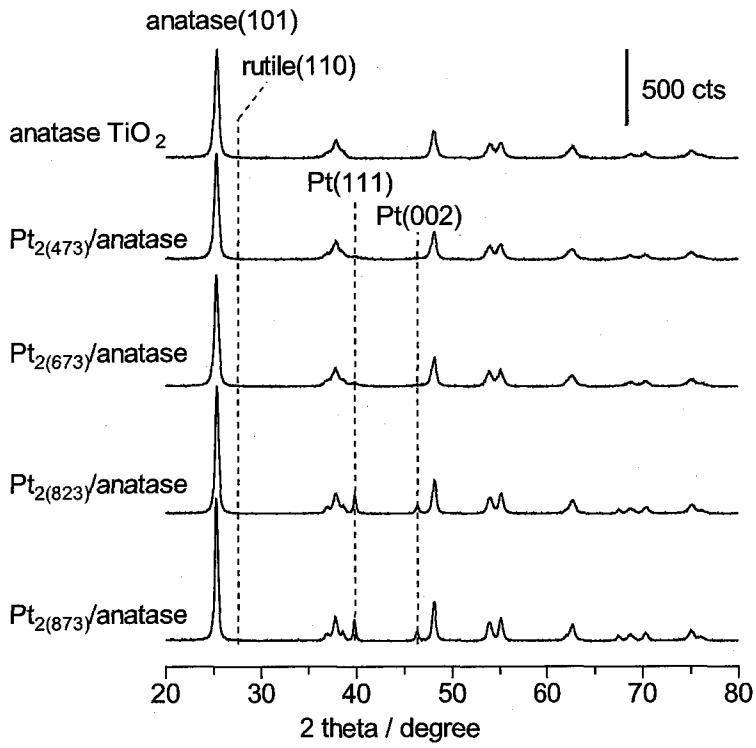

Figure 6-10. XRD patterns of $Pt_{2(y)}$/anatase catalysts. The measurements were performed on a Philips XXX diffractometer with Cu Kα radiation.

As shown by the white bars in **Figure 6-8b**, the photocatalytic activity of $Pt_{2(y)}$/anatase shows d_{Pt} dependence similar to the dark activity. The $Pt_{2(673)}$ catalyst shows the highest activity, and the catalysts with smaller or larger Pt particles show decreased activity. As shown in **Figure 6-9b**, absorbance of the catalysts in the visible region is similar, although their d_{Pt} are different (**Figure 6-8b**). This indicates that

the light absorption efficiencies for these catalysts are similar. The low photocatalytic activity of the catalysts with smaller Pt particles is due to the higher ϕ_B created at the Pt/anatase heterojunction. As reported,[54] the work function of metal particles (W_M) increases with a decrease in their particle size and is expressed by the following equation:

$$W_M\ (\mathrm{eV}) = W_{M\infty} + \frac{1.08}{d_M} \tag{1}$$

$W_{M\infty}$ and d_M are the work function of planar metal and the diameter of metal particles, respectively. $W_{Pt\infty}$ is 5.65 eV,[55] and W_{Pt} for Pt particles on the $Pt_{2(473)}$, $Pt_{2(573)}$, $Pt_{2(673)}$, $Pt_{2(773)}$, $Pt_{2(823)}$, and $Pt_{2(873)}$ catalysts are determined using their d_{Pt} values to be 6.16, 6.08, 5.97, 5.87, 5.68, and 5.67 eV, respectively. As summarized in **Figure 6-11** (black), W_{Pt} for Pt particles indeed becomes more positive with a decrease in the particle size. As shown in **Scheme 6-3**, ϕ_B is defined as the difference between the work function of Pt particles and the electron affinity of anatase E_{CB} ($\phi_B = W_{Pt} - \chi$).[56] This suggests that the catalysts with smaller Pt particles create higher ϕ_B. This may suppress smooth e^- transfer from the photoactivated Pt particles to anatase, resulting in lower photocatalytic activity (**Figure 6-8b**).

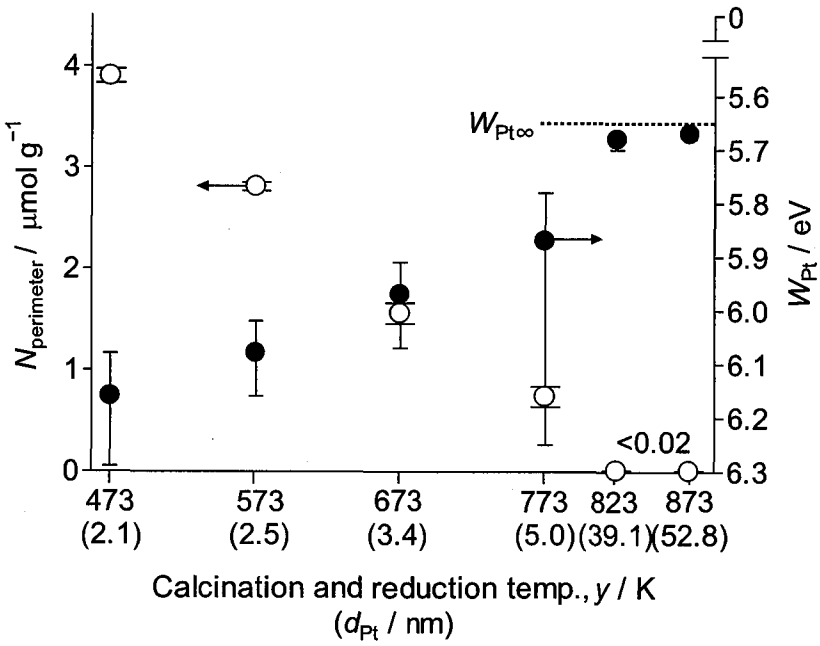

Figure 6-11. The work function of Pt particles (W_{Pt}) and the number of perimeter Pt atoms ($N_{perimeter}$) for $Pt_{2(y)}$/anatase catalysts, determined with the eqs. 1–5 using d_{Pt} values. The detailed calculation results are shown in **Table 6-1**.

Table 6-1. Calculation details for the number of perimeter Pt atoms on $Pt_{2(y)}$/anatase catalysts.

y / K	d_{Pt} [a] / nm	N_{total}* [b] / -	m [c] / -	$N_{perimeter}$* [d] / -	$N_{particle}$ [e] /μmol g^{-1}	$N_{perimeter}$ [f] /μmol g^{-1}
473	2.1 ± 0.4	319 ± 10	5.1 ± 0.1	12.2 ± 0.1	(3.21 ± 0.11) × 10^{-1}	3.9 ± 0.1
573	2.5 ± 0.4	539 ± 14	5.9 ± 0.1	14.8 ± 0.1	(1.90 ± 0.05) × 10^{-1}	2.8 ± 0.1
673	3.4 ± 0.6	(136 ± 7) × 10^{1}	7.9 ± 0.2	20.7 ± 0.4	(7.6 ± 2.1) × 10^{-2}	1.6 ± 0.1
773	5.0 ± 3.2	(431 ± 270) × 10^{1}	11.4 ± 0.4	31.2 ± 1.3	(2.4 ± 0.9) × 10^{-2}	(7.4 ± 0.9) × 10^{-1}
823	39.1 ± 14.3	(206 ± 26) × 10^{4}	85.7 ± 2.5	254 ± 8	(5.0 ± 2.3) × 10^{-5}	(1.3 ± 0.2) × 10^{-2}
873	52.8 ± 15.5	(508 ± 50) × 10^{4}	116 ± 3	344 ± 10	(2.0 ± 1.1) × 10^{-5}	(6.9 ± 1.0) × 10^{-3}

[a] Average diameter of Pt particles determined by TEM observations. [b] The number of total Pt atoms per particle. [c] The number of shells. [d] The number of perimeter Pt atoms per particle. [e] The number of Pt particles per gram catalyst. [f] The number of perimeter Pt atoms per gram catalyst.

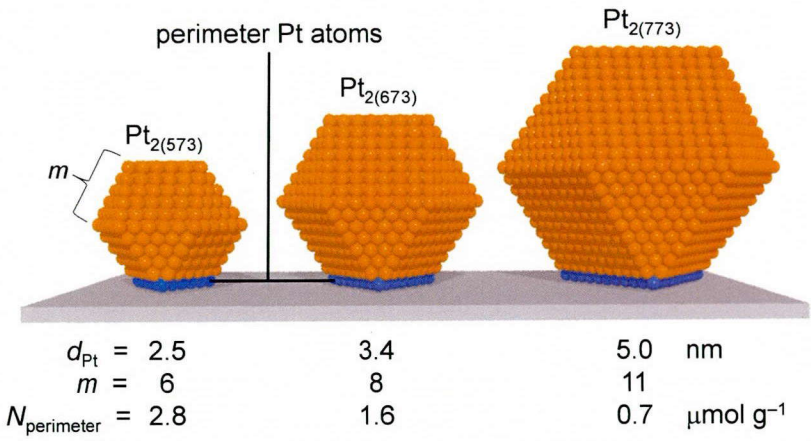

Scheme 6-4. Relationship between the Pt Particle Size and the Number of Perimeter Pt Atoms for $Pt_{2(y)}$/anatase. The calculation details for $N_{perimeter}$ are summarized in **Table 6-1**.

In contrast, larger Pt particles create lower ϕ_B due to their lower W_{Pt}; therefore, the e^- transfer to anatase would occur more easily. However, as shown in **Figure 6-8b**, photocatalytic activity of the catalysts with larger Pt particles is much lower than that of $Pt_{2(673)}$. As shown in **Scheme 6-4**, the e^- transfer from photoactivated Pt particles to anatase occurs through the perimeter Pt atoms indicated by the blue spheres and, hence, the number of perimeter Pt atoms may affect the e^- transfer efficiency. As shown in **Figure 6-1b**, the high-resolution TEM images of catalysts revealed that the shape of Pt particles is a part of cuboctahedron, which is surrounded by (111) and (100) surfaces. The Pt particles on anatase surface therefore can simply be modeled as a *fcc* cuboctahedron,[57] as often used for related systems.[58,59] This thus allows rough determination of the number of perimeter Pt atoms. Considering the full shell close packing cuboctahedron for Pt particle where one Pt atom is surrounded by twelve others, the number of total Pt atoms per particle (N_{total}*) can be expressed by eq. 2 using the number of shells (m). N_{total}* is rewritten with the average diameter of Pt particle (d_{Pt}) and the atomic diameter of Pt [$d_{atom,Pt}$ (=0.278 nm)].[60] The number of perimeter Pt atoms per particle ($N_{perimeter}$*) is expressed by eq. 3.[57]

$$N_{total}*(-) = \frac{10m^3 - 15m^2 + 11m - 3}{3} = \left(\frac{d_{Pt}}{1.105 \times d_{atom,Pt}}\right)^3 \quad (2)$$

$$N_{perimeter}*(-) = 3m - 3 \quad (3)$$

The number of Pt particles per gram catalyst ($N_{particle}$) is expressed by eq. 4, using the percent amount of Pt loaded onto the catalyst [x (= 2 wt %)], molecular weight of Pt [M_W (= 195.1 g mol^{-1})], and N_{total}*. The number of perimeter Pt atoms per gram catalyst ($N_{perimeter}$) is therefore expressed by eq. 5.

$$N_{particle}\ (\mathrm{mol\ g^{-1}}) = \frac{x}{100 \times M_W \times N_{total}*} \quad (4)$$

$$N_{perimeter}\ (\mathrm{mol\ g^{-1}}) = N_{perimeter}* \times N_{particle} \quad (5)$$

The $N_{perimeter}$ values for respective $Pt_{2(y)}$/anatase catalysts can therefore be calculated using their d_{Pt} determined by the TEM observations (**Table 6-1**). As shown in **Figure 6-11** (white), the $N_{perimeter}$ values decrease with an increase in the Pt particle size; the value for $Pt_{2(473)}$ is 3.9 μmol g^{-1}, but that for $Pt_{2(873)}$ is only 6.9×10^{-3} μmol g^{-1}. This suggests that the particle size increase leads to significant decrease in $N_{perimeter}$. As shown in **Figure 6-7e**, ESR analysis of the $Pt_{2(873)}$ catalyst after treatment with O_2 under visible light irradiation shows O_2^- signal much weaker than that of $Pt_{2(673)}$ (**Figure 6-7b**). This indicates that the catalysts with larger Pt particles are indeed inefficient for e^- transfer to anatase, although their ϕ_B values are lower. These findings clearly suggest that the decreased number of perimeter Pt atoms

Table 6-2. Effect of Sunlight Exposure on Aerobic Oxidation of Alcohols with Pt and Au Catalysts.[a]

Entry	Substrate	Catalyst	Sunlight[b]	Conversion / %[c]	Product	Yield / %[d]
1		$Pt_{2(673)}$/anatase	+	75		72
2	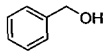	$Pt_{2(673)}$/anatase	−	13	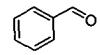	12
3		Au_2/P25	+	37		35
4		$Pt_{2(673)}$/anatase	+	84		80
5	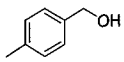	$Pt_{2(673)}$/anatase	−	9	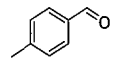	9
6		Au_2/P25	+	60		59
7		$Pt_{2(673)}$/anatase	+	>99		99
8	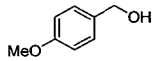	$Pt_{2(673)}$/anatase	−	14	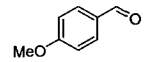	14
9		Au_2/P25	+	77		77
10		$Pt_{2(673)}$/anatase	+	73		73
11	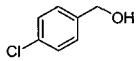	$Pt_{2(673)}$/anatase	−	7	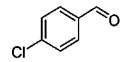	7
12		Au_2/P25	+	43		40
13		$Pt_{2(673)}$/anatase	+	72		72
14		$Pt_{2(673)}$/anatase	−	11		10
15		Au_2/P25	+	34		34
16		$Pt_{2(673)}$/anatase	+	85		84
17	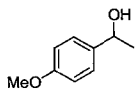	$Pt_{2(673)}$/anatase	−	5	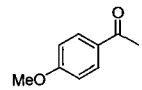	5
18		Au_2/P25	+	49		49

[a] Reaction conditions: toluene (5 mL), alcohol (25 μmol), catalyst (5 mg), O_2 (1 atm), exposure time (4 h). The average light intensity at 300–800 nm was 8.1 mW cm^{-2}, which involves λ <400 nm light with only ca. 2%. The solution temperature during exposure was 288–293 K. [b] The dark reaction (−) was performed at 293 K. [c] = (alcohol converted) / (initial amount of alcohol) × 100. [d] = (product formed) / (initial amount of alcohol) × 100.

suppresses e^- transfer from photoactivated Pt particles to anatase and results in lower photocatalytic activity. As shown in **Figure 6-8b**, the $Pt_{2(573)}$, $Pt_{2(673)}$, and $Pt_{2(773)}$ catalysts contain Pt particles with similar sizes (2–5 nm), but the $Pt_{2(673)}$ catalyst shows the highest photocatalytic activity. This means that, as shown in **Figure 6-11**, the Pt particle size strongly affects W_{Pt} and $N_{perimeter}$, and this trade-off relationship is critical for the activity of photocatalysis. As summarized in **Scheme 6-4**, the 3–4 nm Pt

particles with shell number 7–10, create relatively low ϕ_B and relatively large number of perimeter Pt atoms at the Pt/anatase heterojunction and, hence, act as highly active photocatalysts.

The $Pt_{2(673)}$/anatase catalyst successfully promotes aerobic oxidation of alcohols under sunlight irradiation at ambient temperature. **Table 6-2** summarizes the results for oxidation of various alcohols obtained with $Pt_{2(673)}$/anatase catalyst under sunlight exposure, where the temperature of solution during reaction was 288–293 K. Sunlight exposure selectively oxidizes alcohols to the corresponding carbonyl compounds with very high yields (72–99%). These yields are much higher than those obtained with $Pt_{2(673)}$/anatase in the dark at 293 K or with the Au_2/P25 catalyst[19] under sunlight exposure. These data suggest that the Pt/anatase catalyst is successfully activated by sunlight and acts as efficient photocatalyst.

4. Conclusion

We found that Pt nanoparticles loaded on anatase TiO_2 behave as highly efficient photocatalysts driven by visible light irradiation. The high photocatalytic activity of this system is due to the smooth e^- transfer from photoactivated Pt particles to anatase. This promotes efficient O_2 reduction on the anatase surface and facilitates charge separation at the Pt/anatase interface. The activity of this photocatalysis depends on the height of Schottky barrier and the number of perimeter Pt atoms. The catalyst with 2 wt % Pt, containing 3–4 nm Pt nanoparticles, facilitates efficient e^- transfer from the photoactivated Pt particles to anatase and shows the highest photocatalytic activity. Sunlight activation of the catalyst successfully promotes selective and efficient oxidation of alcohols. The efficient charge separation at the Pt/anatase heterojunction clarified here may contribute to the development of more active catalysts and the design of photocatalytic systems for selective organic transformations by sunlight.

5. References

[1] Sheldon, R. A.; Arends, I. W. C. E.; Dijksman, A. *Catal. Today* **2000**, *57*, 157.

[2] Fox, M. A.; Dulay, M. T. *Chem. Rev.* **1993**, *93*, 341.

[3] Maldotti, A.; Molinari, A.; Amadelli, R. *Chem. Rev.* **2002**, *102*, 3811.

[4] Palmisano, G.; Augugliaro, V.; Pagliaro, M.; Palmisano, L. *Chem. Commun.* **2007**, 3425.

[5] Fagnoni, M.; Dondi, D.; Ravelli, D.; Albini, A. *Chem. Rev.* **2007**, *107*, 2725.

[6] Shiraishi, Y.; Hirai, T. *J. Photochem. Photobiol. C* **2008**, *9*, 157.

[7] Asahi, R.; Morikawa, T.; Ohwaki, T.; Aoki, K.; Taga, Y. *Science* **2001**, *293*, 269.

[8] Miyauchi, M.; Ikezawa, A.; Tobimatsu, H.; Irie, H.; Hashimoto, K. *Phys. Chem. Chem. Phys.* **2004**, *6*, 865.

[9] Ohno, T.; Akiyoshi, M.; Umebayashi, T.; Asai, K.; Mitsui, T.; Matsumura, M. *Appl. Catal. A* **2004**, *265*, 115.

[10] Yan, X.; Ohno, T.; Nishijima, K.; Abe, R.; Ohtani, B. *Chem. Phys. Lett.* **2006**, *429*, 606–610.

[11] Sakthivel, S.; Kisch, H. *Angew. Chem. Int. Ed.* **2003**, *42*, 4908.

[12] Irie, H.; Watanabe, Y.; Hashimoto, K. *Chem. Lett.* **2003**, *32*, 772.

[13] Zhao, W.; Ma, W.; Chen, C.; Zhao, J.; Shuai, Z. *J. Am. Chem. Soc.* **2004**, *126*, 4782.

[14] Chen, X.; Mao. S. S. *Chem. Rev.* **2007**, *107*, 2891.

[15] Jain, P. K.; Huang, X.; El-Sayed, I. H.; El-Sayed, M. A. *Acc. Chem. Res.* **2008**, *41*, 1578.

[16] Tian, Y.; Tatsuma, T. *J. Am. Chem. Soc.* **2005**, *127*, 7632.

[17] Primo, A.; Corma, A.; García, H. *Phys. Chem. Chem. Phys.* **2011**, *13*, 886.

[18] Linic, S.; Christopher, P.; Ingram, D. B. *Nat. Mater.* **2011**, *10*, 911.

[19] Tsukamoto, D.; Shiraishi, Y.; Sugano, Y.; Ichikawa, S.; Tanaka, S.; Hirai, T. *J. Am. Chem. Soc.* **2012**, *134*, 6309.

[20] Ishida, T.; Nagaoka, M.; Akita, T.; Haruta, M. *Chem.–Eur. J.* **2008**, *14*, 8456.

[21] Ohno, T.; Sarukawa, K.; Matsumura, M. *J. Phys. Chem. B* **2001**, *105*, 2417.

[22] Dunn, W. W.; Aikawa, Y.; Bard, A. J. *J. Am. Chem. Soc.* **1981**, *103*, 3456.

[23] Fujii, M.; Kawai, T.; Kawai, S. *Chem. Phys. Lett.* **1984**, *106*, 517.

[24] Hao, Q.; Juluri, B. K.; Zheng, Y. B.; Wang, B.; Chiang, I.-K.; Jensen, L.; Crespi, V.; Eklund, P. C.; Huang, T. J. *J. Phys. Chem. C* **2010**, *114*, 18059.

[25] Zhai, W.; Xue, S.; Zhu, A.; Luo, Y. Tian, Y. *ChemCatChem* **2011**, *3*, 127.

[26] Shiraishi, Y.; Ikeda, M.; Tsukamoto, D.; Tanaka, S.; Hirai, T. *Chem. Commun.* **2011**, *47*, 4811.

[27] Shiraishi, Y.; Takeda, Y.; Sugano, Y.; Ichikawa, S.; Tanaka, S.; Hirai, T. *Chem. Commun.* **2011**, *47*, 7863.

[28] Silvestre-Albero, J.; Sepúlveda-Escribano, A.; Rodríguez-Reinoso, F.; Anderson, J. A. *J. Catal.* **2004**, *223*, 179.

[29] Bigall, N. C.; Härtling, T.; Klose, M.; Simon, P.; Eng, L. M.; Eychmüller, A. *Nano Lett.* **2008**, *8*, 4588.

[30] Abad, A.; Corma, A.; García, H. *Chem.–Eur. J.* **2008**, *14*, 212.

[31] Proch, S.; Herrmannsdörfer, J.; Kempe, R.; Kern, C.; Jess, A.; Seyfarth, L.; Senker, J. *Chem.–Eur. J.* **2008**, *14*, 8204.

[32] Ng, Y. H.; Ikeda, S.; Harada, T.; Morita, Y.; Matsumura, M. *Chem. Commun.* **2008**, 3181.

[33] Hong, H.; Hu, L.; Li, M.; Zheng, J.; Sun, X.; Lu, X.; Cao, X.; Lu, J.; Gu, H. *Chem.–Eur. J.* **2011**, *17*,

8726.

[34] The amount of **2** formed is proportional to the intensity of incident light. Photoreaction of **1** was performed with different light intensity by changing the distance from the light source to the samples. The amount of **2** formed by 12 h photoirradiation was 25 μmol (16.8 mW cm^{-2}), 35 μmol (38.0 mW cm^{-2}), and 45 μmol (54.9 mW cm^{-2}), respectively.

[35] Sun, B.; Smirniotis, P. G.; Boolchand, P. *Langmuir* **2005**, *21*, 11397.

[36] Chen, H.-W.; Ku, Y.; Kuo, Y.-L. *Water Res.* **2007**, *41*, 2069.

[37] Fenoglio, I.; Greco, G.; Livraghi, S.; Fubini, B. *Chem.–Eur. J.* **2009**, *15*, 4614.

[38] Coronado, J. M.; Soria, J. *Catal. Today* **2007**, *123*, 37.

[39] Anpo, M.; Che, M.; Fubini, B.; Garrone, E.; Giamello, E.; Paganini, M. C. *Top. Catal.* **1999**, *8*, 189.

[40] Chen, X.; Zhu, H.-Y.; Zhao, J.-C.; Zheng, Z.-F.; Gao, X.-P. *Angew. Chem., Int. Ed.* **2008**, *47*, 5353.

[41] Photo-thermal conversion on the photoirradiated Pt particles scarcely occurs in the present system. The temperature increase on the surface of an individual Pt particle in solution under photoirradiation can roughly be estimated by the equation, $\Delta T = \sigma_{abs} I/(4\pi R_{eq}\beta\kappa)$, where σ_{abs} = absorption cross section, I = intensity of the incident light, R_{eq} = radius of a sphere with the same volume as the particle, β = thermal capacitance coefficient dependent on nanoparticle aspect ratio, κ = thermal conductivity of solvent (ref 42). The σ_{abs} value for <100 nm Pt particles is reported to be $<1 \times 10^{-14}$ m^2 (ref 43). Other parameters for our catalysts are: R_{eq} <30 nm, I = 168 W m^{-2}, β = 1, κ = 0.13 W m^{-1} K^{-1} (ref 44). The theoretical temperature increase, ΔT, is determined with these parameters to be 3.4×10^{-5} K. This very small temperature increase suggests that photo-thermal conversion scarcely occur in the present Pt/anatase system.

[42] Baffou, G.; Quidant, R.; Abajo, F. J. G. *ACS Nano* **2010**, *4*, 709.

[43] Langhammer, C.; Kasemo, B.; Zorić, I. *J. Chem. Phys.* **2007**, *126*, 194702.

[44] Zhang, Z.; Gu, H.; Fujii, M. *Experiment. Therm. Fluid Sci.* **2007**, *31*, 593.

[45] Gong, X.-Q.; Selloni, A.; Dulub, O.; Jacobson, P.; Diebold, U. *J. Am. Chem. Soc.* **2008**, *130*, 370.

[46] Chowdhury, B.; Bravo-Suárez, J. J.; Mimura, N.; Lu, J.; Bando, K. K.; Tsubota, S.; Haruta, M. *J. Phys. Chem. B* **2006**, *110*, 22995.

[47] Sun, B.; Vorontsov, A. V.; Smirniotis, P. G. *Langmuir* **2003**, *19*, 3151.

[48] Fukuto, J. M.; Di Stefano, E. W.; Burstyn, J. N.; Valentine, J. S.; Cho, A. K. *Biochemistry* **1985**, *24*, 4161.

[49] Schottky, W. *Z. Phys.* **1939**, *113*, 367.

[50] Furube, A.; Du, L.; Hara, K.; Katoh, R.; Tachiya, M. *J. Am. Chem. Soc.* **2007**, *129*, 14852.

[51] Nishijima, Y.; Ueno, K.; Yokota, Y.; Murakoshi, K.; Misawa, H. *J. Phys. Chem. Lett.* **2010**, *1*, 2031.

[52] Uchihara, T.; Matsumura, M.; Yamamoto, A.; Tsubomura, H. *J. Phys. Chem.* **1989**, *93*, 5870.

[53] Liu, Y.; Tsunoyama, H.; Akita, T.; Xie, S.; Tsukuda, T. *ACS Catal.* **2011**, *1*, 2.

[54] Wood, D. M. *Phys. Rev. Lett.* **1981**, *46*, 749.

[55] Eastman, D. E. *Phys. Rev. B* **1970**, *2*, 1.

[56] Nakato, Y.; Ueda, K.; Yano, H.; Tsubomura, H. *J. Phys. Chem.* **1988**, *92*, 2316.

[57] Benfield, R. E. *J. Chem. Soc. Faraday Trans.* **1992**, *88*, 1107.

[58] Arruda, T. M.; Shyam, B.; Ziegelbauer, J. M.; Mukerjee, S.; Ramaker, D. E. *J. Phys. Chem. C* **2008**, *112*, 18087.

[59] Wilson, O. M.; Knecht, M. R.; Garcia-Marthinez, J. C.; Crooks, R. M. *J. Am. Chem. Soc.* **2006**, *128*, 4510.

[60] Murthi, V. S.; Urian, R. C.; Mukerjee, S. *J. Phys. Chem. B* **2004**, *108*, 11011.

[61] Tsukamoto, D.; Shiro, A.; Shiraishi, Y.; Sugano, Y.; Ichikawa, S.; Tanaka, S.; Hirai, T. *ACS Catal.* **2012**, *2*, 599.

[62] Shiraishi, Y.; Sugano, Y.; Tanaka, S.; Hirai, T. *Angew. Chem. Int. Ed.* **2010**, *49*, 1656.

[63] Shiraishi, Y.; Saito, N.; Hirai, T. *J. Am. Chem. Soc.* **2005**, *127*, 8304.

[64] Shiraishi, Y.; Saito, N.; Hirai, T. *J. Am. Chem. Soc.* **2005**, *127*, 12820.

General Conclusions

This dissertation work described selective organic transformations by semiconductor photocatalysts loaded with Pt and Pd nanoparticles to achieve "photocatalytic organic synthesis". In the first four chapters (I-IV), photocatalytic activation of substrates by UV light irradiation was described. In the two other chapters (V and VI), the author described the photocatalytic activation of substrates by visible light irradiation.

In Chapter I, the author found that a new strategy for the acid- and oxidant-free synthesis of benzimidazoles using *o*-arylenediamines and alcohols as the reactants at room temperature under UV light irradiation condition (λ >300 nm). This process employs nanoparticles that comprise of a titanium dioxide (TiO_2) semiconductor loaded with Pt nanoparticles. This is promoted by one-pot multiple catalytic transformations on Pt/TiO_2, which involve a platinum-assisted photocatalytic oxidation of alcohols on TiO_2 and a catalytic dehydrogenation on the surface of the platinum particles. The amount and size of platinum particles are important factors. The catalyst containing 0.2 wt% Pt, with a relatively large amount of Pt atoms and a small Pt particle size (<4 nm), exhibits the highest activity and selectivity. This process has significant advantages when compared with other methods: (i) a cheap and stable reactant (alcohol), (ii) it does not require the use of acids or oxidants, (iii) the by-products formed are harmless (only water and molecular hydrogen form during the reaction), and (iv) the reaction proceeds under milder ambient conditions. Therefore, this process has the potential to enable a more sustainable benzimidazole synthesis.

In Chapter II, TiO_2 loaded with Pd nanoparticles were used as catalysts for photocatalytic hydrodenitrogenation of aromatic cyanide in ethanol as a hydrogen source. These catalysts promote denitrogenation and produce toluene derivatives and triethylamine with very high selectivity under UV light (λ >300 nm) irradiation at room temperature. Photoexcited Pd/TiO_2 catalysts produce acetaldehyde and the active H-Pd species. Consecutive reactions involving the hydrogenation by H-Pd species and the condensation with aldehyde facilitate efficient hydrodenitrogenation of aromatic cyanides. The amount of Pd loaded and the size of Pd particles strongly affect the denitrogenation activity. The Pd/TiO_2 catalyst with a relatively low Schottky barrier height at the Pd/TiO_2 heterojunction and a large number of surface Pd atoms is necessary for efficient denitrogenation.

In Chapter III, the author found that Pd/TiO_2 catalyst promotes *N*-monoalkylation of primary amine with alcohol under UV light irradiation (λ >300 nm) at room temperature. Several kinds of secondary amines are successfully produced with high yields. Tandem photocatalytic and catalytic reactions

promote three consecutive reactions, consisting of Pd-assisted alcohol oxidation on the photoactivated TiO_2, catalytic condensation of the formed aldehydes with amines on the TiO_2 surface, and hydrogenation of formed imine with H atoms on the Pd particles. The rate-determining step is the imine hydrogenation via an adsorption of imine on Pd surface. The imine adsorption onto the larger triangle site is strongly suppressed by competitive adsorption of alcohol. As a result of this, the catalyst with 2-2.5 nm Pd particles, which contain relatively larger number of triangular Pd atoms and do not promote strong alcohol adsorption, shows the highest activity for imine hydrogenation and promotes efficient *N*-alkylation. This tandem catalytic system offers significant advantages: (i) no harmful byproduct forms; (ii) the reaction proceeds at room temperature; and (iii) several secondary amines are successfully produced. The tandem reaction promoted by photocatalytic and catalytic action, therefore, have a potential to be a powerful method for one-pot synthesis of organic compounds in an environmentally-friendly way.

In Chapter IV, the author found that UV irradiation (λ >300 nm) of TiO_2 loaded with Pd-Pt alloy promotes efficient dehalogenation of organic halides with alcohol. The activity is more than three times that of TiO_2 loaded with Pd nanoparticles and higher than the conventional method with molecular hydrogen. Photoexcited catalysts produce carbonyl compounds and H^+, whereas the photoformed e^- reduces H^+ on the Pt site. Sequentially, the formed H atom transfers to the adjacent Pd site and promotes dehalogenation. This high activity is due to the enhanced consumption of photoformed e^- on the Pt site by H^+ reduction and sequential efficient transfer of the formed hydrogen atom to the adjacent Pd site within the alloy particles. This offers crucial advantages: (i) safe alcohols can be used as a hydrogen source; and, (ii) the reaction proceeds much faster. Therefore, this Pd-Pt bimetallic alloy system has a potential to proceed a Pd-based hydrogenation process.

In Chapter V, tungsten trioxide (WO_3) loaded Pt nanoparticles (Pt/WO_3) were used as catalysts for oxidation of cyclohexane (CHA) with molecular oxygen (O_2) under visible light irradiation (λ >420 nm). These catalysts successfully promote partial oxidation of CHA to produce cyclohexanol (CHA-ol) and cyclohexanone (CHA-one) with ca. 93% selectivity. The ESR measurement with a spin trapping reagent and the photocatalytic reaction with a superoxide radical ($O_2\bullet^-$) scavenger indicate that the high selectivity for CHA oxidation on Pt/WO_3 is because subsequent photocatalytic decomposition of CHA-ol and CHA-one is suppressed. In the Pt/WO_3 system, the photoformed electrons on the conduction band of WO_3 are consumed by a multi-electron reduction of O_2 on the Pt particles (formation of H_2O and H_2O_2), where a single-electron reduction of O_2 is unfavored. This suppresses the formation of $O_2\bullet^-$ that promotes decomposition of CHA-ol and CHA-one and, hence, results in selective formation

of these products.

In Chapter VI, the author found that Pt nanoparticles loaded on anatase TiO_2 behave as highly efficient photocatalysts driven by visible light irradiation (λ >450 nm). The high photocatalytic activity of this system is due to the smooth e^- transfer from photoactivated Pt particles to anatase. This promotes efficient O_2 reduction on the anatase surface and facilitates charge separation at the Pt/anatase interface. The activity of this photocatalysis depends on the height of Schottky barrier and the number of perimeter Pt atoms. The catalyst with 2 wt% Pt, containing 3-4 nm Pt nanoparticles, facilitates efficient e^- transfer from the photoactivated Pt particles to anatase and shows the highest photocatalytic activity. Sunlight activation of the catalyst successfully promotes selective and efficient oxidation of alcohols. The efficient charge separation at the Pt/anatase heterojunction clarified here may contribute to the development of more active catalysts and the design of photocatalytic systems for selective organic transformation by sunlight.

Suggestions for Future Work

This dissertation work described the selective organic transformations by semiconductor photocatalysts loaded with Pt and Pd nanoparticles. The author points out here the extension of this work for the design of visible light-driven photocatalysis towards the application of sunlight as a light source for organic synthesis.

Previously, our research group found that Au nanoparticles with small particle size (<5 nm) located at the interface of anatase/rutile TiO_2 particles behave as highly active sites for plasmonic catalysts under visible light.[1] In Chapter VI, by applying the Au/TiO_2 system, the author also found that Pt nanoparticles with appropriate particle size (3-4 nm) located at anatase TiO_2 particles behave as highly active sites for photocatalysts under visible light. ESR analysis clearly revealed that the heterojunction of Pt/anatase facilitates direct transfer of e^- from the photoactivated Pt particles to anatase TiO_2 and efficient O_2 reduction. The catalyst successfully promotes aerobic oxidation of alcohols under sunlight. In addition, On the basis of the catalyst architecture clarified from these results, the author proposes more efficient visible light-induced photocatalysts. **Figure 7** shows the proposal of new catalysts: they are (1) TiO_2 loaded with *Au–Cu bimetallic alloy* nanoparticles, and (2) TiO_2 loaded with *Pt-Cu bimetallic alloy* nanoparticles.

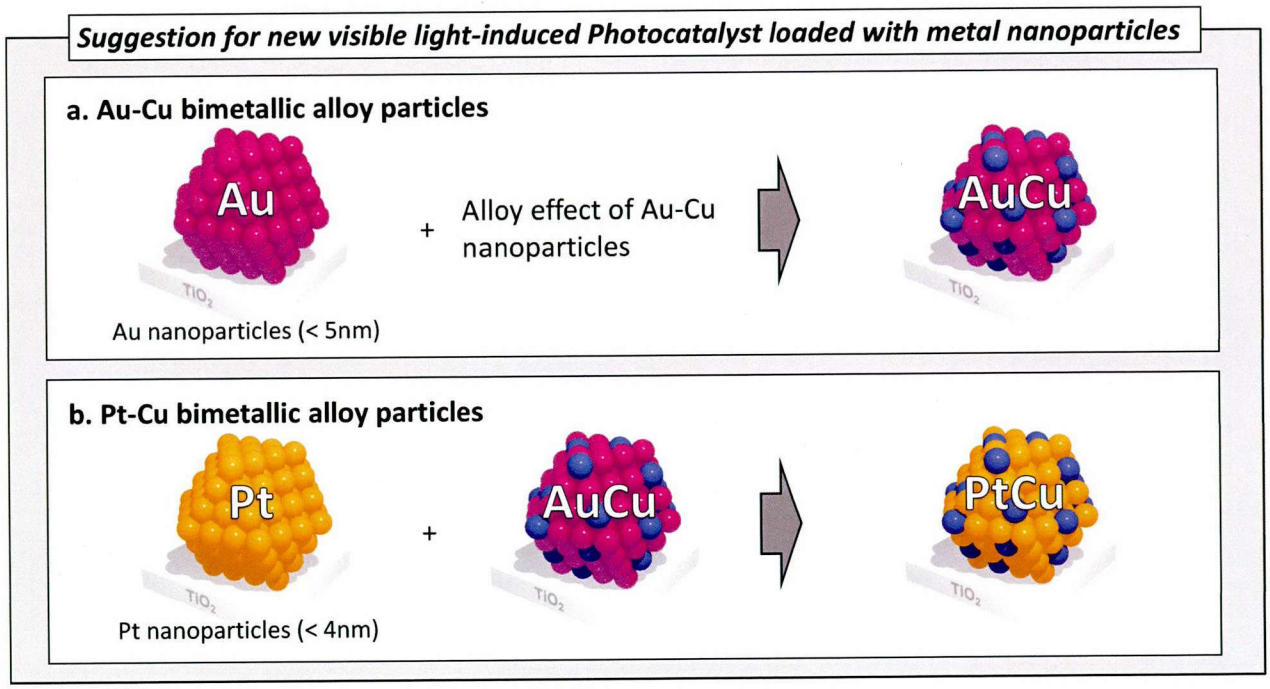

Figure 7. Suggestion for new visible light-induced photocatalyst loaded with metal nanoparticles

(1) TiO_2 loaded with Au–Cu bimetallic alloy nanoparticles

As reported,[2] alloying of Au with other noble metals affects strongly on the catalytic activity. This alloy effect is probably due to the e^- transfer phenomena from the metal with small electronegativity[3] to the metal with large electronegativity (**Figure 8a**). In addition, as reported,[4] Au-Cu alloy particles with ca. 3 nm diameter loaded on silica promotes aerobic oxidation of alcohols with 1.5-fold higher than the monometallic Au particles. The enhanced activity of Au-Cu alloy is considered to be due to the efficient activation of O_2 on the alloy site. These alloy particles, however, rapidly lose their activity during the reaction, because O_2 oxidizes the surface Cu atoms and eliminates the alloying effect.[5] Therefore, creation of Au-Cu alloy catalysts which enable to avoid the oxidation of surface Cu atoms by O_2 is necessary for highly efficient aerobic oxidation under ambient conditions. The Au–Cu bimetallic alloy nanoparticles with visible light irradiation are probably one of the new approaches to avoid the oxidation of surface Cu atoms (**Figure 7a**). Au-Cu alloy particles activate molecular oxygen and promote aerobic oxidation of alcohols (**Figure 9a**). Simultaneously, the oxidized Cu species on the surface of catalyst with visible light is reduced to Cu^0 by a transfer of the plasmon electrons of photoactivated Au particle to oxidized Cu species, leading to suppression of oxidation of Cu on the surface (**Figure 9b**). This may promote efficient aerobic oxidation of alcohols without decreasing the activity. We have already made Au–Cu bimetallic alloy particles loaded on TiO_2 particles, with ca. 2.5 nm diameter and shows enhanced photocatalytic activity for aerobic oxidation than Au/TiO_2 catalyst under visible light irradiation. Although the detailed reaction mechanisms remain to be clarified, this alloy system with visible light irradiation would be one of the candidates for the improvement of catalytic activity.

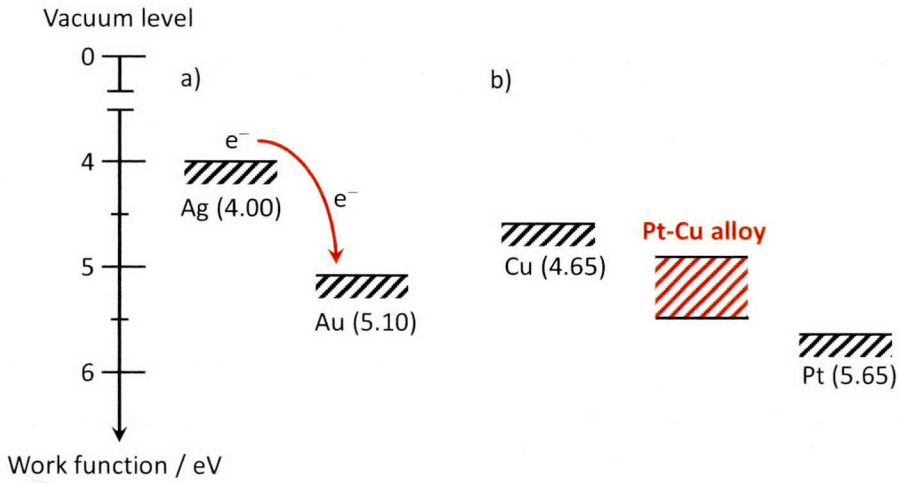

Figure 8. Work functions of noble metals.

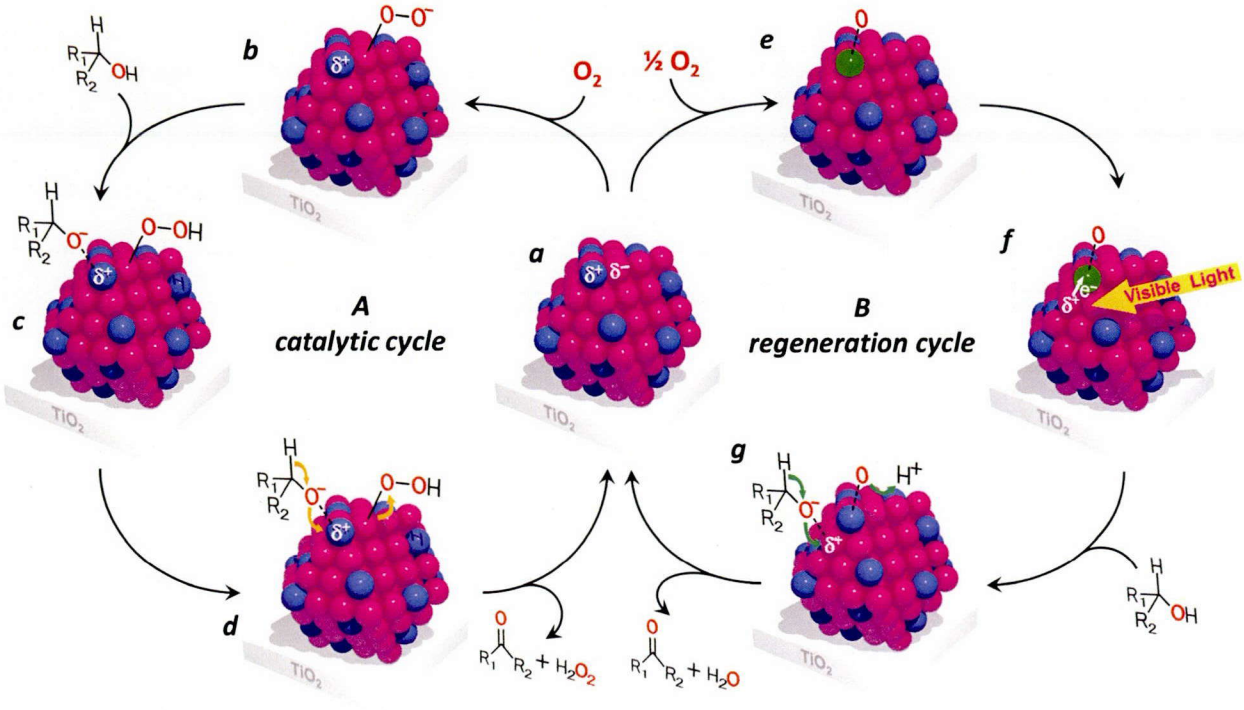

Figure 9. Proposed mechanism for aerobic oxidation on AuCu/TiO_2 catalyst. (purple) gold atom, (blue) copper atom, (gray) oxidized copper atom, and (red) oxygen atom.

(2) TiO_2 loaded with Pt-Cu bimetallic alloy nanoparticles

As noted above, alloying of Au and Cu affects strongly in the catalytic activity. This is probably because visible light-induced plasmon activation of e^- on Au reduces the oxidized surface Cu atoms. As shown in Chapter VI, visible light-induced photocatalysis on Pt/TiO_2 is initiated by direct e^- injection from photoactivated Pt particles to anatase TiO_2 conduction. Therefore, Pt-Cu alloying system may also enhance the catalytic activity (**Figure 7b**). When the photoactivated Pt particles inject e^- to TiO_2 conduction band, the e^- have to overcome the Schottky barrier. The height of the barrier decreases with decrease of work function of metal. The work function of Pt-Cu alloying metal, therefore, becomes smaller than Pt (**Figure 8b**), leading to more efficient e^- transfer to TiO_2 conduction band. The authors have already made PdCu/TiO_2 catalysts and the catalyst shows very high activity for aerobic oxidation of alcohols. It must be noted that the catalytic activity is much higher than Pt/TiO_2 catalyst. Although the detailed reaction mechanisms remain to be clarified, this alloy system would also possess one of the possibilities for the improvement of catalytic activity under visible light.

References

[1] Tsukamoto, D.; Shiraishi, Y.; Sugano, Y.; Ichikawa, S.; Tanaka, S.; Hirai, T. *J. Am. Chem. Soc.* **2012**, *134*, 6309.

[2] Tsukamoto, D.; Shiro, A.; Shiraishi, Y.; Sugano, Y.; Ichikawa, S.; Tanaka, S.; Hirai, T. *ACS Catal.* **2012**, *2*, 599.

[3] Eastman, D. E. *Phys. Rev. B* **1970**, *2*, 1.

[4] Pina, C. D.; Falletta, E.; Rossi, M. *J. Catal.* **2008**, *260*, 384.

[5] Liu, X.; Wang, A.; Li, L.; Zhang, T.; Mou, C. Y.; Lee, J. F. *J. Catal.* **2011**, *278*, 288.

List of Publication

Papers:

(1) **Shiraishi, Y.; Sugano, Y.; Tanaka, S.; Hirai, T.** One-Pot Synthesis of Benzimidazoles by Simultaneous Photocatalytic and Catalytic Reactions on Pt@TiO_2 Nanoparticles, *Angew. Chem.* **2010**, *122*, 1700–1704; *Angew. Chem. Int. Ed.* **2010**, *49*, 1656–1660.

(2) **Sugano, Y.; Fujiwara, K.; Shiraishi, Y.; Ichikawa, S.; Hirai, T.** Photocatalytic hydrodenitrogenation of aromatic cyanides on TiO_2 loaded with Pd nanoparticles, *Catal. Sci. Technol.* **DOI:** 10.1039/C3CY20748J.

(3) **Shiraishi, Y.; Fujiwara, K.; Sugano, Y.; Ichikawa, S.; Hirai, T.** N-Monoalkylation of Amines with Alcohols by Tandem Photocatalytic and Catalytic Reactions on TiO_2 Loaded with Pd Nanoparticles, *ACS Catal.* **2013**, *3*, 312-320.

(4) **Shiraishi, Y.; Takeda, Y.; Sugano, Y.; Ichikawa, S.; Tanaka, S.; Hirai, T.** Highly efficient photocatalytic dehalogenation of organic halides on TiO_2 loaded with bimetallic Pd-Pt alloy nanoparticles, *Chem. Commun.* **2011**, *47*, 7863–7865.

(5) **Shiraishi, Y.; Sugano, Y.; Ichikawa, S.; Hirai, T.** Visible light-induced partial oxidation of cyclohexane on WO_3 loaded with Pt nanoparticles, *Catal. Sci. Technol.* **2012**, *2*, 400–405.

(6) **Shiraishi, Y.; Tsukamoto, D.; Sugano, Y.; Shiro, A.; Ichikawa, S.; Tanaka, S.; Hirai, T.** Platinum Nanoparticles Supported on Anatase Titanium Dioxide as Highly Active Catalysts for Aerobic Oxidation under Visible Light Irradiation, *ACS Catal.* **2012**, *2*, 1984–1992.

Related works:

(1) **Shiraishi, Y.; Sugano, Y.; Inoue, D.; Hirai, T.** Effect of substrate polarity on photocatalytic activity of titanium dioxide particles embedded in mesoporous silica, *J. Catal.* **2009**, *264*, 175-182.

(2) **Tsukamoto, D.; Shiro, A.; Shiraishi, Y.; Sugano, Y.; Ichikawa, S.; Tanaka, S.; Hirai, T.** Photocatalytic H_2O_2 Production from Ethanol/O_2 System Using TiO_2 Loaded with Au-Ag Bimetallic Alloy Nanoparticles, *ACS Catal.* **2012**, *2*, 599-603.

(3) **Tsukamoto, D.; Shiraishi, Y.; Sugano, Y.; Ichikawa, S.; Tanaka, S.; Hirai, T.** Gold Nanoparticles Located at the Interface of Anatase/Rutile TiO_2 Particles as Active Plasmonic Photocatalysts for Aerobic Oxidation, *J. Am. Chem. Soc.* **2012**, *134*, 6309-6315.

Acknowledgment

The author is greatly indebted to Professor Dr. Takayuki Hirai and Associate Professor Dr. Yasuhiro Shiraishi (Research Center for Solar Energy Chemistry, Osaka University) for their constant guidance and helpful advice throughout this work. The author is sincerely grateful to Professor Dr. Koichiro Jitsukawa (Graduate School of Engineering Science, Osaka University) and to Professor Dr. Michio Matsumura (Research Center for Solar Energy Chemistry, Osaka University) for a number of valuable comments and criticisms during the completion of this thesis.

The author deeply thanks Dr. Satoshi Ichikawa (Institute for NanoScience Design, Osaka University) for TEM measurements and Dr. Shunsuke Tanaka (Department of Chemical, Energy and Environmental Engineering, Kansai University) for TEM and XPS measurements. The author also thanks Mr. Shinzo Koshida (Graduate School of Engineering Science, Osaka University) for ESR measurements.

The author acknowledges all members of the Hirai laboratory for their friendship. Special thanks are given to the following colleagues for their experimental cooperation: Dr. Daijiro Tsukamoto, Messrs. Satoshi Takaki, Mokoto Ikeda, Yoshinori Takeda, Akimitsu Shiro, and Keisuke Fujiwara.

Finally, the author also wishes to thank his family, Kazuyoshi Sugano and Katsuko Sugano for their continuous encouragement and supports.

This study was supported financially by Global Center of Excellence (GCOE) program "Global Educaton and Research Center for Bio-Environmental Chemistry" of Osaka University.